

...E#i#

3 1293 10064 7951





OVERDUE FINES: 25¢ per day per item

#### RETURNING LIBRARY MATERIALS:

Place in book return to remove charge from circulation records

		:
		•
		; ;
		:
		•
		*

This is an authorized facsimile
and was produced by microfilm-xerography
in 1980 by
UNIVERSITY MICROFILMS INTERNATIONAL
Ann Arbor, Michigan, U.S.A.
London, England

# A THEORETICAL INVESTIGATION OF ROTATIONAL NONEQUILIBRIUM PHENOMENA IN THE PULSED HYDROGEN FLUORIDE LASER SYSTEM

Ву

Keith Emery

#### A DISSERTATION

Submitted to

Michigan State University
in partial fulfillment of the degree of

MASTER OF SCIENCE

Department of Electrical Engineering

1979

#### ABSTRACT

A THEORETICAL INVESTIGATION OF ROTATIONAL NONEQUILIBRIUM PHENOMENA IN THE PULSED HYDROGEN FLUORIDE LASER SYSTEM

By

#### Keith Emery

A rate equation model of a pulsed  $H_2 + F_2$  chemical laser is used to examine the relative effect of rotational nonequilibrium mechanisms on laser performance. This computer model yields the population time histories for the first seven vibrational and thirty rotational level of HF. The model also yiel'ds the time resolved spectra for the first twelve vibrational - rotational P branch transitions. The major thrust of the present work was to evaluate the relative importance of vibrational to rotational (VR), vibrational to vibrational (VV), rotational to rotational (RR) and rotational to translational (RT) energy transfer on laser performance. The character of the spectra is significantly different from that of other  $F + H_2$ and  $H_2$  +  $F_2$  models which assume that rotational equilibrium is present in VR,T and VV reactions. The effect of single and multi vibrational quanta VR are assessed. The effect of increasing the multiquanta VR rate was found to populate higher rotational levels of HF, increase P branch pulse energy and duration.

#### **ACKNOWLEDGEMENTS**

I would like to thank the many people who have helped bring this thesis to completion. My advisor, Dr. Ron Kerber has provided much needed technical advice and assistance. I would like to thank Captain Larry Rapognani for providing information on the CYBER 176 operating system at Kirkland Air Force Base in Albuquerque, New Mexico where the model was executed.

I would also like to thank the Division of Engineering Research at Michigan State University for assistance in preparing the manuscript. Finally, I would like to thank Betty Hutcheson at Colorado State University for assistance in typing this thesis.

# TABLE OF CONTENTS

		Page
1.	PREVIOUS STUDIES OF ROTATIONAL NONEQUILIBRIUM PHENOMENA	1
	1.1 Nonequilibrium Pumping	2
	1.1.2 Hot Pumping	6 10
	1.2.1 Experimental Studies	10
	1.2.2 Rotational Lasing	12
	1.2.3 Theoretical Studies	15
	1.3 Vibrational Relaxation of HF	18
	1.3.1 Theoretical Investigations of VR	19
	1.3.2 Theoretical Investigations of VV	26
2.	STUDIES OF ROTATIONAL NONEQUILIBRIUM IN	
	THE PULSED H <sub>2</sub> + F <sub>2</sub> SYSTEMS	32
	2.1 Time Resolved Spectroscopy	32
	2.2 Computer Modeling of Rotational	
	Nonequilibrium Phenomena	36
3.	MODEL FORMULATION	42
4.	RESULTS AND DISCUSSIONS	55
	4.1 Effect of Vibrational to Rotational	
	Relaxation on HF Population	55
	4.2 Effect of Vibrational to Rotational	
	Relaxation on the Power and Energy	61
<b>5.</b>	SUMMARY	69
	APPENDIX A: RATE COEFFICIENTS FOR THE	
	H <sub>2</sub> + F <sub>2</sub> CHEMICAL LASER	70
	APPENDIX B: DERIVATION OF X rad	88
	APPENDIX C: DESCRIPTION OF COMPUTER SIMULATIONS FOR THE PULSED	
	HF CHEMICAL LASER	93
	RELAXATION	109
	REFERENCES	115

# LIST OF TABLES

Table		Page
1.1	Relative Pumping Efficiencies for $F + H_2$ (0',J') $K_2^C(V)$ $HF(v) + H \dots \dots \dots \dots$	4
1.2	Relative Pumping Efficiencies for $H + F \xrightarrow{f} (v) HF(v) + F \dots \dots \dots$	7
1.3	Observed HF Rotational Laser Transitions	13
1.4	Multiquanta VR Rates of Wilkins [51] $HF(v,J) + M \downarrow HF(v',J') + M $	14
1.5	Vibrational to Vibrational Rate Coefficients	
	in 10 <sup>12</sup> cc/mol-sec at 300°K for HF(v-1) + HF(v'=1) + HF(v) + HF(v'=0)	27
1.6	Single Quanta VV Rates of Wilkins [51] $HF(v,J_1) + HF(v^*,J_2) \stackrel{\rightarrow}{\leftarrow} HF(v-1,J_1') +$	
	$HF(v*+1,J_2')$	29
1.7	Vibrational Dependence of the Total VR, T Rate Coefficient	30
2.1	Comparison of Computer Models Incorporating Rotational Nonequilibrium Phenomena in HF	
	or DF	33
3.1	Relative Rotational Relaxation Efficiencies	49
4.1	Possible VR Relaxation Distributions About  J max for HF(v,J) + M + HF(v',J') + M	56
A.1	Rate Coefficients for the H <sub>2</sub> + F <sub>2</sub> Chemical Laser	72
c.1	Nomenclature	103
D.1	Most Probable Multiquanta VR Transitions	
	and Their Energy Defect AE in cm	109

# LIST OF FIGURES

Figure		Page
1.1	Rotational distribution for the cold pumping reaction. The solid line is the distribution of Polany; et al. [11] and the dashed line is a 300°K equilibrium rotational distribution	5
1.2	Rotational distribution for the hot pumping reaction. The solid line is the distribution of Polany; et al. [26] and the dashed line is a 300°K equilibrium rotational distribution	9
1.3	Calculated rotational transition probabilities versus rotational level [51]. The equation for line A is 0.788 exp( 0.1357 J). The equation for line B is 0.0406 exp(-0.1376 J)	17
1.4	A typical VR relaxation path. Multiquanta vibrational relaxation is allowed. The values of J' range from J -4 to J +2 where J is the value of J' with smallest energy defect	20
1.5	Schematic of a typical VV reaction path. The specific reaction shown is $HF(2,10) + HF(0,4)$ $2HF(1,10) + HF(1,4) + 102.8 \text{ cm}^{-1}$ . If zero rotational energy is assumed then $\Delta E = 171.2 \text{ cm}^{-1}$	21
2.1	Comparison of time-resolved spectral output.  (a) Experimental data reported in Ref. 69 for a 1 $H_2$ :1 $F_2$ :60 He mixture at 50 Torr	34
2.2	Time resolved spectra of Nichols et al. [69] for a 1:1:10 mixture of $H_2:F_2:N_2$ at 90 Torr with $F/F_2 = 0.23\%$ and 0.002 HF. The active medium length is 30 cm and the mirror spacing	25
	is 113 cm, $R_0 = 0.7$ and $R_r = 1.0 \dots$	35

# LIST OF FIGURES - CONTINUED

Figure		Page
2.3	Time resolved spectra of Parker and Stephens [70] for a 1:1:10:0.25 mixture of $F_2:H_2He:0_2$ at 35 Torr with $F/F_2=5\%$ .	
	The active medium length is 15 cm and the mirror spacing is 60 cm, $R_0 = 0.8$	
	and $R_L = 1.0$ . The lower level of a P	
	branch transition is denoted by v and J. The length of the lines correspond to the duration of lasing on a given line. The dot on the line corresponds to the time at which the maximum power was achieved on that line	38
	actiteved on that line	30
A.1	Pumping rates for the cold reaction. The pumping rates employed in the present formulation have been suggested by	
	Cohen [24]	74
A.2	Rate coefficients for the hot pumping reaction. The present formulation uses the rate coefficients that have been suggested by Cohen [24]	83
A.3	The temperature dependence of selected vibrational to vibrational exchange rate coefficients. The VV rates calculated by Wilkins [51] and given in Table 1.5 are employed in the present formulation	84
A.4	Vibrational to rotational, translational rates. Note that for HF+H <sub>2</sub> , H, F <sub>2</sub> , H, Wilkins [51]	
	rates are scaled according to Cohen's [22] rates and are employed in the present formulation	85
<b>c.1</b>	A Warnier-Orr [90] diagram of the Fortran program MSUHFVR, a comprehensive computer model of the pulsed H <sub>2</sub> + F <sub>2</sub> laser system	96

#### 1. PREVIOUS STUDIES OF ROTATIONAL NONEQUILIBRIUM PHENOMENA

Laser action from the hydrogen fluoride (HF) molecule initiated by flash photolysis of UF<sub>6</sub>-H<sub>2</sub> mixtures was reported by Kompa and Pimentel [1] in 1967 shortly after the first HCl chemical laser was demonstrated in 1965 by Kasper and Pimentel [2]. At about the same time, Deutsch [3] reported similar laser action resulting from initiation by pulsed electrical discharge from Freon-H<sub>2</sub> mixtures. Since the advent of this first laser important advances in the development and understanding of the HF laser have occurred.

With the discovery of the chemical laser, it was recognized that one essential advantage of this laser was its potential for high efficiency, and that this efficiency could be realized through the use of a chain reaction to achieve a population inversion. The chain consists of a cold pumping reaction,

$$F + H_2 (v,J') \stackrel{\rightarrow}{\leftarrow} HF(v,J) + H \quad \Delta H = 31.9 \text{ kcal/mole}$$
 (1.1)

and a hot pumping reaction,

$$H + F_2 + HF(v,J) + F$$
  $\Delta H = 97.9 \text{ kcal/mole}$  (1.2)

where cold and hot refers to the relative exothermicity of the reactions. The vibrational energy level of HF is denoted by v, the rotational energy levels of HF are given by J, and the net change in molar enthapy of the reaction is denoted as  $\Delta H$ . The vibrational and rotational levels of  $H_2$  are denoted as v', J'. We note that the nascent vibrational and rotational distribution of HF is significantly different from the thermal equilibrium population.

Many initiation techniques for the H<sub>2</sub>+F<sub>2</sub> chain reaction laser, e.g., electron-beam-irradiated discharge, electrical discharge and laser photolysis, with a large assortment of experimental apparatus and a variety of gas mixing procedures have been developed yielding a wide range of results [4]. A review of the literature by Gross and Bott [4] indicate that electrical efficiencies of 160% have been obtained in converting electrical energy to laser output energy with electrical initiation [5]. Output energies of 2500 J [6] have been demonstrated using electron-beam initiation. Current efforts in high-energy pulsed systems are directed toward achieving successful large-volume initiation of the laser medium. The electron beam is considered a prime candidate for accomplishing this objective because of its ability to deposit large amounts of energy uniformly over a large volume of the gas mixture.

Several theoretical models for the analysis of the H<sub>2</sub>+F<sub>2</sub> chemical laser have been developed. The assumption that lasing begins when gain reaches threshold and that gain equals loss during the lasing period have been used in the models developed by references [7,8,9,10]. The assumption of thermal equilibrium in the rotational population yields a rigid J-shifting pattern and multiline lasing in a given branch is minimal. The study of the role of rotational nonequilibrium mechanisms in HF lasers is a major part of this study.

### 1.1 Nonequilibrium Pumping

The nascent vibrational and rotational distributions for the cold pumping reaction Equation (1.1) and the hot pumping reaction Equation (1.2) have been measured by several workers [11,12,13,14,26,27]. Theoretically predicted distributions have also been determined [15,16,17,18,19,28,29].

#### 1.1.1 Cold Pumping

The nascent vibrational and rotational distribution for the cold pumping reaction has been measured by Polanyi and coworkers [11,12, 13,14]. Theoretically predicted distributions have also been determined using classical trajectory [15,16,17,18,19] and quantum mechanical methods [20]. The measured and calculated relative vibrational distributions of HF produced by the cold reaction are presented in Table 1.1.

The results of Polanyi and Woodall [11] using the arrested relaxation variation [21] of the infrared chemiluminescence (IRC) technique indicated that the mean fraction of available energy entering into vibration, <fv>, rotation, <fr> and translation, <ft> are 0.66, 0.08 and 0.26 respectively. The arrested relaxation method allows the nascent product distribution to be measured before relaxation becomes significant. The fraction of energy entering into rotation and vibration is far from the thermal equilibrium distribution at the translational temperature. The rotational energy distributions observed by Polanyi, et al. [11] for the vibrational levels pumped by the cold pumping reaction are compared with a 300°K thermal equilibrium rotational distribution in Figure 1.1.

Douglas and Polanyi [12] investigated the effect of rotationally excited H<sub>2</sub> on the vibrational and rotational distribution of HF.

Their work showed that rotationally excited H<sub>2</sub> has a small but noticeable effect on the nascent vibrational distribution and no observable effect on the nascent rotational distribution of HF. Perry and Polanyi [13] using the infrared chemiluminescence technique obtained the vibrational and rotational distribution of HF from 77K to 1315K.

Berry [14] has obtained vibrational distributions for the cold pumping

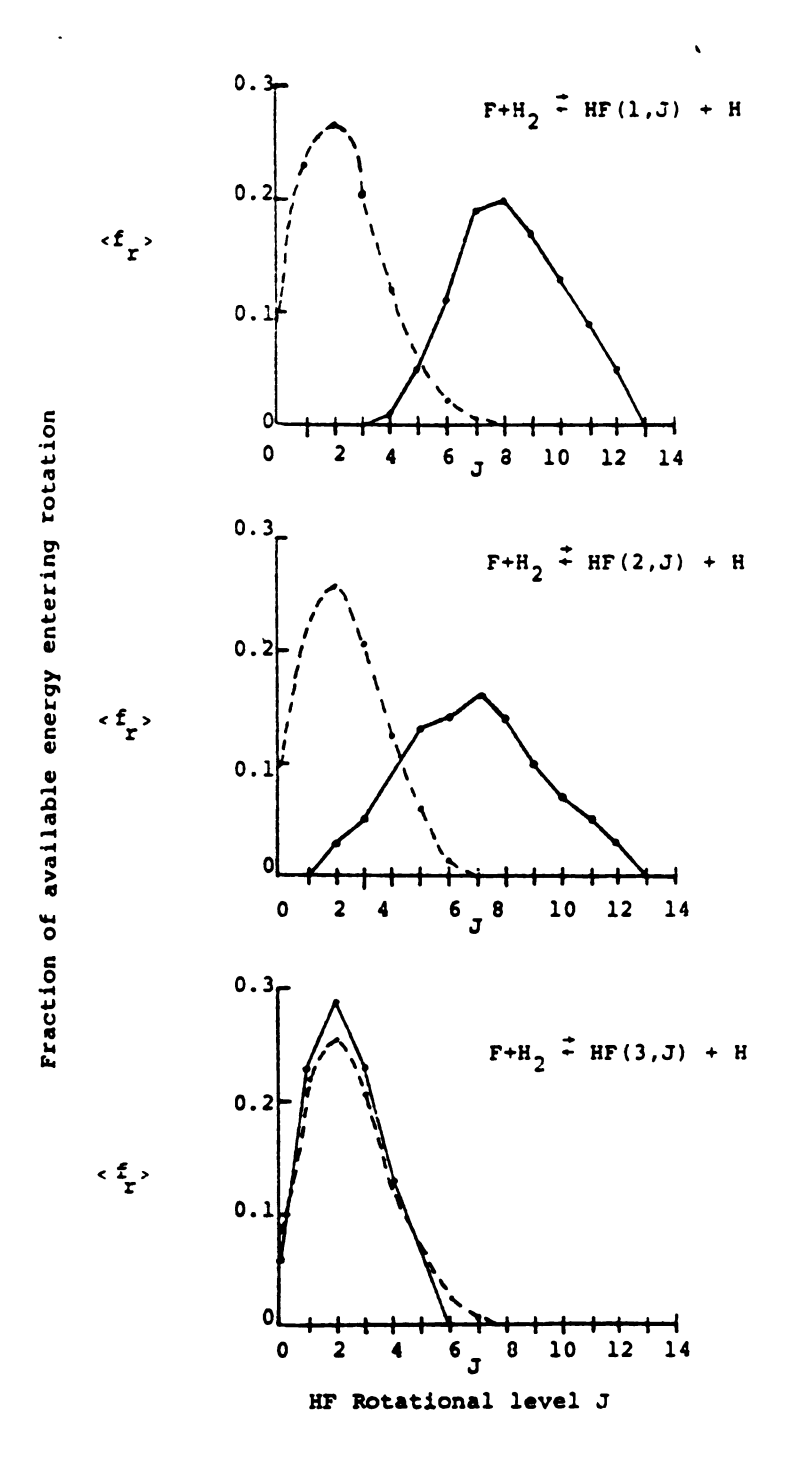
Table 1.1 Relative Pumping Efficiencies for  $F + H_2(0',J') \xrightarrow{K_f^c(v)} HF(v) + H^a$ 

J'	$J' \qquad f_v(0) \qquad f_v(1)$		f <sub>v</sub> (2)	f <sub>v</sub> (3)	Technique	Referenc	•
					Experimental		
0	-	0.6	0.4	-	Laser Experiment	Kompa	[22]
O	-	0.07	0.40	<0.53	Laser Experiment (534K)	Parker	[22]
9	-	0.23	0.77	-	Laser Experiment	Krough	[22]
0	0.03	0.15	0.50	0.32	Laser Experiment	Berry	[14]
0	-	0.16	0.57	×0.27	IRC	Polanyi	[22]
0	-	0.17	0.56	0.27	IRC	Anlauf	[22]
0	-	0.14	0.49	0.37	IRC	Jenathan	[22]
0	-	0.17	0.56	0.27	IRC	Jonathan	[22]
0	-	0.17	0.56	0.27	IRC	Polanyi	[11]
0	-	0.14	0.55	0.41	IRC	Douglas	[12]
1	-	0.17	0.56	0.27	IRC	Douglas	[12]
2	-	0.14	0.53	0.33	IRC	Douglas	[12]
ŋ	0.02	0.15	0.53	0.30	IRC	Perry	[13]
					<u>Theoretical</u>		
0	-	0.09	0.61	0.30	Semi-empirical Monte Carlo	Wilkins	[16]
0	-	0.15	0.67	0.18	Semi-classical Monte Carlo	Polanyi	[17]
1	-	0.31	0.58	0.11	Semi-classical Monte Carlo	Jaffe	[18]
0	-	0.561	0.438	0.001	Variation theory Monte Carlo	Jaffe	[22]
0	-	0.016	0.665	0.319	Information Theoretic Suprisal	Connor	[20]
0	0.001	0.006	0.483	0.510	Information Theoretic Suprisal	Connor	[20]
					Recommended		
0	0	0.17	0.55	0.28	******	Cohen [	22,23
0	0.07	0.15	0.52	0.26	Used in this article	Cohen	[24]

The forward vibrational pumping rate  $K_f^c(v)$  is given by  $K_f^c(v) = 1.6 \times 10^{14} \exp{(-2400/RT)}$  f<sub>v</sub>(v) cc/mol-sec.

 $<sup>^{5}</sup>$ The distribution was calculated assuming that the total available energy is 35.40 k cal/mol.

 $<sup>^{\</sup>rm c}$  The distribution was calculated assuming that the total available energy is 37.40 k csl/mol.



Pigure 1.1. Rotational distrubution for the cold pumping reaction.

The solid line is the distribution of Polanyi et al. [11] and the dashed line is a 300 K equilibrium rotational distribution.

reaction using a chemical laser technique which measures the time to threshold while minimizing the effects of vibrational deactivation. His results were in agreement with those of Polanyi, et al. [13].

Muckerman [17], Jaffe, et al. [18] and Polanyi, et al. [19] have calculated the nascent vibrational and rotational distribution of HF from three dimensional classical trajectory calculations. Connor, et al. [20] applied information theory to extract vibrational and rotational distributions of HF populated by the hot and cold pumping reaction. The product distribution obtained by Polanyi, et al. [19] and Connor, et al. [20] compared favorably with infrared chemiluminescence measurements. The classical trajectory and quantum mechanical calculations predict larger rotational energies than have been observed experimentally.

The vibrational distribution recommended by Cohen [22,23,23] will be used in a comprehensive model of the  $H_2+F_2$  pulsed chain reaction laser system. The reaction rate recommended by Cohen [22,23,24] for the cold reaction is:

$$K_f^c(v) = 1.6 \cdot 10^{14} \exp(-1600/RT) f_v(v) cc/mol-sec$$
 (1.3)

where R is in units of Kcal/mol-K. This recomendation concurs with the subsequent analysis of Cummings, et al. [25].

#### 1.1.2 Hot Pumping

The relative vibrational distribution for the hot pumping reaction has been measured and calculated using various methods. Results of these calculations are listed in Table 1.2.

Polanyi and Sloan [26] have investigated the product vibrational and rotational distribution for the hot reaction (1.2) and found that the mean fraction of energy entering into vibration, rotation and

Table 1.2. Relative Pumping Efficiencies for  $\mathrm{H}^{\mathrm{R}}_{2}$  . Relative Pumping Efficiencies for  $\mathrm{H}^{\mathrm{R}}_{2}$ 

1	[22]	[22]	[7]	[27]	[97]	[36]	[36]		[53]	28]	[20]		,23]	_
Reference	Jonathan [22]	Jonathan [22]	Jonathan [7]	Jonathen [27]	Polanyi	Polanyi	Polanyi		Wilkins [	Polanyi [28]	Connor		Cohen [22,23]	Cohen [24]
Pe.	-4	Jon	Jon	Top.	Pol	Pol	Pol						8	8
f <sub>v</sub> (10) Technique	Experimental	IRC	IRC	IRC	IRC	. IRC <sup>b</sup>	IRC	Theoretical	3D classical Monte Carlo	3D classical Monte Carlo	Information Theoretic Suprisal	Recommended	1	used in this study
f (10)	ı	•	0.012	0.004	1	1	1		1	1	ı			•
f <sub>v</sub> (9)	1	•	0.012	0.004	0.045	0.017	ı		ı	1	ı	•	1	•
f <sub>v</sub> (8)	•	ı	0.059	0.03	0.073	0.028	•		ı	ı	1		•	0.02
f,(7)	•	<0.0>	0.13	0.046	0.113	9.70	ı		ı	0.15	0.003		•	0.05
f <sub>v</sub> (5) f <sub>v</sub> (6)	0.26	0.23	0.29	0.40	0.28	0.35	0.43		0.25	0.45	0.218		0.44	0.40
f <sub>v</sub> (5)	0.28	0.24	0.26	0.30	0.22	0.28	0.35		0.43	0.30	0.287		0.35	0.30
f <sub>v</sub> (4)	0.18	0.17	0.13	0.134	0.10	0.11	0.14		0.23	0.00	0.346		0.13	0.13
f <sub>v</sub> (3)	0.14	0.14	0.038	0.030	0.000	0.062	0.0		0.10	0.01	0.135		90.0	0.03
f <sub>v</sub> (2)	0.08	0.0	0.032	0.029	0.037	0.038			ı	ı	0.010		•	0.03
f,(1)	90.0	0.03	0.026	0.021	0.034	0.03	•		1	ı	ı		1	0.02
<b>(</b> 0)	1	ı	0.012	0.00	<0.03	0.025	•		ı	1 .	ı		•	0.01

The forward vibrational pumping rate  $K_{\tilde{f}}^h(v)$  is given by  $K_{\tilde{f}}^h(v) = 1.2 \times 10^{14}$  exp(-2400/RT)  $f_{\psi}(v)$  cc/mol-sec.

<sup>\*</sup>Corrected for Einstein transition probability [20]

The fraction of available energy in vibrational v was obtained by neglecting vibrational levels outside of the v=3-6 manifold.

translation were 0.53, 0.03 and 0.44 respectively. The rotational distribution of HF for the hot reaction is presented in Figure 1.2. The vibrational distribution of the constants measured by Jonathan, et al. [27] compared favorably with those obtained by Polanyi, et al. [26] using the arrested relaxation method.

The three dimensional Monte Carlo classical trajectory calculations of Polanyi [28] and Wilkins [29] and the quantum mechanical results of Connor [20] yield vibrational and rotational energy distributions which are compared in Table 1.2 to observations of Polanyi [26], Jonathon [27] and others [22].

In a comprehensive review of the literature, Cohen [22] suggests that HF is not formed by the hot pumping reaction for vibrational levels less than three or vibrational levels greater than five. This conclusion is based upon the classical Monte Carlo trajectory calculations of Wilkins [29]. The experimental results of Polanyi and Sloan [26] were renormalized so that vibrational levels outside of the v=3 to 6 manifold are neglected,

$$\sum_{\mathbf{v}} \langle \mathbf{f}_{\mathbf{v}}(\mathbf{v}) \rangle = 1 \tag{1.4}$$

giving the values listed in Table 1.2 which are recommended by Cohen [22,23]. Subsequent analysis by Cummings, et al. [25] supports the recommendation of Cohen [22,23]. It is assumed that the forward rate coefficient for the hot pumping reaction measured by Albright [30] and recommended by Cohen [22,23,24] and Cummings, et al. [25] is:

$$K_f^h(v) = 1.2 \times 10^{14} \exp (-2400/RT) f_v(v) cc/mole-sec$$
 (1.5)

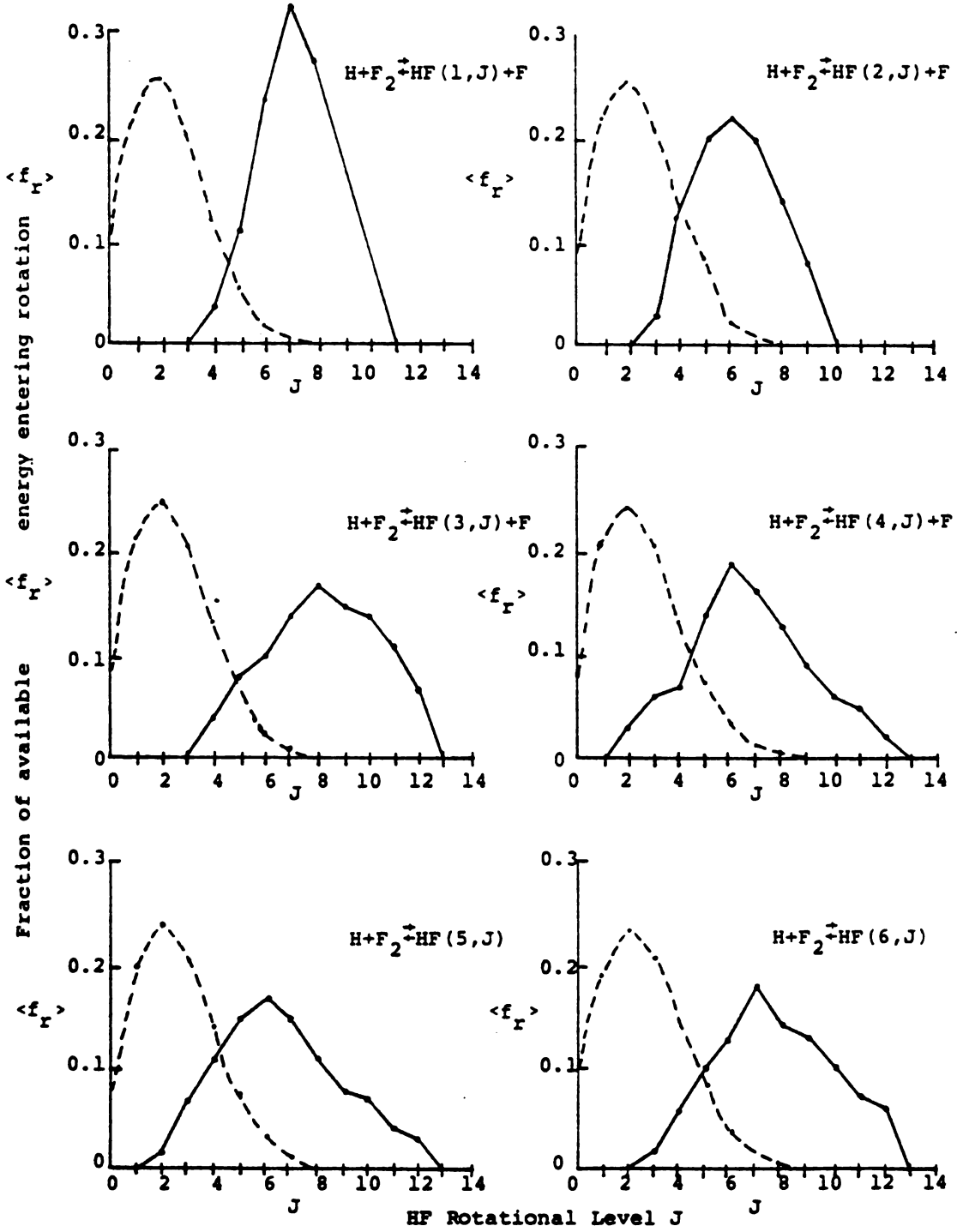


Figure 1.2. Rotational distribution for the hot pumping reaction. The solid line is the distribution of Polanyi, et. al. [26] and the dashed line is a 300 K equilibrium rotational distribution.

#### 1.2 Rotational Population Transfer

#### 1.2.1 Experimental Studies

Once the HF molecule is formed in a vibrationally and rotationally excited state, rotational relaxation may occur. The rate of rotational population transfer from a given vibrational and rotational level has been measured by Polanyi, et al. [31,32], Hinchen and Hobbs [33,34], Peterson, et al. [35], Vasilev, et al. [36], Gur'ev [37] and Emanuel [38]. Polanyi and Woodall [31] used the infrared chemiluminescence method to observe the rotational distribution of HCl pumped by the hot reaction (1.2) with Cl<sub>2</sub> replacing F<sub>2</sub>. Polanyi, et al. [31] determined that the empirical formula for the rate of rotational relaxation out of a given rotational level is of the form

$$K_{J,J-\Delta J} = P_r Z_{HF-M} e^{-B\Delta E/kT} = \frac{1}{\tau_r P}$$
 (1.6)

where  $P_r$  is the probability of rotational relaxation, and  $Z_{HF-M}$  is the binary collision frequency for unit concentration of HF with M. The gas pressure is P and  $\tau_r$  is the rotational relaxation time constant. When rotational relaxation occurs the rotational quantum number J undergoes a change from J to  $J-\Delta J$ . The change in energy  $\Delta E$  due to rotational relaxation is

$$\Delta E = E(v,J) - E(v,J-\Delta J) . \qquad (1.7)$$

The rotational energy in vibrational level v is denoted as E(v,J). The parametric constant B approximates the decrease in transition probability with increasing  $\Delta J$ . For  $\Delta J = \pm 1$  Polanyi [31] determined that B was 0.016. Ding and Polanyi [32], using a heated supersonic primary beam of HCl or HF and a target beam containing He, Ar, Kr,

 $HX(X\equiv F, Cl, Br, I)$ ,  $H_2S$  or propane, examined the infrared emission from colliding molecular beams. Ding, et al. [32] observed that the parametric constant B was also a function of collision energy. Emanuel [38] investigated the sensitivity of temperature and gas non-uniformities in chemiluminescent experiments and concluded that these nonuniformities can have a significant impact on the observed rotational distributions. Vasil'ev, et al. [36] studied rotational relaxation of HF with  $H_2$ ,  $D_2$ , He and Xe. Their results indicated that  $H_2$  and  $D_2$  depleted the rotational levels of HF, through a resonant transfer of rotational energy an order of magnitude more rapidly than He or Xe.

Gur'ev, et al. [37] obtained rate coefficients for rotational relaxation of HF(v=0, J=8) by several chaperon gases by monitoring the relaxation losses that occur when light is passed through a resonantly absorbing medium. Their rate coefficients for rotational relaxation of HF(v=0, J=8) by a chaperon M correspond to relative rotational relaxation efficiencies of 1.0 for M=HF, 0.03 for M=H<sub>2</sub> or D<sub>2</sub> and less than 0.005 for M=He, Ar, Kr or Xe.

Peterson, et al. [35] obtained rotational relaxation rates of HF from specific vibrational and rotational levels by using a pump laser to populate a particular level of HF and then observing an exponential decay out of that level with a probe laser. They assumed that the rotational relaxation rate is related to the collisional linewidth  $\gamma_{\rm L}$  of HF by

$$\tau_{r} = \frac{1}{2\pi c \gamma_{L}} \tag{1.8}$$

where c is the velocity of light in vacuum and  $\gamma_L$  is in cm<sup>-1</sup>. The relaxation time  $\tau_r$  was obtained by Peterson, et al. [39] by conducting high resolution linewidth measurements of HF.

Hinchen and Hobbs [33,34] observed rotational relaxation effects in HF using infrared double resonance. This technique employed a pulsed pump laser to populate a particular vibrational and rotational level of HF and a continuous wave probe laser to monitor the rotational relaxation of HF to adjacent HF levels. The relative rotational relaxation efficiencies for HF, H<sub>2</sub> and He were found by Hinchen, et al. [33] to be 1.0, 0.1 and 0.03 respectively. Specific relaxation rates for HF indicated that a mechanism, in addition to rotational relaxation, was preferentially transferring population to a lower level ( $\Delta J=1,2,3,etc.$ ). This additional mechanism was observed by Hinchen [33,34] to be lasing between adjacent rotational levels.

#### 1.2.2 Rotational Lasing

Deutsch [40] observed laser action on pure rotational bands of HF produced by a pulsed electrical discharge in a mixture containing CF<sub>4</sub> and H<sub>2</sub>. Table 1.3 contains a list of rotational lasing transitions that have been observed by Deutsch [40], Sirken, et al. [41], Krogh, et al. [42], Skribanowitz, et al. [43], Chen, et al. [44], Hinchen [33,34], Akitt, et al. [45], Cueller, et al. [46] and Rice [47]. Rotational lasing occurs by the following mechanism

$$Hf(v,J+1) + h\frac{c}{\lambda} + HF(v,J) + 2 h\frac{c}{\lambda}$$
 (1.9)

where observed values of  $\,\lambda\,$  range from 12 microns to more than 100 microns. Overtone rotational lasing has not been observed.

Table 1.3. Observed HF rotational laser transitions

Wavelength	$W_{c\underline{R}_1}(v,J)$	(v:J·	+1 <b>+</b> J)	Reference
Micron	cm_T	v	J	
9.381	1065.0	0	31	41
9.960	1004.0	1	30	44
12.262	815.53	1	22	40,45,47
12.767	783.27	2	22	47
13.303	751.71	3	22	47
13.726	728.54	2	20	40,47
13.730	728.33	1	19	40,47
13.774	726.01	3	21	47
13.785	725.43	0	18	40,47
14.336	697.54	1	18	47
14.441	692.47	0	17	40,46,47
15.017	665.91	1	17	40,47
15.624	660.04	2	17	47
15.785	633.51	1	16	47
16.021	624.18	0	15	40,47
16.422	608.94	2	16	45,47
16.657	603.61	1	15	45,47
16.981	588.89	0	14	45,47
17.328	577.10	2	15	45,47
17.654	566.44	1	14	45,47
18.086	552.91	0	13	45,46,47
18.801	531.89	1	13	40,46,47
19.369	516.29	0	12	46,47
36.475	274.16	1	6	33,43
42.432	235.67	1	5	33,43
50.800	196.85	1	4	33,43
63.383	157.77	1	3	33,43
84.388	118.50	1	2	33,43
126.41	79.107	1	1	33,43

Sirken, et al. [41] observed laser emission between high rotational states of HF by the photolysis of halogenated olefins ( ${
m CH}_2{-}{
m CF}_2$ ,  ${
m CHF-CH}_2$ etc.). Rotational lasing from levels as high as  $\mbox{HF}(v=0,J=31)$  and HF(v=1,J=30) were observed. Similar results were observed by Krogh [42] using ClF<sub>y</sub>-F<sub>2</sub>. Skribanowitz, et al. [43] and Hinchen, et al. [33,34] observed rotational lasing by using a pump laser to populate the upper level of the rotational lasing transition. Skribanowitz [43] used a helical transverse discharge HF pin laser with a mixture of  $SF_6$  and  $H_2$  as a pump laser. The sample cell used a ring laser cavity configuration allowing the gain to be monitored in the same or opposite direction that the light from the pump laser entered. Pressures in the sample cell ranged from 50 millitorr for the  $P_1(3)$  and  $P_1(4)$  pump lines to 6 torr for the  $P_1(8)$  pump line. The variation in cell pressure compensates for the changing absorption coefficient of HF. Skribanowitz [43] estimates that under certain conditions the incremental gain for rotational lasing to be in excess of 1 cm<sup>-1</sup>. Using an infrared double resonance experiment utilizing a separate HF pump and probe laser Hinchen, et al. [33,34] observed the same transitions as Skribanowitz [43]. The gain at pressures from 0.007 torr to 0.85 torr ranged from 0.02 cm<sup>-1</sup> to a maximum of 1.15 cm<sup>-1</sup> for the HF(1,3) to HF(1,2) transition at 0.17 torr. The gain expression for rotational lasing is given in Appendix B. The large gain for single quanta rotational lasing effectively blocks rotational lasing for AJ larger than 1. Chen, et al. [44], in an atmospheric pulsed HF laser, observed indirect evidence of rotational lasing. Their method of observation involved placing black polyetheylene which absorbs light with a wavelength less than 15 microns over an energy meter. Chen, et al. [44],

observed that approximately 10% of the total energy of 1.5 joules was transmitted through the polyetheylene. Akitt, et al. [45] observed laser emission at 16 wavelengths between 11 and 18 microns in a pulsed discharge containing  $FB_3$ .  $N_2$  and  $H_20$  were found to decrease the lasing energy while He increased the total emission energy by a factor of 4. Cuellar, et al. [46] observed laser emission from rotational transitions of HF formed through chemically activated  $CH_3CF_3$  and from photo-excited  $CH_2CF_2$ . Rice, et al. [47] observed rotational lasing by exploding wires in  $F_2$  and an inert gas mixture at pressures up to 500 torr.

There is clear experimental evidence that rotational lasing can and does occur. Lasing can occur from very high rotational levels indicating a nonequilibrium rotational distribution that is well above what would be expected from pumping. One mechanism that can populate high rotational levels is vibrational to rotational energy transfer.

#### 1.2.3 Theoretical Studies

Sentman [48] developed a computer model to determine  $P_r Z_{HF-M}$  and B in Equation (1.3) and found that for rotational relaxation of HF by HF to be  $P_r Z_{HF-HF}$ =2.45 and B=0.359. Sentman [48] found that  $P_r Z_{HF-HF}$  and B determined from Hinchen's [34] experiment were comparable to those obtained from Polanyi and Woodall's [31] data.

The rotational relaxation of polar gases such as HF was investigated by Zeleznik [49] using two dimensional classical dynamics to investigate the rotational relaxation of polar molecules. Zeleznik [49] found that the change in rotational energy per collision averaged over the number of collisions per unit time can be expressed as

$$\frac{d \text{ HF(v,J)}}{dt} = \frac{\text{HF(v) Boltz(v,J) - HF(v,J)}}{\tau_r}$$
 (1.10)

where  $\mathrm{HF}(v,J)$  represents the hydrogen fluoride and  $\tau_{\Gamma}$  corresponds to the mean time for rotational relaxation, and  $\mathrm{HF}(v)$  represents the total rotational population of a specific vibrational level of  $\mathrm{HF}$ . Boltz (v,J) is the Boltzman distribution for the rotational populations at the translational temperature T and is given by

Boltz (v,J) = 
$$\frac{2J+1}{Q_v^r(T)}$$
 e<sup>-hcE(v,J)/kT</sup> (1.11)

where the value of the rotational partition function  $Q_{\mathbf{v}}^{\mathbf{r}}(\mathbf{T})$  may be taken from the data given in reference [7] and  $\mathbf{E}(\mathbf{v},\mathbf{J})$  is the rotational energy calculated from Dunham coefficients [50].

From three dimensional trajectory calculations Wilkins [51,52] obtained detailed rate coefficients for rotational to rotational (RR) and rotational to translational (RT) energy transfer. Wilkins [51,52] found that the rate coefficients for de-excitation from the upper rotational levels were much smaller than rate coefficients for de-excitation from the lower rotational levels in agreement with the exponential dependence of the energy defect in Equation (1.6), the anharmicity of the energy levels of HF, and observations of Polanyi and coworkers [31,32]. The rotational transition probabilities calculated by Wilkins [51]  $\Delta J=1,2$ , and 3 are presented in Figure 1.3. The probabilities for rotational relaxation with J greater than 15 were extrapolated from the probabilities between J=10 and J=15. The extrapolation technique was a mean square regression fit to an exponential curve.

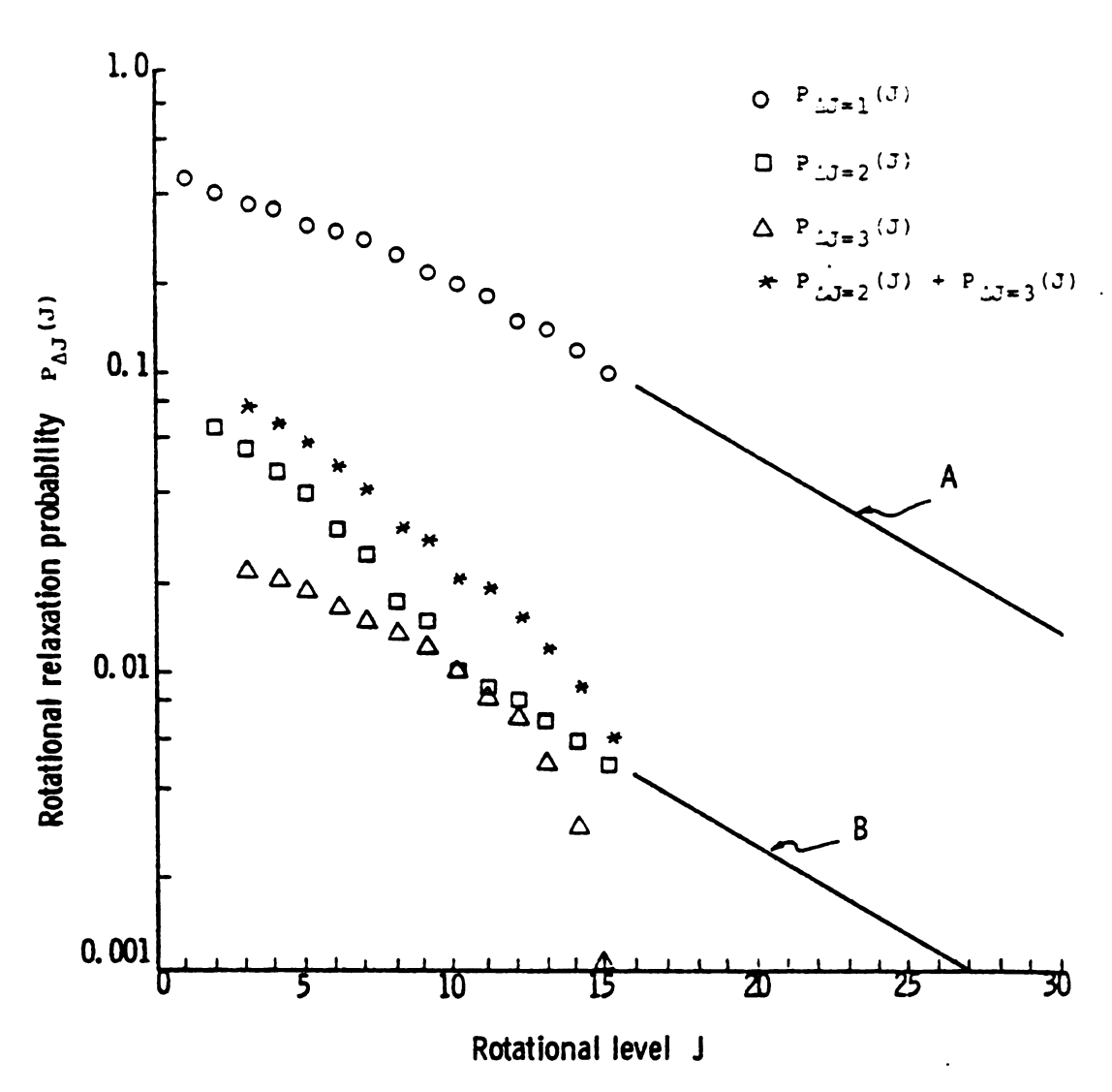


Figure 1.3. Calculated rotational transition probabilities versus rotational level [51]. The equation for line A is 0.788 exp(-0.1357 J). The equation for line B is 0.0406 exp(-0.1376 J).

A small rotational relaxation probability at high rotational levels is consistent with observations of rotational lasing at high J levels.

#### 1.3 Vibrational Relaxation of HF

The vibrational relaxation of HF may be expressed by vibrational to rotational, translational energy transfer (VR,T) and vibrational to vibrational energy transfer (VV) reaction

$$HF(v,J) + M + HF(v',J') + M + \Delta E$$
 (1.12)

$$HF(v, J_1) + HF(v_J^*J_2) \neq HF(v-1,J_1') + HF(v_J^*+1,J_2') + \Delta E$$
 (1.13)

where M is a collision partner and  $\Delta E$  is the energy defect. Until very recently, the interpretation of experiments reported in the literature usually assumed that rotational levels J and J' are in thermal equilibrium at the translational temperature with the energy defect being released to the thermal bath [4]. This interpretation results in energy defects of several thousand cm<sup>-1</sup> for Reaction (1.12). The recent results of Wilkins [51,52] and others [34] suggest that Reaction (1.12) occurs by a near resonant multiquanta VR process where the resultant HF(v',J') loses one or more quanta of vibrational energy with the excess energy going into rotation. The "optimum" value of J' is obtained by minimizing the energy defect

$$\Delta E = Minimum \left[ E_{total}(v,J) - E_{total}(v',J') \right]$$
 (1.14)

where  $E_{total}(v,J)$  and  $E_{total}(v',J')$  are the sum of the vibrational and rotational energy of HF(v,J) and HF(v',J'), respectively. A

typical multiquanta VR reaction path is shown in Figure 1.4. The values of v', J' and  $\Delta E$  are given in Table D.1 for the range of v and J of interest in HF chemical lasers. The first column contains the rotational level J associated with the upper vibrational level v. The rotational level  $J_{max}$  that yields a minimum energy defect given v, J and v' is found in columns 3, 5, 7, 9, 11, and 13. The energy defect associated with a given multiquanta VR reaction is found in columns 4, 6, 8, 10, 12, and 14. The energy defect is quite small even when there are large changes in vibrational quanta, indicative that the multiquanta VR rates are near resonant.

It has usually been assumed that Reaction (1.13) occurs through intermolecular VV energy exchange while neglecting rotational energy resulting in an energy defect of several hundred cm $^{-1}$  [7]. The recent results of Wilkins [51, 52] suggests that rotational energy levels should be included in Reaction (1.13) and that  $J_1$  and  $J_1'$  are equal and  $J_2$  and  $J_2'$  are equal. The energy defect for Reaction (1.13) is typically one hundred cm $^{-1}$  indicating a near resonant VV process. A typical VV reaction path is shown in Figure 1.5.

#### 1.3.1 Theoretical Investigations of VR Relaxation

The role of vibrational to rotational energy transfer in diatomic-diatomic or diatomic-atomic collisions has been investigated by many researchers. The role of rotational motion in the deactivation of vibrationally excited diatomic molecules by collision with an atom has been investigated by Kelly [53]. His theory is based upon the solution of the two dimensional classical equations of motion, for an initially vibrating rotationless oscillator bound by a Morse potential, colliding with a particle of mass m. The importance of VR energy transfer was

$$HF(v,J) + M \stackrel{+}{\leftarrow} HF(v',J') + M$$

Energy of HF(v,J)

Energy of HF(v',J')

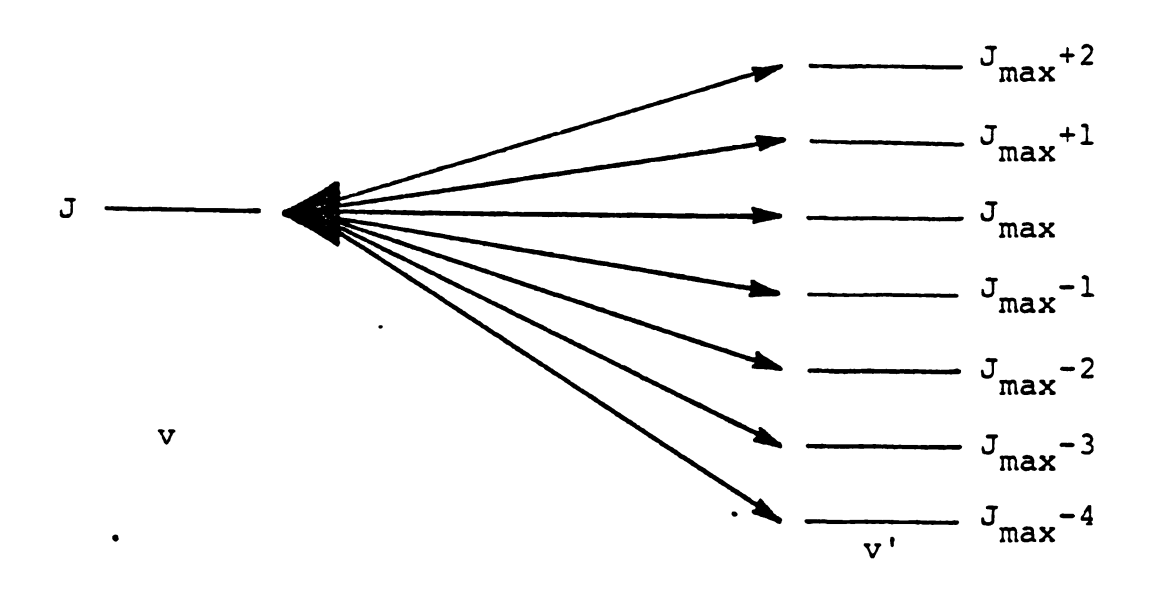


Figure 1.4. A typical VR relaxation path.

Multiquanta vibrational relaxation is allowed. The values of J' range from J<sub>max</sub>-4 to J<sub>max</sub>+2 where

J<sub>max</sub> is the value of J' with smallest energy defect.

$$HF(v,J_1) + HF(v^*,J_2) HF(v-1,J_1^*) + HF(v^*+1,J_2^*)$$

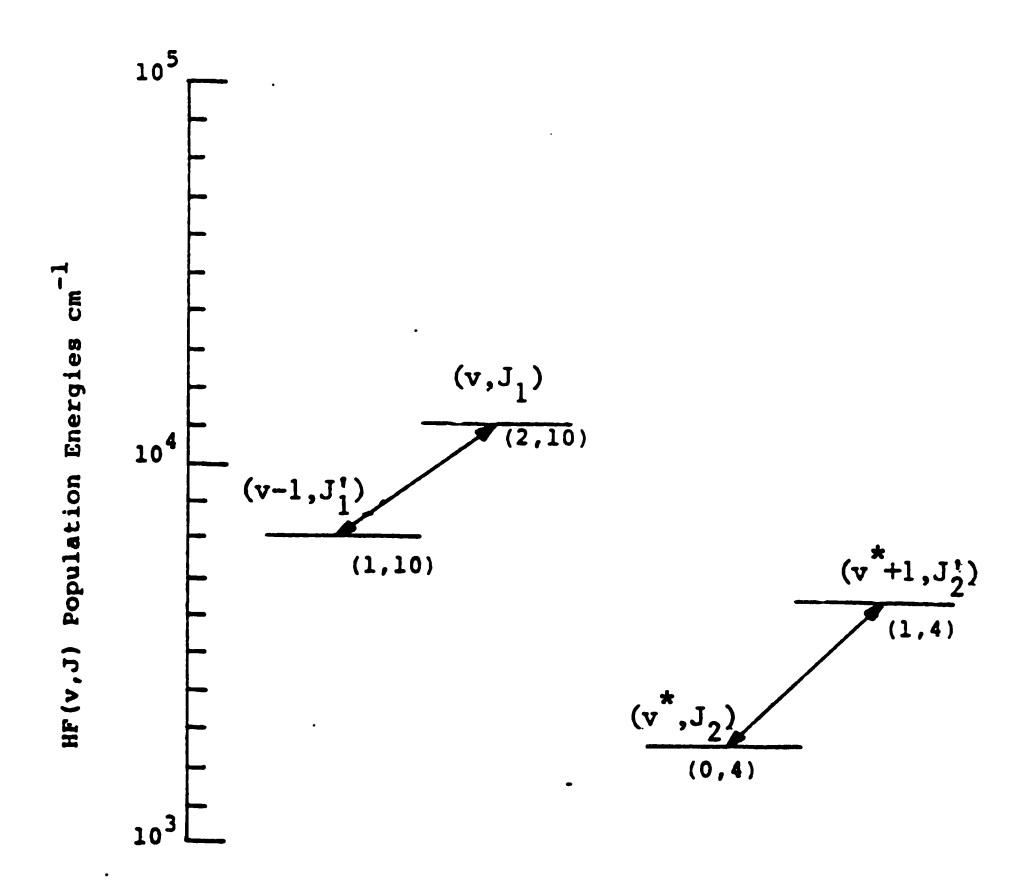


Figure 1.5 Schematic of a typical VV reaction path. The specific reaction shown is  $HF(2,10) + HF(0,4) \stackrel{+}{\rightarrow} HF(1,10) + HF(1,4) + 102.8 cm^{-1}$  If zero rotational energy is assumed then  $\Delta E=171.2$  cm<sup>-1</sup>.

found by Kelly [53] to increase with m, indicating the intramolecular VR processes should be important in HF. The role of near resonant VR energy transfer in BCl, diatomic collisions have been investigated by Poulsen et al. [54] and Frankel et al. [55]. The model of Poulsen et al. [54] accounted for near resonant transitions between a quantized oscillator (BCl $_3$ ) and a quantized rotor (HCl, DCl, H $_2$ , O $_2$ ). Further refinement of the theory of Poulsen et al. [54] by Frankel et al. [55] indicated that attractive long range forces were necessary for BCl3 deactivation rates to compare reasonably with infrared double resonance experiments [54] at temperatures above 300°K. Poulsen [54] noted that his theory was most useful for systems in which a small quantum of vibrational energy is relaxed by a hydrogen containing species where the vibrational and rotational quanta are comparable. A fully quantum mechanical 'coupled states' approximation was used by McGuire and Toennies [56] to be a dominant process in He-H, relaxation even though the rotational coupling for this system is weak. Multiquanta rotational and vibrational relaxation processes were found by Dillon and Stephenson [57] to be important when transition moments are large as in the case for collisions involving HF. Infrared chemiluminescence experiments conducted by Nazar et al. [67] with highly excited rotational levels in hydrides suggest that relaxation occurs through a resonant VR process. This cascading process involves near resonant vibrational exchange in which the vibrationally excited hydride is vibrationally deactivated with retention of its initial rotational quantum number. The quantum mechanical theory of Dillon and Stephenson [57] indicates that multiquantum rotational transitions play an important role in vibrational

energy exchange involving diatomic-diatomic collisions by allowing the vibrational energy defect to be absorbed by the rotational energy levels.

A one-dimensional analytical model which includes the effects of dipole-dipole and hydrogen-bond interactions has been formulated by Shin [58,59] to explain the efficient vibrational deactivation of HF at low temperatures. For HF-HF collisions Shin [58,59] predicted that VR energy transfer was more efficient than VT energy transfer. The results of Shin [58,59] compare favorably with experimental data over a wide range of temperatures. Shin noted that as a result of the strong dipole-dipole attractive forces the HF molecules attract each other at large distances even when each molecule is rotating rapidly and this attractive force between HF molecules would tend to form an HF dimer intermediary at low temperatures.

The 3-dimensional classical trajectory calculations of Wilkins [51] provide for the first time detailed rate coefficients for multiquantum VR, VV and rotational relaxation for reactions involving HF with HF. The potential that Wilkins [51] employed for HF-HF interactions is a combination of two functions, a London-Eyring-Polanyi-Sato (LEPS) potential energy function for short range interactions and a point-charge dipole-dipole potential energy function for long range interactions between the four atoms. The energy surface is capable of supporting the HF dimer concept which has been suggested as being responsible for the efficient VV energy transfer in the experiment of Airey and Fried [60]. The fast self-relaxation rates of HF measured by Airey and Fried [60] in their opinion are not the result of dimer formation. At the pressures and temperature of their experiment less

Table 1.4. Multiquanta VR Rates of Wilkins [51]  $HF(v,J) + M \stackrel{+}{\leftarrow} HF(v',J') + M^a$ 

v	Total	0	1	2	3	4	5	6	7
1	30±3.0	30.		•					
2	39±3.1	15.	24.						
3	43±3.2	11.	17.	15.					
4	49.8±3.2	9.9	8.9	14.	17.				
5	53.6±3.2	9.4	7.1	11.	7.1	19.			
6	58.0±3.0	8.5	5.6	8.5	7.5	8.9	18.0		
7	60.6 <sup>b</sup>	7.6	7.6	7.6	7.6	7.6	7.6	15.	
8	63.6 <sup>b</sup>	7.0	7.0	7.0	7.0	7.0	7.0	7.0	14.6

<sup>&</sup>lt;sup>a</sup>The forward VR rates in this table should be multiplied by  $10^{12}(\frac{T}{300})^{0.5}$ 

<sup>&</sup>lt;sup>b</sup>The values for v=7.8 were obtained from a least squares power fit to the total rates from v=1 to 6 of the form  $29.89v^{0.363}$ 

than 0.001% of the HF exists as dimers. Thompson [67] points out that this view is correct if it is assumed that vibrational relaxation occurs between an excited HF molecule and the dimer, but it is not necessarily true if the effective intermediate is a long-lived complex. If a longlived complex is formed then the vibrational relaxation rates are critically dependent on the rate of formation and dissociation of the dimer.

The following qualitative results were noted by Wilkins [51]: (1) HF dimers are not formed in the typical HF-HF collision in the tempera-(2) The vibrational energy of the ture range at or above 300°K. vibrationally excited incident HF molecule is transferred into rotational energy of the same HF molecule implying that there is little or no change in the internal energy of the target HF molecule. This result allows the HF-M rates to be inferred from Wilkins [51] HF-HF rates based upon previously measured or calculated HF-M VT rates. Similar results were obtained for HF-DF trajectory calculations of Wilkins [52]. (3) Very high rotational states of the incident HF molecules are popu-

- lated by single and multiple quanta VR reactions listed in Table D.1.
- (4) The energy defect for these multiquantum VR reactions are much less than the energy defect for the corresponding multiquantum VT reaction where the energy defect is given up to the thermal bath.

The rate coefficients for vibrational to rotational energy transfer process

$$HF(v,J_1) + HF(0,J_2) \neq HF(v',J_1') + HF(0,J_2')$$
 (1.15)

calculated by Wilkins [51] are presented in Table 1.4. For vibrational energy levels greater than 6 a least squares fit of the form

$$Av^{n} = 29.89v^{0.36}$$
 (1.16)

was obtained for the vibrational dependence of this rate based upon the overall rate coefficient. The resultant total rate was then converted to a multiquanta rate with the single quantum rate twice the multiquantum rates.

## 1.3.2 Theoretical Investigations of VV Relaxation

Theoretical calculations of VV exchange rates for HF-HF collisions were conducted by Shin and Kim [61] and Wilkins [51]. The one dimensional arrested rotational relaxation model used by Shin and Kim [61] gives VV rates for the temperature range of 200°K to 2000°K. The transfer of energy was assumed by Shin and Kim [61] to occur through the formation of non-rigid dimers at low temperatures (T<300°K) and through the rotational motion of the colliding molecules at temperatures above 300°K. In the non-rigid dimer model the energy defect in Reaction (1.13) is transferred to the restricted translational motion of individual molecules of the dimer. At temperatures above 300°K the energy defect is transferred to the rapid rotational motion of the colliding molecules. Shin and Kim's model confirmed previous predictions that two quantum VV processes HF(v) + HF(0) + HF(v-2) + HF(2) have very low probability. Their theory does not indicate the mechanism by which vibrational energy is converted to rotational energy and it does not include multiquantum VR processes. The VV rate coefficients for v = 2 to 5 and v' = 0 have been calculated by Wilkins [51] and measured by Kwok and Wilkins [62], Airey and Smith [63], and Osgood et al. [64] are compared in Table 1.5. In the analysis of vibrational relaxation data a v<sup>2.3</sup> dependence on the VR.T is assumed.

Table 1.5. Vibrational to Vibrational rate coefficients in  $10^{12}$  cc/mol-sec at 300°K for HF(v-1) + HF(v'=1) - HF(v) + HF(v'=0)

v	Wilkins forward r	[51] everse	Shin, Kim [61]	Kwok, Wilkins [62]	Airey, Smith	Osgood et <sub>a</sub> al. [64]
2	8.5±1.9		8.5	5.0	6.1	11.0
3	5.2±1.4	7.8±1.8	9.8	3.2	b	18.4
4	3.3±1.2	5.0±1.4	10.		>7.7	3.7
5	1.9±0.9	2.8±1.2	2.3		>7.5	
6	1.2±0.7	1.7±0.9	)			

 $<sup>^{</sup>a}$ The VV rate was extracted from the total vibrational relaxation rate by assuming a  $v^{2\cdot3}$  dependence for the contribution due to VR,T

 $<sup>^{\</sup>text{b}}$ Subtracting the  $v^{2\cdot 3}$  contribution due to VR.T resulted in a negative rate.

The three dimensional trajectory calculations of Wilkins [51] predict that the formation of a dimer is not necessary to account for VV processes. The VV rate coefficients calculated by Wilkins [51] and presented in Table 1.6 indicate that the VR rates in Table 1.4 are larger than VV rates.

In order to interpret the experimentally determined rate coefficients for the deactivation of HF by HF the effects of VR,T (Reaction 1.12) and VV (Reaction 1.3) must be uncoupled. There is very little data available except for systems involving v = 1 single quantum transitions and only a linear v dependence of VR,T rates. A vibrational dependence of  $v^{2.3}$  has been suggested by Kwok and Wilkins [62] based upon flow tube studies. The vibrational dependence due to VR,T is summarized in Table 1.7. The experimental data of Kwok [62], Osgood [64], and Airey [63] are compared with the theoretical data of Shin [59] and Wilkins [51] in Table 1.5 assuming a  $v^{2.3}$  dependence. A linear v dependence for VR,T in interpreting experimental data to deduce VV rate coefficients for HF(v) + HF(1) + HF(v+1) + HF(0) results in a rate coefficient larger than gas kinetic.

The lack of direct experimental confirmation of the findings of Wilkins [51] indicates a need for experimental study of multiquanta VR reactions, VV reactions and rotational relaxation processes under well defined conditions..

One of the goals of the present effort is to assess the effect of VR processes on laser performance. This goal may be achieved in part through the introduction of mechanisms for VR, VV and rotational relaxation with rotational and P branch lasing in a comprehensive computer model. Time resolved spectroscopy of pulsed  $H_2+F_2$  lasers and computer

Table 1.6 Single Quanta VV Rates of Wilkins [51]  $HF(v,J_1) + HF(v*,J_2) \stackrel{?}{\rightarrow} HF(v-1,J_1') + HF(v*+1,J_2')^a$ 

v* 1	2	3	4	5	6	7
1 12.0	7.8	5.0	2.8	1.7	0.85	0.42
2	6.6	3.3	1.65	0.825	0.413	0.207
3		3.9	1.95	0.975	0.488	0.244
4			2.3	1.15	0.575	0.289
5				1.2	0.6	0.3
6					0.7	0.35

<sup>&</sup>lt;sup>a</sup>The forward rates in this table should be multiplied by  $10^{12} \left(\frac{T}{300}\right)^{0.5}$ .

<sup>&</sup>lt;sup>b</sup>The values for v = 6 and v = 7 were obtained by assuming a vibrational dependence of  $2^{v-v}$ .

Table 1.7 Vibrational dependence of the total VR,T rate coefficient

Single or Multiquanta	g <sup>v</sup> (1)	g <sup>v</sup> (2)	<b>g</b> <sup>V</sup> (3)	g <sup>v</sup> (4)	<b>g</b> <sup>V</sup> (5)	g <sup>v</sup> (6)	g <sup>v</sup> (7)	g v(8)	g'(3) $g'(4)$ $g'(5)$ $g'(6)$ $g'(7)$ $g'(8)$ v dependence Reference	Reference
single	-	7	æ	4	<b>~</b>	9	7	<b>©</b>	>	Harmonic Oscillator
single	1	<b>&amp;</b>	28	25	2	S	٠	<b>S</b>	t	Cohen [22]
Bultí	1	9	6	12 b 17	30	20	1	ı	1	Cohen [23]
multi		6.4	12.5	24.3	40.5	61.6	87.8	119.4	v <sup>2.3</sup>	Kwok [62]
multi	1	1.3	1.4	1.7	1.8	1.9	2 <sup>a</sup>	2.1 <sup>8</sup>	vv 0.363	Wilkins [51]
multí	1	4	6	6	\$	3	1.5	ı	ı	Cummangs [25

 $^{
m a}$ These values were obtained from a least squares power fit to the total v rates for v=1 to 6. bow otbrational dependences for the v=3 and 4 rate coefficient were obtained by Cohen [23]

models incorporating rotational nonequilibrium effects are discussed in the next section.

# 2. STUDIES OF ROTATIONAL NONEQUILIBRIUM IN THE PULSED H<sub>2</sub>+F<sub>2</sub> SYSTEM

#### 2.1 Time Resolved Spectroscopy

Experimental measurements of the time resolved spectra of pulsed H<sub>2</sub>+F<sub>2</sub> lasers have been made by Suchard, Gross and Whittier [68], Suchard [71], Nichols, et al. [69] and Parker and Stephens [70]. The duration of transitions and initial conditions are shown in Figure 2.1, 2.2 and 2.3 for the data reported by Suchard, et al. [68], Nichols, et al. [69] and Parker, et al. [70]; respectively. In the figures, the duration of the P-branch spectra is denoted by a line at an elevation associated with the v,J state corresponding to the lower level of the P-branch transition. The dot corresponds to the point where power peaked on the given transition. Theoretical models that assume rotational equilibrium do not permit simultaneous lasing on adjacent transitions in the same band. This phenomena can be seen by comparing the spectra predicted by the comprehensive model reference [7] in Figure 2.1 with the spectra of Suchard, et al. [68].

In laser systems initiated by flashlamps [68], [71], the sequence of appearance of individual lines is irregular within a given vibrational band. One possible explanation of this phenomena is nonuniform absorption of the light from the flashlamps. The initial F atom concentration is difficult to determine in flashlamp initiated systems, and F atom generation by photolysis occurs well into and often beyond the duration of the laser pulse. The time resolved spectra observed by Nichols, et al. [69] and shown in Figure 2.2 was obtained with carefully defined initial conditions. The second harmonic emission (3471 Å) from a 30n sec variable amplitude Q-switched ruby laser initiated the

Table 2.1 Comparison of Computer Models Incorporating Rotational Nouequilibrium Phenomena in 11F or DF.

	÷ •	F + H2+HF(v, J) + H	9+==	$11 + F_2 + 11F(v, J) + F$	Vibrational			Broadening		Energy Levels	evels		
Hodel	Ref.	Rotational Distribution	Ref.	Rotational Distribution	Relaxation W	VR,T	Rotational Relaxation	Lineshape Profile	Lesing	Considered Vibration Re	red Rotation	Diluent	Temperature Dependence
Pulsed HF This work	[11]	IRC Boltzmann	[34]	IRC, Boltzmann	0-FV	VR (a)	RT AJ-1,2(F)	Voigt	۳ <b>వ</b>	8×N	J<29 for V<6	N2, He, Ar, SF,	Variable
Pulsed HF Kerber, Hough, Emery [73,74]	[11]	Strong preferential, IRC,	[54]	Strong preferential, IRC, Boltzmann	Rot. equil.	Ţ	RT 6J-1	Voigt	Da.	8×1	J<12 for V<6	N2.He. Ar.SF6	Variable
Pulsed HF Kerber, Hough [72]	[16]	Trajectory	[54]	Bol t zmenn	Rot. equil.	5	RT 6J-1	Voigt		V<4 or V<8	$\frac{3<15}{3=J}$ or (c) $\frac{1}{3}$ (+2, -1)	N2, He. At. SF	Variable
Pulsed IIF Ben Shaul [75]	[11]	Statistical, IRC, Boltzmann			0-۲۹	a t	RT 6J-1	Doppler	p.,	Ç <u>ī</u>	J<20	Ar.SF6	Constant
Pulsed HF Superradiant Moreno [76]	[91]	Trajectory	[26] [29]	IRC	Rot. equil.	Ţ	RT AJ-1	rectangle	•	, v. 7	J <u>4</u> 11	11e, 0 <sub>2</sub> , Ar	Variable
Pulsed IIF Creighton (77)	[11]	IRC				5	RT AJ-1	Doppler at	۵.	V<3	J<20	NF.	Constant
CV NF Sentman [78,79]	<u>=</u>	IRC			Rot, equil.	ţ	RT 6J-1	Doppler	•	V<3	J<20	<b>.</b>	Constant
CV IIF Skiffstad [80]	[11]	IRC			Rot. equil.		RT 4J-1 <sup>(6)</sup>		£		(c)	; ;	300, 600°K
CV DF Hall [81]	Π	IRC			Rot. equil.	7	RT &J-1	Doppler	<u>a</u> .		. p.₁ J≤16	¥ .	Variable

Multiquanta VR transitions relax from HF(v,J) to HF(v',J'), where J' is 2 above or 3 below Jax transition with the minimum energy defect.

This model has been modified to include rotational lasing effects.

The rotational transition on a given vibrational band of maximum gain in denoted as J.

Single quanta VR transitions for collisions of HF with HF and F relax to the J that satisfies Equation (2.2).

IRC represents infrared chemiluminescence data.

Rotational relaxation rates obtained from values calculated by Wilkins [51].

۩€

3533

Cain equals loss during lasing.

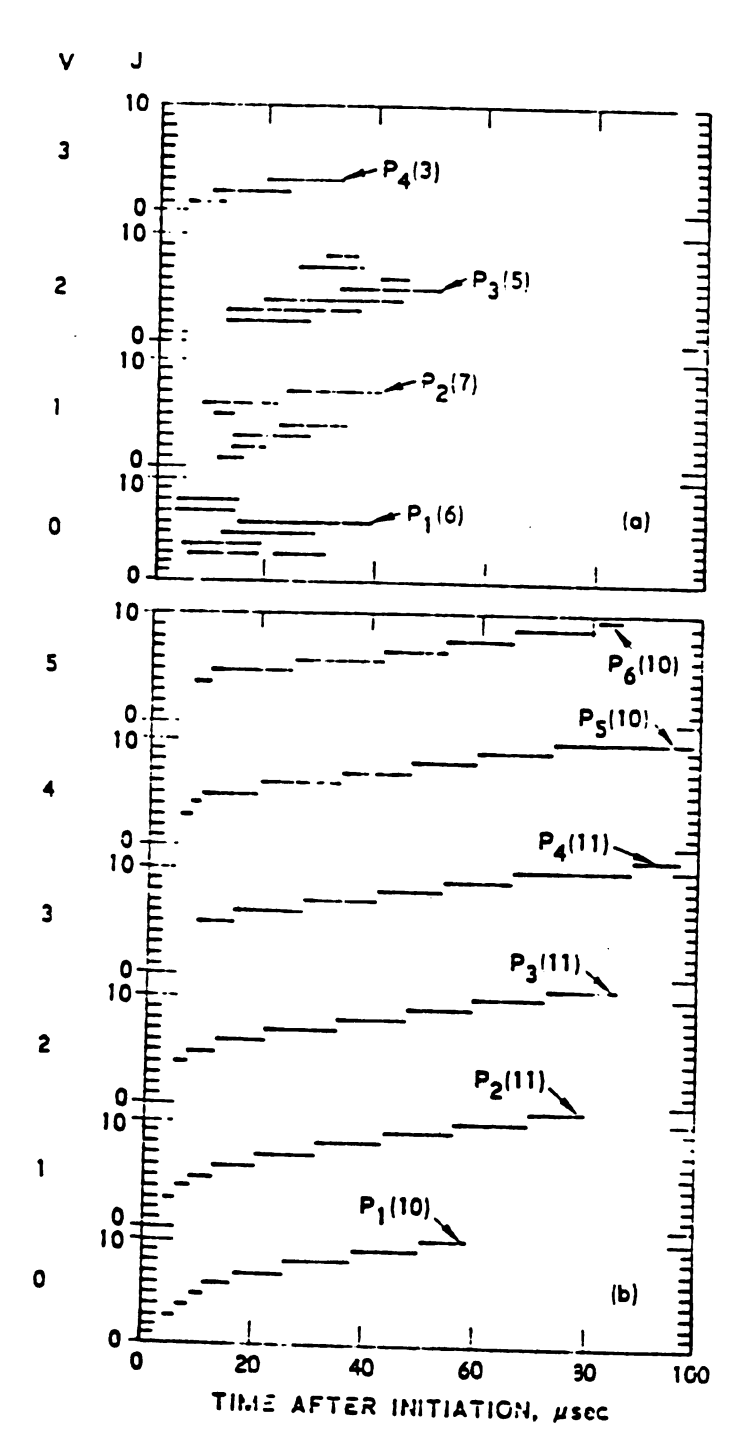
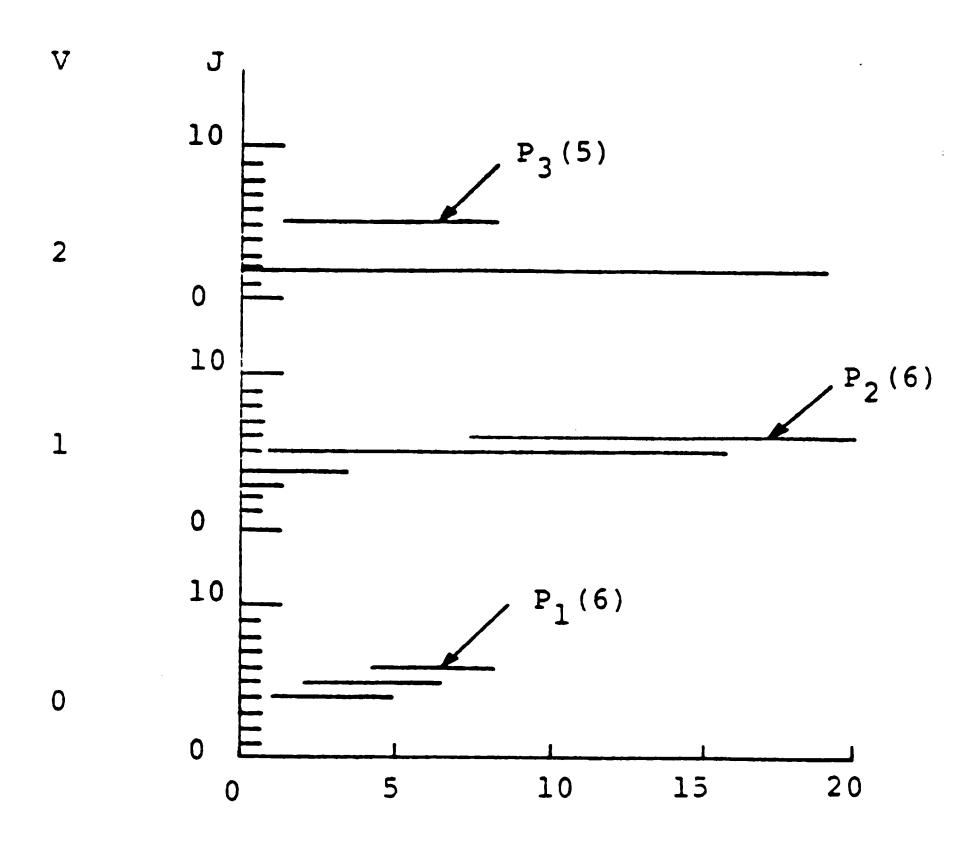


Figure 2.1. Comparison of time-resolved spectral output. (a) Experimental data reported in Reference 69 for a 1 H<sub>2</sub>:1 F<sub>2</sub>:60 He mixture at 50 Torr: (b) calculated spectrum for the same mixture from Reference 7 where rotational equilibrium was assumed.



Time After Initiation (usec)

Figure 2.2. Time resolved spectra of Nichols et al. [69] for a 1:1:10 mixture of  $H_2:F_2N_2$  at 90 torr with  $F/F_2$  = 0.23% and 0.002 HF. The active medium length is 30 cm and the mirror spacing is 113 cm,  $R_0$  = 0.7 and  $R_L$  = 1.0

 ${
m H_2+F_2}$  chain reaction laser by the photodissociation of  ${
m F_2}$ . The level of initiation was obtained by considering the mirror and window transmissities, the photodissociation cross section of  ${
m F_2}$  and the energy of the initiating ruby pulse with the assumption that the energy is uniformly absorbed.

Small amounts of initial HF can have a significant effect on laser performance. The initial HF concentration was measured by Nichols, et al. [69] by utilizing an HF probe laser operating on the  $P_1(2)$  transition to measure the ground state concentration of HF. The experimental apparatus of Nichols, et al. [69] is limited to measuring the time resolved power on 9 transitions and the total power.

The time resolved spectroscopy of Parker and Stephens [70] shown in Figure 2.3 was obtained utilizing transverse electric discharge initiation. A preionizer consisting of a linear array of spark discharges was used to provide a background of electrons insuring a uniform glow discharge. The sequence of appearance and disappearance of transitions within a band is quite regular with positive J-shift as observed by Nichols, et al. [69] and Parker and Stephens [70]. However, there is strong simultaneous lasing on adjacent transitions within a given band which is not possible with rotational equilibrium population distributions. The initial F atom concentration was obtained by comparing the peak power and pulse duration with the predictions of a computer model of the H<sub>2</sub>+F<sub>2</sub> laser [71].

## 2.2 Computer Modeling of Rotational Nonequilibrium Phenomena

The effects of rotational nonequilibrium in pulsed HF lasers have been modeled by Kerber and coworkers [72,73], Ben-Shaul, et al. [75],

Figure 2.3

Time resolved spectra of Parker and Stephens [70] for a 1:1:10:0.25 mixture of  $F_2$ : $H_2$ He: $0_2$  at 36 Torr with  $F/F_2$ =5%. The active medium length is 15 cm and the mirror spacing is 60 cm, $R_0$ =0.8 and  $R_L$ =1.0. The lower level of a P branch transition is denoted by v and J. The length of the lines correspond to the duration of lasing on a given line. The dot on the line corresponds to the time at which the maximum power was achieved on that line.

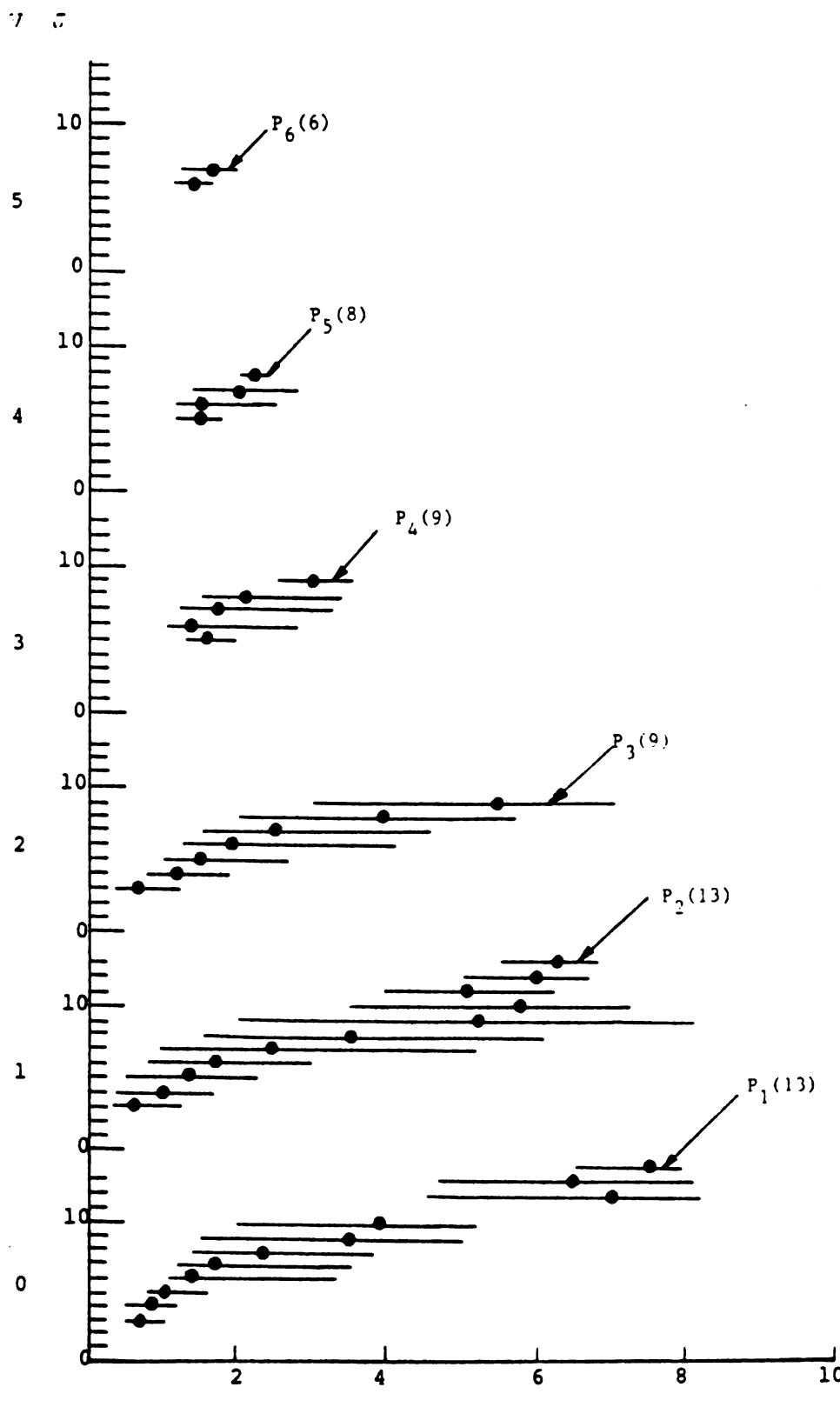


Figure 2.3 Time After Initiation ( $\mu sec$ )

•

Moreno [76] and Creighton [77]. Rotational nonequilibrium phenomena have been modeled by Sentman [78,79] and Skifstad, et al. [80] for the continuous wave (cw) HF laser system and by Hall [81] for the cw DF laser. These models vary significantly in their ability to model rotational nonequilibrium phenomena in a manner that approximates the actual physical mechanisms. The major characteristics and assumptions of these models are outlined in Table 2.1.

The cold pumping reaction is included in every model listed in the table. The rotational distribution suggested by Polanyi, et al. [11] (see Figure 1.1) was used by references [73-75 and 77-79] and this work. The Boltzmann rotational distribution is used by reference [80] and the effect on the pumping distribution is examined in references [73-75]. The rotational distribution for references [73,74] and this work is a given fraction of a Boltzmann distribution and the distribution of Polanyi [1]. The distribution computed by Wilkens [16] is used by references [72,76].

The hot pumping reaction is included in the models of Kerber and coworkers [72,74] and Moreno [76] with the rotational distribution measured by Polanyi, et al. [26]. The rotational distribution for references [73,74] and this work is a given fraction of a Boltzmann distribution and the distribution of Polanyi [76] (see Figure 1.2). The inclusion of the hot pumping reaction is essential in modeling the  $H_2+F_2$  chain reaction, but greatly increases the complexity of a model by increasing the number of vibrational levels that must be considered from 3 to 8.

The vibrational to vibrational (VV) energy transfer process is one of the energy transfer mechanisms that is responsible for the excitation

and de-excitation of vibrationally excited HF. Rotational levels are at their equilibrium values during the intermolecular VV energy exchange process in all models considered with the exception of the present work and that of Ben-Shaul, et al. [75] The present work and that of reference [75] require that the rotational levels are not perturbed during VV relaxation.

Vibrational relaxation can also occur by the following VR,T reaction:

$$HF(v,J) + M + HF(v',J') + M$$
 (2.1)

This reaction is a VT reaction if J and J' are given by their thermal equilibrium values. With the exception of the present work and reference [75], reaction (2.1) is treated as a VT reaction. The effects of multiquantum VT were considered by Kerber, et al [73] who found as one would expect that multiquanta deactivation tended to decrease the pulse energy, peak power and shorten the pulse duration over single quantum (v'=v-1) cases. Ben-Shaul, et al. [75] incorporated the effects of vibrational to rotational energy transfer (VR) in his model for reactions of HF(v,J) with HF and F. The rates for this process increase linearly with vibrational energy. The change in rotational energy due to the VR process was determined by the relationship [87],[88]

$$\langle \Delta E_{rot} \rangle = \frac{2}{3} \langle \Delta E_{vib} \rangle$$
 (2.2)

Ben-Shaul concluded that VR cannot serve as an efficient pumping mechanism of high rotational levels since his mechanisms for depopulating

high rotational levels were more efficient than his VR mechanism for populating high rotational levels. Although these results are contrary to the results of the present efforts this is the first attempt to model VR processes.

Rotational relaxation for all models with the exception of the present work is assumed to consist of  $\Delta J \pm 1$  RT relaxations of the form

$$HF(v,J) + M + HF(v,J-1) + M$$
 (2.3)

These models, with the exception of reference [80], employ the rotational relaxation model of Polanyi, et al. [31] as discussed in Section 1.2. Two approaches to modeling RT relaxation are discussed by Kerber [73]. These methods consist of the rotational relaxation time constant approach where rotational levels relax towards their equilibrium values (Equation 1.11) and the detailed kinetic approach where explicit RT reactions are modeled. The results of Kerber indicate that (1) the major temporal characteristics are the same including the sequential J-shift pattern, (2) the detailed kinetic model predicts a smaller fraction of energy in the vibrational levels pumped by the hot reaction than the time constant model predicts, (3) the detailed kinetic model predicts higher pulse energies and less power over the time constant model, and (4) the detailed kinetic model predicts a sharper distribution of energy as a function of rotational quantum number for each band. The detailed kinetic model also predicts that the rotational transitions undergoing lasing will appear and terminate sooner than what is predicted by the time constant model.

The line shape in references [75,77,79] is assumed to be Doppler broadened. The Doppler broadening profile is valid only at pressures under a few torr. In the model of the H<sub>2</sub>+F<sub>2</sub> superradient laser of reference [76], the line shape is approximated by a rectangle. The line shape used by Kerber and coworkers [72,74] is a Voigt profile which includes the effects of Doppler boradening and Lorentz broadening [7, 86].

All of the models listed in Table 2.1 include P branch lasing.

The model of Skifstad [80] restricts lasing to only single lines.

The effects of R branch lasing were found by Sentman [78] to decrease with increasing rotational relaxation rates. The present study includes the effects of P branch lasing.

The only models which adjust the gas temperature according to the energy balance equation are those of Kerber and coworkers [72,74], Moreno [76], and Hall [81] and the present model. The other models maintain a fixed temperature throughout the simulation.

The effect of rotational nonequilibrium on the time resolved spectra was found by Kerber and coworkers [72,74] (1) to increase the number of transitions that lase simultaneously, (2) to lower the intensity of each transition, (3) to extend the duration of lasing on each transition, and (4) to shift the laser energy to higher rotational levels. These conclusions appear to be consistent with the other models in Table 2.1. The rotational distribution was noted by references [35,37] to approximate the pumping rotational distribution for early times and approach but not reach an equilibrium rotational distribution towards the end of the pulse.

#### 3. MODEL FORMULATION

The computer model of the pulsed hydrogen fluoride laser system is described. The mechanisms for a rate equation model of the pulsed  $H_2+F_2$  chain reaction laser with P branch and RR lasing are presented.

The present formulation yields the time history of the first seven vibrational levels of hydrogen fluoride and their first thirty rotational levels. In addition vibrational levels (v=7,8) are included and their rotational levels are assumed to be in rotational equilibrium at the translational temperature.

The cold pumping reaction is

$$F + H_{2}(0) = \frac{K_{f}^{c}(v) P_{c}(v,J)}{K_{b}^{c}(v,J)} HF(v,J) + H$$
 (3.1)

where  $K_{\mathbf{f}}^{\mathbf{C}}(\mathbf{v})$  is the forward rate coefficient recommended by Cohen [24]. The normalized rotational pumping distribution is given by  $P_{\mathbf{C}}(\mathbf{v},\mathbf{J})$ . The present formulation assumes this to be a variable fraction of the distribution suggested by Polanyi [11] and the Boltzmann distribution. The backward pumping rate is denoted as  $K_{\mathbf{b}}^{\mathbf{C}}(\mathbf{v},\mathbf{J})$  and is obtained from the forward rate  $K_{\mathbf{f}}^{\mathbf{C}}(\mathbf{v})$   $P_{\mathbf{C}}(\mathbf{v},\mathbf{J})$  by considering detailed balancing. The cold reaction is exothermic for  $\mathbf{v}=0$  to 3 and endothermic for  $\mathbf{v}=4$  to 6. Pumping of  $\mathbf{v}=0$  has not been observed experimentally.  $P_{\mathbf{C}}(\mathbf{v},\mathbf{J})$  is shown in Figure 1.1 and  $K_{\mathbf{f}}^{\mathbf{C}}(\mathbf{v})$  is given in Appendix A.

The hot pumping reaction is

$$H + F_2 \frac{K_f^h(v) P_h(v,J)}{K_f^h(v,J)} HF(v,J) + F$$
 (3.2)

where  $K_f^h(v)$  is the forward rate coefficient recommended by Cohen [24]. The normalized pumping distribution  $P_h(v,J)$  for the hot pumping reaction is also assumed to be a fraction of the distribution suggested by Polanyi [26] and the Boltzmann distribution. The backward rate coefficient,  $K_b^h(v,J)$ , is computed from the equilibrium constant for the cold reaction. The hot reaction forms vibrationally excited HF from v=0 to v=8. The forward rate  $K_f^h(v)$  is given in Appendix A and  $P_h(v,J)$  is illustrated in Figure 1.2.

The HF vibrational to rotational (VR) quantum exchange mechanism is given by

$$HF(v,J) + M = \frac{K_f^{VR}(v,v')}{K_f^{VR}(v,v',J,J')} HF(v',J') + M$$
 (3.3)

where  $K_f^{VR}(\mathbf{v},\mathbf{v}')$  is the forward rate coefficient. The forward rates,  $K_f^{VR}(\mathbf{v},\mathbf{v}')$ , are obtained from the overall rate coefficients recommended by Wilkins [51] for a given  $\mathbf{v}$  by making the rate for single quantum transitions two times the rate for multiple quantum transitions. Thus if only single quantum transitions are to be considered  $K_f^{VR}(\mathbf{v},\mathbf{v}-1)$  would be the total rate for a given vibrational level. The forward rate constants  $K_f^{VR}(\mathbf{v},\mathbf{v}')$  for a change in vibrational quanta up to 7 are given in Table 3.1. The backward rate  $K_b^{VR}(\mathbf{v},\mathbf{v}',\mathbf{J},\mathbf{J}')$  is obtained from detailed balancing considerations. A typical multiquanta VR reaction path is illustrated in Figure 1.4.

The rotational level yielding a minimum energy defect between HF(v,J) and HF(v',J') is given in Table 1.4. Equal probability is assigned to each of the allowed vibrational to rotational transitions from HF(v,J) to HF(v',J'). In the results given by Wilkins [51],

only self relaxation of HF is considered. Collision partners other than HF must be considered for VR relaxation. Single quantum VR processes are assumed for all other species with the exception of H atoms. A temperature dependent scale parameter was formulated based upon Cohen's [23] recommended HF-M VT rates. For H<sub>2</sub> this parameter is the M=H<sub>2</sub> rate divided by Cohen's [23] HF+HF VT rate K<sub>HF</sub>

$$\frac{6 \times 10^7 \text{ T}}{10 \text{K}_{\text{HF}}} \tag{3.4}$$

For  $F_2$ , Ar,  $N_2$  and  $SF_6$  this parameter is,

$$\frac{7.7 \times 10^{-7} \text{ T}}{50 \text{K}_{HF}} \tag{3.5}$$

where the scale factor for He is twice that of Ar. The factor for F is

$$\frac{1.5 \times 10^{12} \, e^{-700/RT}}{10 \, \text{K}_{\text{HF}}} \tag{3.6}$$

and for H, this factor is

$$\frac{1.6 \times 10^{13} e^{-2700/RT}}{200K_{HF}}$$
 (3.7)

where T is the temperature in degrees Kelvin and R is the gas constant in calories/mole-K. The scale factor for M=HF is 1. The HF-HF VT rate  $K_{\rm HF}$  is given by

$$3 \times 10^{14} \text{ T}^{-1} + 3.5 \times 10^{4} \text{ T}^{2.26}$$

Vibrational to vibrational (VV) quantum exchange for HF-HF collisions are modeled as

$$HF(v,J_{1}) + HF(v^{*},J_{2}) = \frac{K_{f}^{VV}(v,v^{*})}{K_{b}^{VV}(v,v^{*},J_{1},J_{2})} + HF(v^{-1},J_{1}') + K_{b}^{VV}(v,v^{*},J_{1},J_{2}') + HF(v^{*}+1,J_{2}')$$
(3.8)

where the forward rate coefficient  $K_f^{VV}(v,v^*)$  is obtained from the three-dimensional trajectory calculations of Wilkins [51] (Table 1.7). The rotational levels  $J_1$  and  $J_2$  are held fixed and as before  $K_b^{VV}(v,v^*,J_1,J_2)$  is obtained from detailed balance considerations. To prevent duplications in the HF-HF VV reactions considered  $v,v^*,J_1$  and  $J_2$  are given by

$$6 \ge v \ge v \ge 1$$
 and  $29 \ge J_2 \ge J_1 \ge 0$  . (3.9)

Vibrational to vibrational energy transfer of HF-H, is modeled as

$$HF(v,J) + H_{2}(v^{*}) \underbrace{\frac{K_{f}^{HF-H_{2}}(v,v^{*})}{K_{h}^{HF-H_{2}}(v,v^{*})}}_{HF(v+1,J) + H_{2}(v^{*}-1)$$
(3.10)

where the forward rate  $K_f^{\mathrm{HF}-\mathrm{H}}2(\mathrm{v},\mathrm{v}^*)$  is obtained from the recommended rate coefficients of Cohen [24]. For  $\mathrm{v}^*=1$ , the first 4 (v=0 to 3) vibrational levels of HF are considered. For  $\mathrm{v}^*=2$ , the first 2 vibrational levels of HF are considered. Vibrational to translational energy transfer in  $\mathrm{H}_2$  may be modeled as

$$H_2(v) + M = \frac{H_f^{H_2^{-H_2}(v)}}{K_b^{H_2^{-H_2}(v)}} H_2(v-1) + M$$
 (3.11)

where  $K_f^H 2^{-H} 2(v)$  is the forward rate coefficient, M represents all collision partners and v is 1 or 2 as recommended by Cohen [24].

The effects of rotational relaxation excluding lasing are modeled by the following mechanisms; rotational to translational (RT)

$$HF(v,J) + M = \frac{K_f^{RT}(v,J,\Delta J)}{K_b^{RT}(v,J,\Delta J)} \qquad HF(v,J-\Delta J) + M \qquad (3.12)$$

and rotational to rotational (RR) quantum exchange

$$HF(v,J_{1}) + HF(v*,J_{2}) = \frac{K_{f}^{RR}(v,J_{1},\Delta J)}{K_{b}^{RR}(v,J_{1}J_{2},\Delta J)} + HF(v,J_{1}'-\Delta J) + K_{b}^{RR}(v,J_{1}J_{2},\Delta J) + HF(v*,J_{2}'+\Delta J)$$
(3.13)

where  $\Delta J$ , the change in rotational quantum number, is 1 or 2 for RT and  $\Delta J$  is 1 for RR. To prevent duplications in the rotational relaxation reactions considered, we require

$$7 \ge v^* \ge v \ge 0$$
 and  $(29 - \Delta J) \ge J_2 \ge J_1 \ge \Delta J$ . (3.14)

The forward rates for RT and RR processes are based upon the total rate coefficients for the following two reactions:

$$K_{f}^{R}(v=0)$$
HF(0,10) + HF(v,J)  $\xrightarrow{K_{f}^{R}(v=0)}$  HF(0,10- $\Delta$ J) + HF(v,J) (3.15)

where the forward rate  $K_f^R(v=0)$  is

$$K_f^R(v=0) = 1.023 \times 10^{16} T^{-0.805} e^{-2569/RT}$$
 (3.16)

and

$$K_f^R(v=1)$$
HF(1,10) + HF(v,J)  $K_f^R(v=1)$ 
HF(1,10- $\Delta$ J) + HF(v,J) (3.17)

where the forward rate  $K_f^R(v=1)$  is given by

$$K_f^R(v=1) = 3.38 \times 10^{16} T^{-0.893} e^{-2436/RT}$$
 (3.18)

where  $K_f^R(v)$  is in units of cc/mole-sec.

The total rotational relaxation rate  $K_{\mathbf{f}}^{\mathbf{R}}(\mathbf{v})$  was calculated for rotational levels 5, 10 and 15 by Wilkins [51]. The intermediate value J=10 was chosen as a reference. The rate coefficient  $K_{\mathbf{f}}^{\mathbf{R}}(\mathbf{v})$  is scaled according to the transition probabilities presented in Figure 1.4 about J=10.

The present formulation assumes that the rate coefficient for vibrational levels greater than 1 is the same as the  $K_f^R(1)$  rate. Wilkins [51] noted that the contribution due to RR mechanisms contributed to approximately one third of the total rate coefficient. Assuming that indeed one third of the total rate is due to RR and two thirds of the total rate is due to RT mechanisms then the following rates for  $K_f^{RR}(v,J,\Delta J)$  and  $K_f^{RT}(v,J,\Delta J)$  may be obtained:

$$K_f^{RR}(v,J,1) = \frac{K_f(v) P_{\Delta J=1}(J)}{3 P_{\Delta J=1}(10)}$$
 (3.19)

$$K_f^{RT}(v,J,1) = \frac{2}{3} \frac{K_f^R(v) P_{\Delta J=1}(J)}{P_{\Delta J=1}(10) + P_{\Delta J=2}(10)}$$
 (3.20)

$$K_{f}^{RT}(v,J,2) = \frac{2}{3} \frac{K_{f}^{R}(v) P_{\Delta J=2}(J)}{P_{\Delta J=1}(10) + P_{\Delta J=2}(10)}$$
 (3.21)

The chaperon M for RT reactions employs the relative rotational relaxation efficiencies based upon the infrared double resonance experiments of Hinchen [33,34] and are listed in Table 3.1.

Table 3.1 Relative Rotational Relaxation Efficiencies.

Species	Relative Efficiency
нъ	1.0
He	0.03
Ar	0.03
N <sub>2</sub>	0.03
SF <sub>6</sub>	0.03
F <sub>2</sub>	0.03
F	0.03
H <sub>2</sub>	0.1
H	0.03

The dissociation of HF is given by

$$HF(v,J) + M \xrightarrow{K_{f}^{HF}(v)} H + F + M \qquad (3.22)$$

where the rate coefficients are of the form suggested by Cohen [24] and listed in Appendix A.

The dissociation of  $H_2$  is given by

$$H_2(v=0) + M = \frac{K_f^{H_2}}{K_b^{H_2}} + H + H + M$$
 (3.23)

where the rate coefficient  $K_f^{H}2$  has been suggested by Cohen [24].

The dissociation of  $F_2$  is represented by

$$F_2 + M \xrightarrow{K_f^F 2} F + F + M$$
 (3.24)

 $K_f^F$ 2 is the sum of the rate suggested by Cohen [24].

Initiation may be modeled by the instantaneous introduction of F atoms or by a continuous dissociation of  $F_2$  simulating a flashlamp. The rate of photodissociation of  $F_2$  due to a flashlamp is of the form presented in Nest [89].

$$\frac{dF_2}{dt} = \frac{Z_1}{\rho} \sin \left(\frac{\pi t}{t_{flesh}}\right) (1 - e^{-Z_2 F_2}) . \qquad (3.25)$$

The quantity  $Z_1$  is the maximum value of the flashlamp output in moles of photons relative to a unit volume of the gas mixture,  $\rho$  is the density of the mixture, t is the time in seconds from the start of

photodissociation,  $t_{flash}$  is the length of time of the photodissociation of  $F_2$  in moles/cc. The absorption coefficient  $\alpha_v$  in cm<sup>-1</sup> of  $F_2$  and the active medium length L in cm, is related to  $Z_2$  by

$$z_2 = \frac{\alpha_v L}{F_2} \qquad (3.26)$$

The chemical reactions are written in the general form

$$\sum_{i} \alpha_{ri} N_{i} \frac{K_{r}}{K_{-r}} \sum_{i} \beta_{ri} N_{i}$$
 (3.27)

where N<sub>i</sub> is the concentration of species i in mole/cc,  $\alpha_{ri}$  and  $\beta_{ri}$  are stoichometric coefficients, K<sub>r</sub> and K<sub>-r</sub> are the forward and backward rate coefficients. For the specific reactions introduced earlier the chemical reactions yield a concentration rate of change of the form

$$\frac{dN_{i}}{dt} = \sum_{r} (\beta_{ri} - \alpha_{ri}) (K_{r} + \sum_{j} N_{j}^{\alpha_{rj}} - K_{-r} + \sum_{j} N_{j}^{\beta_{ri}}) . \qquad (3.28)$$

The general term for the rate of change of  $\operatorname{HF}(v,J)$  can be written as

$$\frac{dHF(v,J)}{dt} = X_{i} + \frac{1}{x_{rad}(v,J) - X_{rad}(v,J-1)} + \frac{1}{x_{rad}(v,J) + x_{rad}(v,J) + x_{rad}(v,J-1)}$$
(3.29)

where  $X_1$  is the rate of change of HF(v,J) due to kinetics and  $\alpha(v,J)$  is the gain in cm<sup>-1</sup> on the P branch v+l+v transition with lower level J and f(v,J) is the photon flux in mole/cm<sup>2</sup>-sec. The model can be modified to include rotational lasing where the

rate of lasing from rotational level J+l+J is denoted as  $X_{rad}(v,J)$ . The rate equation for the lasing flux if [72]

$$\frac{\mathrm{df}(\mathbf{v},\mathbf{J})}{\mathrm{dt}} = \frac{\mathrm{c} \, \mathbf{L}}{\ell} \left[ \alpha(\mathbf{v},\mathbf{J}) - \alpha_{\mathrm{thr}} \right] \tag{3.30}$$

where c is the speed of light, L is the active medium length and  $\ell$  is the spacing between the mirrors in cm. The threshold gain is

$$\alpha_{\text{thr}} = -\frac{1}{2L} \ln(R_0 R_L)$$
 (3.31)

where  $R_0$  is the reflectivity of the output mirror and  $R_L$  includes the loss at the second mirror and other cavity losses. The gain for a P branch transition at line center is [72]

$$\alpha(v,J) = \frac{h N_A}{4\pi} \omega_c(v,J) \phi(v,J) B(v,J) \left[ \frac{2J+1}{2J-1} HF(v+1,J-1) - HF(v,J) \right]$$
(3.32)

where  $N_A$  is Avagadro's number, h is Planck's constant,  $\omega_{_{\mbox{\scriptsize C}}}(v,J)$  is the wavenumber of the P branch transition, B(v,J) is the Einstein isotropic absorption coefficient based on the intensity, and  $\phi(v,J)$  is the Voigt profile at line center with the Lorentzian linewidth based upon the data of Meredith [27] or Hough [86]. Lasing transitions are assumed to be homogeneously broadened and do not overlap.

The power on a given P branch transition is [72]

$$P_{VR}(v,J) = h c N_A \alpha_{thr} \omega_c(v,J) f(v,J) . \qquad (3.33)$$

The output power through  $R_0$  is [27]

$$P_{VR}^{out}(v,J) = P_{VR}(v,J) \frac{1 - R_0}{\left[1 + \sqrt{\frac{R_0}{R_L}}\right] \left[1 - \sqrt{R_0 R_L}\right]}$$
 (3.34)

The rate of photon emission due to RR lasing for a transition from J+l to J given by  $X_{\rm rad}(v,J)$  can be expressed in terms of a rate equation for the RR lasing flux. An alternate form for  $X_{\rm rad}(v,J)$  that does not require the addition of up to 210 flux terms to the integration list is discussed in Appendix B. The power due to rotational lasing is

$$P_{RR}(v,J) = h c N_A \omega_{cR}(v,J) X_{rad}(v,J)$$
 (3.35)

where  $\omega_{\rm cR}({\rm v,J})$  is the wavenumber of the rotational lasing transition from J+l to J. Research is currently underway assessing the effect of Equation (3.35) on laser performance and will not be presented here. The laser energy extracted in each band is then determined by integrating the power

$$E_{VR}(v,J) = \int_{0}^{c} P_{VR}(v,J) dt$$

$$E_{RR}(v,J) = \int_{0}^{c} P_{RR}(v,J) dt$$
(3.36)

there  $t_c$  is the length of time in seconds of the laser pulse.

The time rate of change of temperature for a constant density gas based on conservation of energy is [72]

$$\frac{dT}{dt} = \frac{- [P_{VR} + P_{RR} + \sum_{i} \frac{dN_{i}}{dt} H_{i}(T)]}{\sum_{i} N_{i}C_{vi}(T)}$$
(3.37)

where  $P_{VR}$  is the total power due to P branch lasing,  $P_{RR}$  is the total power due to rotational lasing,  $C_{V1}(T)$  is the molar specific heat of species i for constant volume at a given temperature and  $H_{i}(T)$  is the molar enthalpy.

A Warnier-Orr [80] diagram outlining the major processes in the model is given in Appendix C.

## 4. RESULTS AND DISCUSSION

A comprehensive computer model has been developed and presented that simulates the performance of the pulsed  $H_2 + F_2$  pulsed chemical laser. Rate equations are used to represent the chemical kinetic and stimulated emissions processes occurring in a representative unit volume within a Fabry-Perot cavity. All processes are assumed uniform throughout the cavity. Lasing is permitted on all P branches in the vibrational - rotational bands at or below v = 6 and J = 12, and may respond to gain fluctuations during the lasing period. This model permits the examination of the effect of vibrational to rotational, rotational to rotational, rotational to rotational, rotational to translational and vibrational to vibrational energy transfer on the spectral distribution. The effect of nonequilibrium pumping distributions and line selection on the spectral content of the laser pulse can also be examined. The major thrust of the present work has been to examine the effects of Wilkins [51] VR, VV and RR, T rate coefficients on laser performance.

4.1 Effect of Vibrational to Rotational Relaxation on HF Population

The present formulation supports the predictions of Wilkins [51,
52] and others [23,34] that VR is the primary mechanism for populating high rotational states of HF. The effect of various distributions of J' about J for the multiquanta VR reaction

$$HF(v,J) + M \rightleftharpoons HF(v',J') + M + \Delta E$$
 (4.1)

where J is the value of J' that minimizes the energy defect. Several distributions both multi quanta and single quanta have been studied and are listed in Table 4.1. The total forward reaction rate

Table 4.1 Possible VR relaxation distributions about  $J_{max}$  for  $HF(v,J) + M \stackrel{?}{\downarrow} HF(v',J') + M$ 

Distri- bution	J <sub>max</sub> -4	J <sub>max</sub> -3	J <sub>max</sub> -2	J -1	J max	J +1	J +2
1	1/7	1/7	1/7	1/7	1/7	1/7	1/7
2	0	0	0	1/3	1/3	1/3	0
3	0	0	0	0	1	. 0	0
4	0.05	0.05	0.05	0.25	0.3	0.25	0.05

is obtained by multiplying  $K_f^{VR}(v,v')$  by a particular distribution. The rate  $K_f^{VR}(v,v')$  was obtained by multiplying a temperature dependent scale parameter based upon Cohen's [22,23] recommended HF + M single quanta VT rate and Wilkins [51] recommended VR rates for HF+HF collisions. These rates are illustrated in Figure A.4.

To assist in understanding the numerous coupled processes occurring in the model, plots were made of the population time history of HF(v,J)and time resolved spectra for all cases. Integration difficulty was encountered for the first distribution where J' is 2 above and 4 below  $J_{\text{max}}$  and all seven levels are equally weighted. The difficulty arose from the integration step size being too large. Prohibitively large computation times would have been necessary to eliminate this problem. The concentration of HF(v,J) versus J at 1 sec, 10 sec, 50 sec and at the end of the lasing pulse when the total power has dropped below 1% of the maximum are illustrated in Figure 4.1 for run 18a. At early times in the simulation the rotational population matches the pumping rotational distribution. As time progresses the population of rotational levels above the levels pumped increases dramatically. The VR relaxation processes were found to be primarily responsible for populating these upper levels. The VV relaxation mechanism will tend to redistribute the specific upper rotational level pumped by VR about the 7 vibrational levels considered. The effect of rotational relaxation on the derivative of HF(v,J) was found to be important even at high rotational levels.

The relative contributions to the derivative of HF(v=1,J) are compared in Figure 4.2. For a typical HF(v,J) there are several hundred contributions to the derivative. A total of 92,398 reactions

# RUN18A VR, W, RR: P LASING

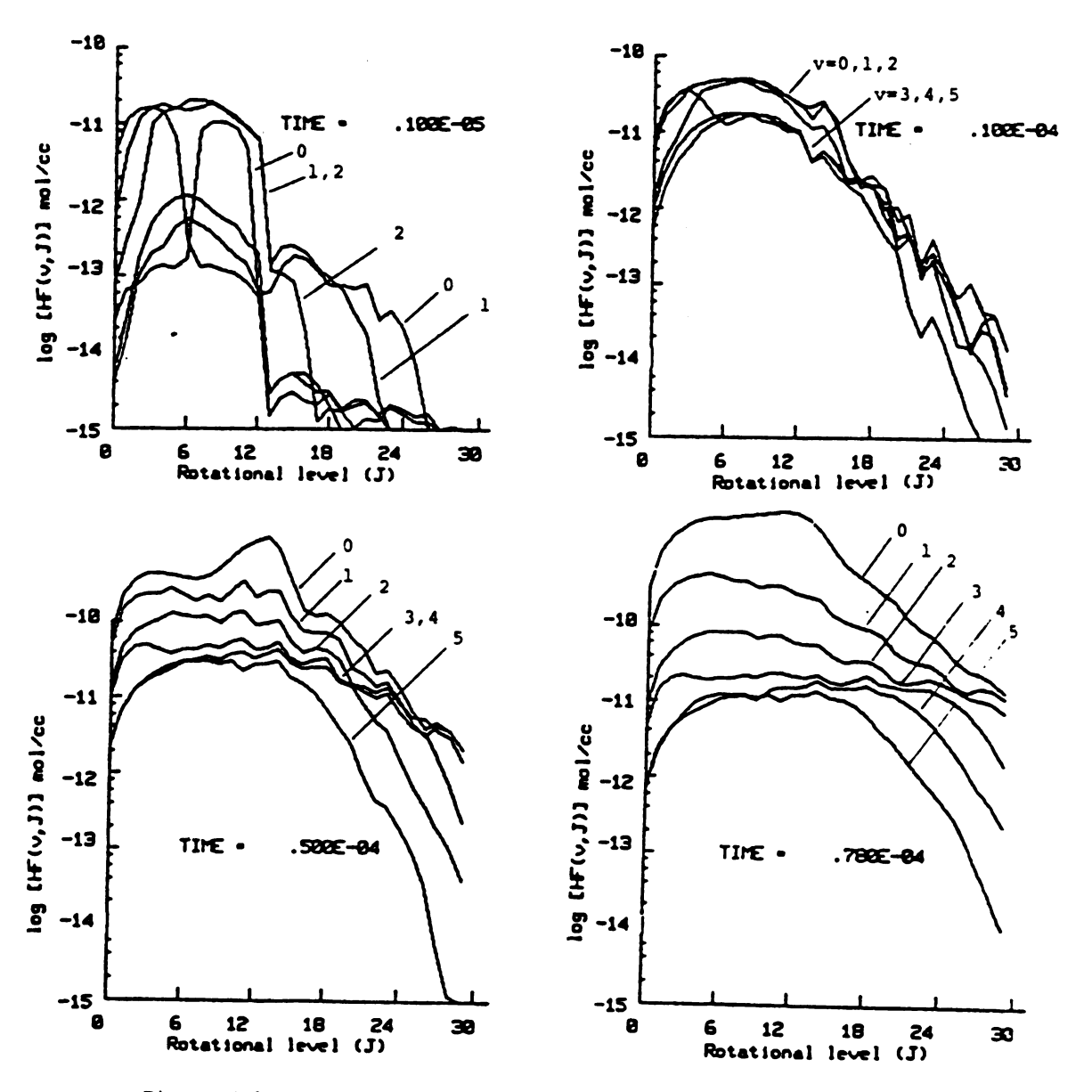


Figure 4.1 Concentration of  $\mathrm{HF}(v,J)$  versus rotational level at selected times.

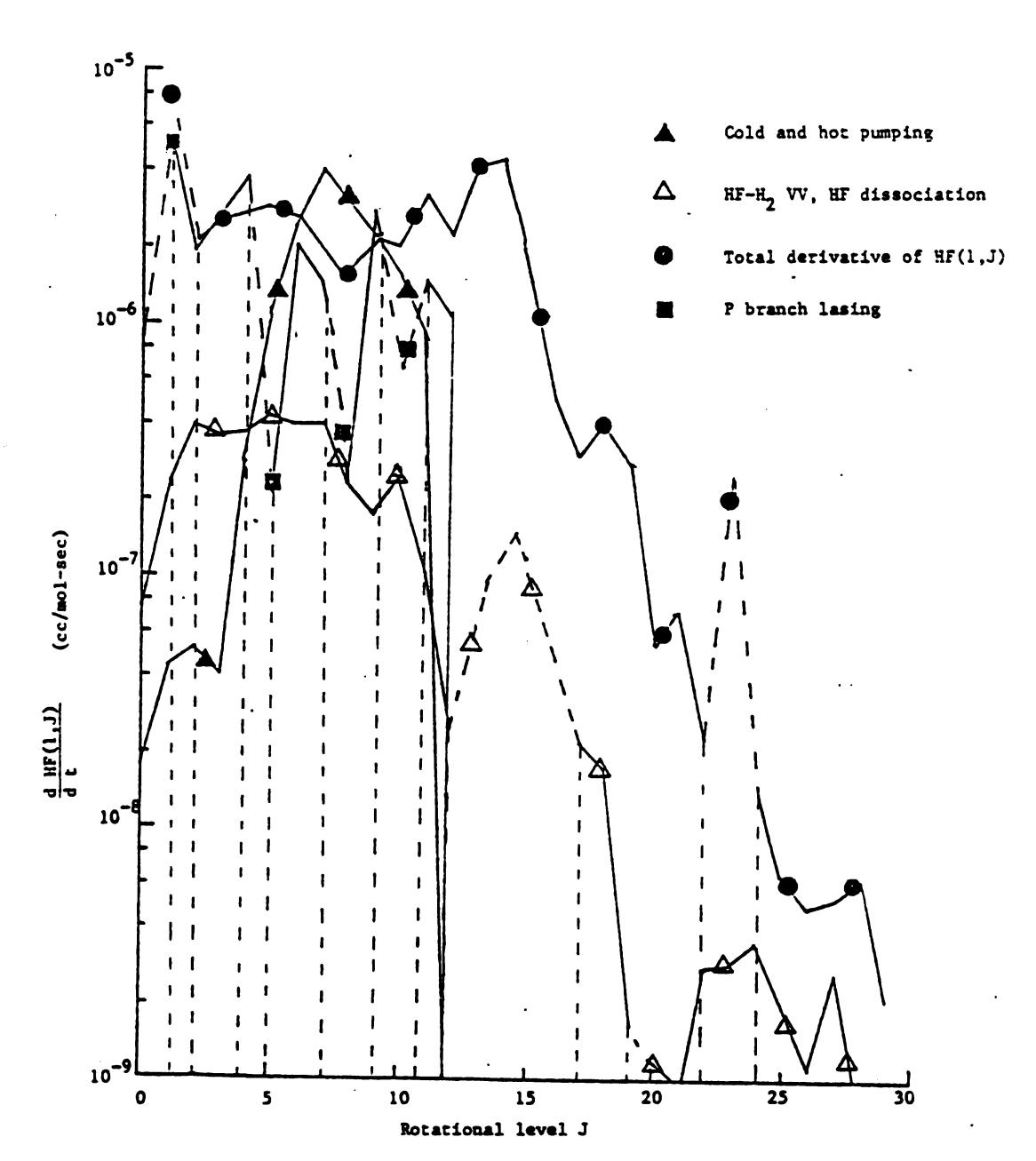


Figure 4.2a. Contribution to the derivative of HF(1,J) at peak power for run 18a. A dashed line denotes a negative contribution to the total derivative.

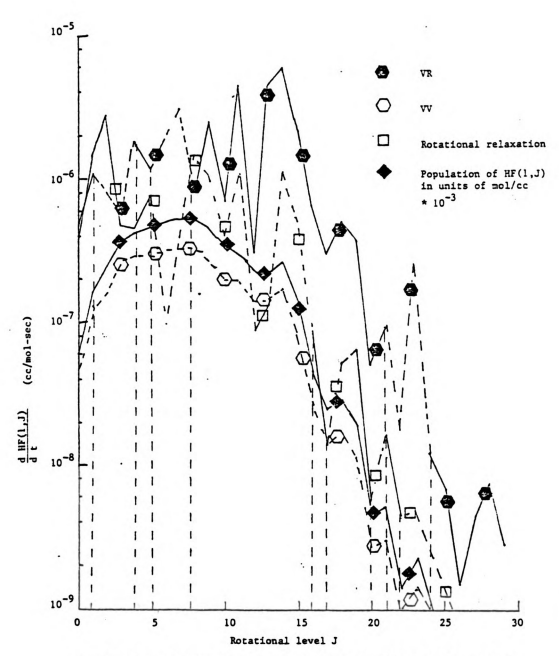


Figure 4.2b. Contribution to the derivative of HF(1,J) at peak power for run 18a.

contribute to the derivative of all 210 vibrational and rotational levels of HF considered. The major contribution to the derivative of HF(1,J) is from VR relaxation. The pumping and P branch lasing processes compete with VR relaxation at rotational levels less than 13. The peak in the derivative of HF(1,J) due to VR at J=15 corresponds to the transition from HF(v=2, J=0-4) to HF(1,15). This peak near J=15 has been observed for all vibrational levels that are considered. The ability of VR to transfer energy from several of the lowest rotational levels to a single rotational level near J=15 provides an efficient mechanism for populating this level. The effect of rotational relaxation is to redistribute the rotational distribution towards thermal equilibrium counteracting the effects of VR at higher rotational levels. The derivative of HF(v,J) due to VV has the effect of redistributing the rotational population among all 7 vibrational levels.

The total derivative of HF(v,J) versus J is illustrated in Figure 4.3. For v=0-2 the derivatives are nearly equal. The large peak in the derivative of HF(0,29) is an artifact of the model and is caused by the VR mechanism. There are 9 separate VR reaction paths which contribute to this derivative [HF(1,J=25,26), HF(2,J=21,22) HF(3,16,17), and HF(4,J=8-10)]. Examination of the derivatives due to VR indicate that the multiquanta VR relaxation path from HF(4,J=9,10) is responsible.

4.2 Effect of Vibrational to Rotational Relaxation on the Power and Energy

The effect of distributions 2, 3 and 4 are examined in Table 4.2 which compares the relative band energies, pulse energy and duration.

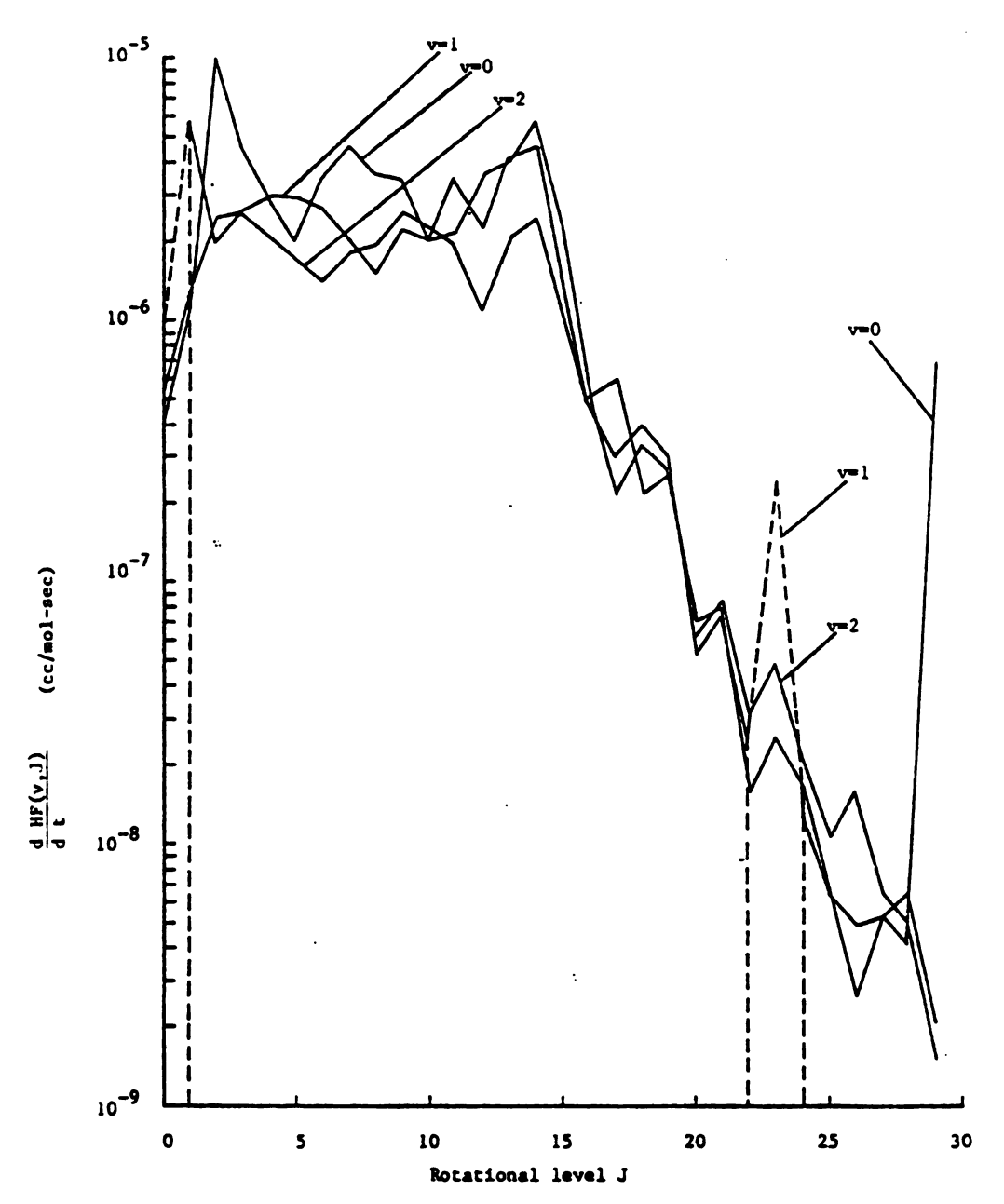


Figure 4.3a. Total contribution to the derivative of HF(v,J) at peak power for run 18a.

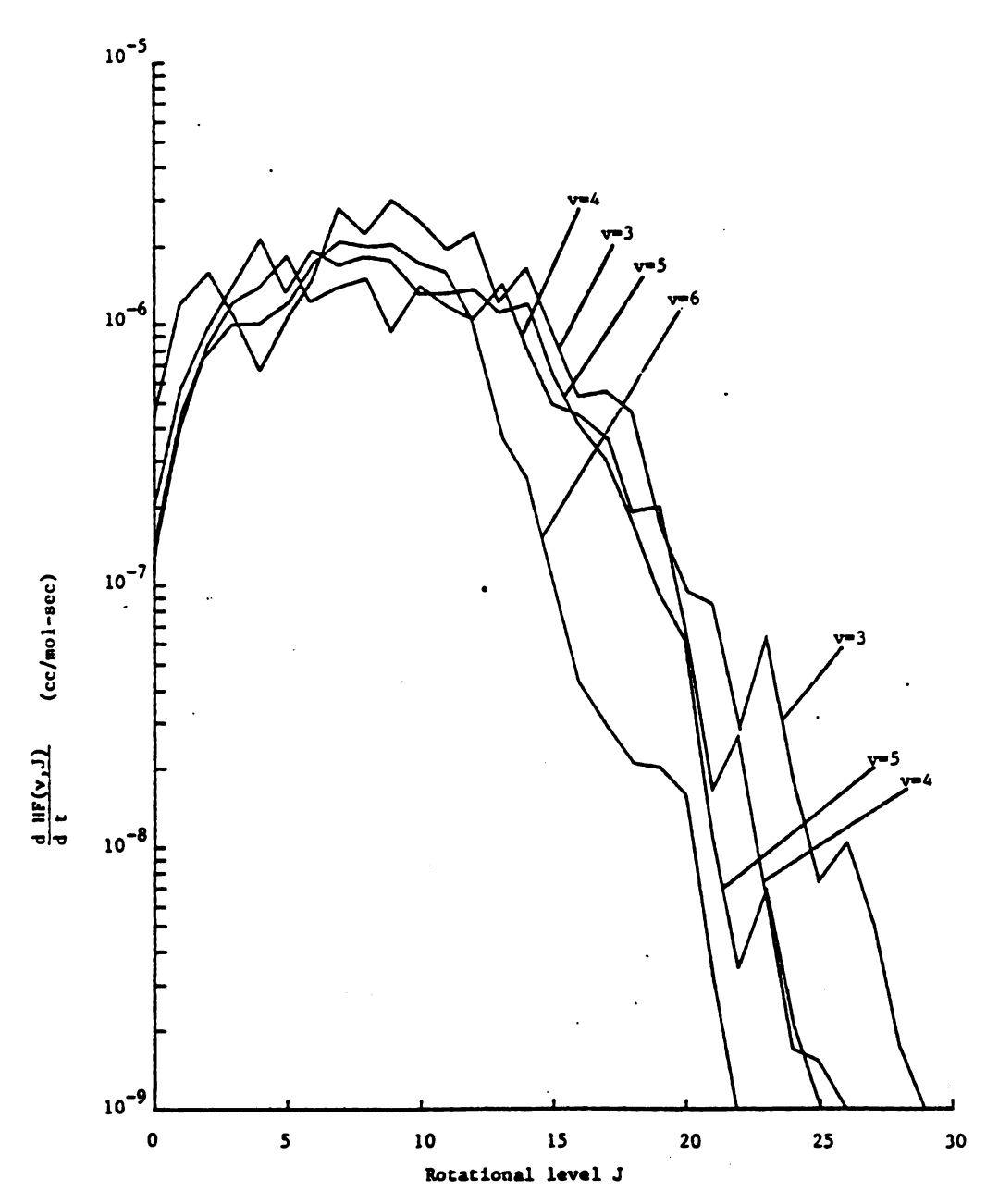


Figure 4.3b. Total contribution to the derivative of HF(v,J) at peak power for run 18a.

The relative band energies in Table 4.2 indicate that the maximum band energy for cases 12a and 12b is found in the 5-4 band which is inconsistent with experimental observations. The maximum band energy for run 12c and 18a are on the 2-1 band which is consistent with experimental observations. The excess energy in the hot bands could be reduced by incorporating the recent recommendation for the vibrational pumping distribution of Cohen [22] or Cummings et al [25]. From Table 1.2 it can be seen that a significant reduction in the direct population of vibrational levels 4 to 8 due to pumping would result if Cohen's [22] or Cummings et al [25] pumping distribution were adopted over the distribution recommended by Cohen [24] and employed in the present formulation. The effect of VR and VV relaxation mechanisms also are believed to contribute to the excess energies observed in the hot bands. The decrease in pulse energy, maximum power and time to maximum power for multiquanta VR cases over single quanta VR cases is consistent with the predictions of the comprehensive VT, RT model of Kerber and co-workers [72-74].

The total power for cases 12a, 12b, 12c, and 18a are compared in Figure 4.4. Comparing cases 12a and 12b in Figure 4.4 illustrates the effect of single and multiquanta VR on pulse energy, maximum power and time to maximum power. As more VR channels about J become available the pulse energy decreases.

The time resolved spectra of Run 18a for all 72 P branch transitions considered are illustrated in Figure 4.5. The initial spike in the power is a result of the instantaneous introduction of a finite amount of F atoms. This effect would be less pronounced if F atoms were introduced over a longer period of time by the dissociation of F,

Table 4.2 Effect of VR<sup>a</sup>

	Single or			Rel	Relative Band Energies	Band Er	nergies	m	R. V.R.	P			
Case	VR	dist. <sup>b</sup> 1-0	1-0	2-1	2-1 3-2 4-3 5-4 6-5	4-3	5-4	95	3/8	w/cc	w/cc max	Final	ບູ
12a	single	3	0.12	0.58	0.30	0.57	1:0	0.58 0.30 0.57 1:0 0.94 0.52	0.52	8.64	8.64 64.0	105.7	0.3
12b	multi	e	0.14	0.43	0.09	0.15	1.0	0.43 0.09 0.15 1.0 0.91	0.32	4.69	4.69 10.4	103.5	0.3
12c	single	7	0.31	1.0	0.38	0.38 0.61		0.86 0.29 0.28	0.28	7.16	7.16 11.1	72.0	9.0
18a	multi	4	0.64	1.0		0.19	0.83	0.22 0.19 0.83 0.51 0.15	0.15	5.45	5.42 10.1	78.9	0.5

cavity conditions:  $R_0 = 1$ .,  $R_L = 0.8$ , L = 20 cm,  $\ell = 20$  cm, P branch lasing. <sup>a</sup>Gas mixture: 0.02F:0.99F<sub>2</sub>:1H<sub>2</sub>:20H<sub>e</sub>, T<sub>1</sub> = 300°k, P<sub>1</sub> = 20 torr

 $^{
m b}$ The distributions for VR relaxation are listed in Table 4.1 with a probability of vibrational relaxation of 1.

<sup>c</sup>The degree of completion  $\varepsilon$  is (F<sub>2</sub>Final)/(F<sub>2</sub>Initial).

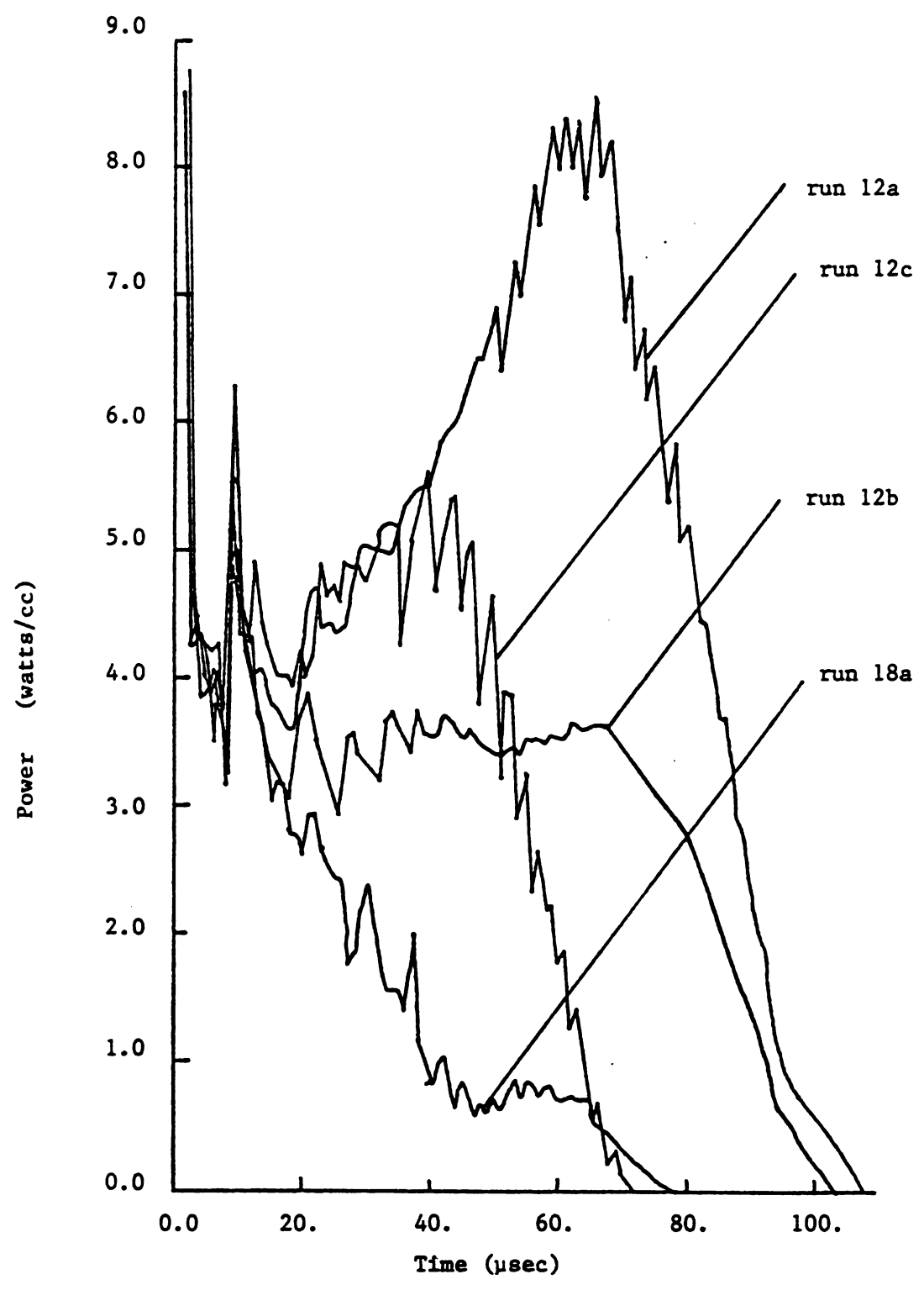
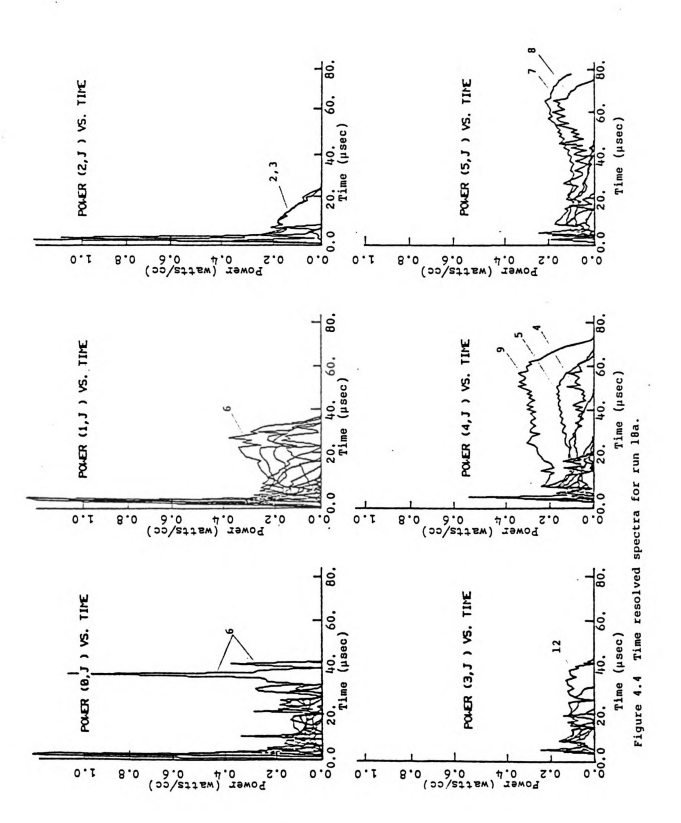


Figure 4.4. Comparison of the total power as a function of time



given by Equation 3.25. The rapid oscillations in the power is much more pronounced than the VR,T model of Kerber et al. [73,74]. This phenomena is believed to be caused in part by the rapid redistribution of energy levels of HF(v,J) by multiquanta VR. The late time powers observed in the hot bands is quite pronounced. The mechanism contributing to the spectra of  $P_4(12)$  is believed to be caused in part from the suppression of P branch lasing from rotational levels greater than 12. The mechanism resulting in lasing from  $P_5(4)$ ,  $P_5(5)$ ,  $P_5(4)$ ,  $P_6(7)$  and  $P_6(8)$  is not clear although examination of the population of HF(v,J) at 50 µsec in Figure 4.1 indicates that the population of HF(4,J) and HF(5,J) are nearly equal from J equals 0 to 12.

## 5. SUMMARY

A comprehensive model of the pulsed  $H_2+F_2$  chemical laser system has been presented. The assumption of rotational equilibrium has been relaxed for all mechanisms contributing to the population of HF(v,J). This model permits examination of the effect of VR, VV, RR and RT relaxation mechanisms on the spectral content of the laser pulse. The model is also capable of examining the effects of various nonequilibrium pumping distributions and line selection on the time resolved spectra.

This comprehensive model supports the conclusion of Wilkins [51] that VR relaxation processes are responsible for populating very high rotational levels of HF. The effect of multiquanta VR relaxation was found to increase the population of the upper rotational levels (J>15) of HF over the entire pulse duration while RR and RT relaxation mechanisms slowly depleted these levels. The VV relaxation mechanism permits the energy of a given HF(v,J) to be transferred to HF(v-1,J) or visa versa which has the effect of redistributing a given rotational level over all vibrational levels.

Recent experimental results indicate that rotational lasing may be significant. The present formulation is being extended to assess the effects of rotational lasing on the population time histories and time resolved spectra.

#### APPENDIX A

RATE COEFFICIENTS FOR THE H<sub>2</sub> + F<sub>2</sub> CHEMICAL LASER

The rate coefficients that have been recommended by Cohen [22] and incorporated in the present formulation for dissociation, recombination, cold and hot pumping,  $HF-H_2$  VV and  $H_2-H_2$  VT energy transfer are presented in Table A.1.

The cold pumping rates that have been suggested by Cohen [22,24] and Cummings et al. [25] are compared in Figure A.1. The specific cold pumping reactions listed in Figure A.1 are plotted as a function of temperature for the listed forward rate. Reactions for all figures in this appendix are shown in the exothermic direction. The cold pumping reaction is exothermic in Figures A.1(a) to A.1(c) and endothermic in Figures A.1(d) to A.1(j). Both the forward and reverse rate coefficients are included in the model. The hot pumping rates are compared in Figure A.2. In the present study the rate coefficients recommended by Cohen [24] listed in Table A.1 are combined with the rate coefficients calculated by Wilkins [51] for VV, VR, and rotational relaxation of HF to form a chemical kinetic model of the pulsed H<sub>2</sub> + F<sub>2</sub> laser system.

The VV rates calculated by Wilkins [51] are compared with the VV exchange rates suggested by Cohen [22,24] and Cummings et al. [25] in Figure A.3. The multiquanta VR rates calculated by Wilkins [51] are only valid for collisions of HF with HF. For collision partners other than HF, Wilkins rate coefficients are scaled according to the recommended VR,T rates of Cohen [22]. These rate coefficients are compared with the suggested rate coefficients of Cohen [22,24] and Cummings et al. [25] in Figure A.4. The recommended rate coefficients

of Cohen [24] assume that the VR-T rates are linear in v and a single quanta, while those rates recommended by Cohen [22] and Cummings et al. [25] have a  $v^{2.3}$  vibrational dependence for multiquanta VR,T reactions.

Table A.1 Rate Coefficients for the  $H_2 + F_2$  Chemical Laser

Reaction	Collision Partner	: M Forward Rate <sup>a</sup>
Di	ssociation Recombi	nation
F <sub>2 +</sub> M + F + F + M	all species	$\kappa_{f}^{F_2} = 5.*10^{13} e^{-35.36}$
$H + H + M + H_2(0) + M$	all species, 2.9H <sub>2</sub> , 20H	$K_f^{H2} = 1.*10^{19}T^{-1}$
$HF(0) + M \stackrel{+}{+} H + F + M$	all species	$K_{f}^{HF}(0) = 1.2*10^{18}T^{-1}e^{-135.89}$
HF(1) + M + H + F + M	all species	$K_{f}^{HF}(1) = 1.2*10^{18}T^{-1}e^{-124.5\theta}$
HF(2) + M + H + F + M	all species	$K_f^{HF}(2) = 1.2*10^{18} T^{-1} e^{-113.60}$
HF(3) + M + H + F + M	all species	$K_{f}^{HF}(3) = 1.2*10^{18} T^{-1} e^{-103.3\theta}$
$HF(4) + M \stackrel{+}{+} H + F + M$	all species	$K_f^{HF}(4) + 1.2*10^{18}T^{-1}e^{-93.39\theta}$
$HF(5) + M \stackrel{+}{+} H + F + M$	all species	$K_f^{HF}(5) + 1.2*10^{18}T^{-1}e^{-83.96\theta}$
$HF(6) + M \stackrel{\Rightarrow}{+} H + F + M$	all species	$K_f^{HF}(6) = 1.2*10^{18} T^{-1} e^{-74.978}$
HF(7) + M + H + F + M	all species	$K_f^{HF}(7) = 1.2*10^{18} T^{-1} e^{-66.439}$
	Cold Pumping	
$F + H_2(0) + HF(1) + H$		$K_{f}^{c}(1) = 2.6*10^{13}e^{-1.66}$
$F + H_2(0) + HF(2) + H$		$K_{f}^{c}(2) = 8.8*10^{13}e^{-1.6\theta}$
$F + H_2(0) \stackrel{+}{+} HF(3) + H$		$K_{f}^{c}(3) = 4.4*10^{13}e^{-1.60}$
$F + H_2(0) \stackrel{?}{=} HF(4) + H$		$K_f^c(4) = 1.46*10^{13}T^{-0.107}e^{-11.34\theta}$
$F + H_2(0) + HF(5) + H$		$K_{f}^{c}(5) = 2.17*10^{13}T^{-0.107}e^{-20.786}$
F+ H <sub>2</sub> (0) + HF(6) + H		$K_f^c(6) = 3.76 * 10^{13} T^{-0.107} e^{-29.82\theta}$

<sup>&</sup>lt;sup>a</sup>With the exception of VV and VR,T reactions this table contains the recommended rate coefficients of Cohen [24]. The value of  $\theta$  is 1000/RT. The gas constant R is 1.98725 Kcal/mol- $^{\circ}$ K.

Table A.1 (continued)

Danation	<b>4.11</b>	
Reaction	Collision Partner M Hot Pumping	Forward Rate
H + F <sub>2</sub> <sup>→</sup> HF(0) + F		$K_f^h(0) = 1.1*10^{12}e^{-2.46}$
H + F <sub>2</sub> + HF(1) + F	·	$K_{f}^{h}(1) = 2.5*10^{12}e^{-2.46}$
$H + F_2 \stackrel{?}{=} HF(2) + F$		$K_{f}^{h}(2) = 3.5 \pm 10^{12} e^{-2.40}$
$H + F_2 + HF(3) + F$		$K_{f}^{h}(3) = 3.6*10^{12}e^{-2.4\theta}$
$H + F_2 \stackrel{+}{+} HF(4) + F$		$K_{f}^{h}(4) = 1.6*10^{13}e^{-2.4\theta}$
$H + F_2 \stackrel{?}{=} HF(5) + F$		$K_{f}^{h}(5) = 3.6*10^{13}e^{-2.4\theta}$
$H + F_2 \Rightarrow HF(6) + F$		$K_{f}^{h}(6) = 4.8*10^{13}e^{-2.4\theta}$
$H + F_2 \rightleftharpoons HF(7) + F$		$K_{f}^{h}(7) = 5.5*10^{12}e^{-2.4\theta}$
$H + F_2 \rightleftharpoons HF(8) + F$		$K_f^h(8) = 2.5*10^{12}e^{-2.4\theta}$
	HF-H <sub>2</sub> VV	
$HF(0) + H_2(1) \rightleftharpoons HF(1)$	+ H <sub>2</sub> (0)	$K_{f}^{HF-H}2(0,0) = 9*10^{10}$
$HF(1) + H_2(1) \rightleftharpoons HF(2)$	+ H <sub>2</sub> (0)	$K_{f}^{HF-H}2(1,0) = 2.9*10^{12}$
$\mathrm{HF}(2) + \mathrm{H}_{2}(1) \rightleftharpoons \mathrm{HF}(3)$	+ H <sub>2</sub> (0)	$K_f^{HF-H}2(2,0) = 9*10^{12}$
$\mathrm{HF}(3) + \mathrm{H}_2(1) \rightleftharpoons \mathrm{HF}(4)$	+ H <sub>2</sub> (0)	$K_{f}^{HF-H}2(3,0) = 2*10^{13}$
$HF(0) + H_2(2) \rightleftharpoons HF(1)$	+ H <sub>2</sub> (1)	$K_f^{HF-H}2(0,1) = 9*10^{11}$
$\mathrm{HF}(1) + \mathrm{H}_2(2) \rightleftharpoons \mathrm{HF}(2)$	+ H <sub>2</sub> (1)	$K_f^{HF-H}2(1,1) = 2.9*10^{12}$
	H <sub>2</sub> -H <sub>2</sub> VT	
$H_2(1) + M \rightleftharpoons H_2(0) + M$	all species <sup>4H</sup> 2, <sup>4H</sup>	$K_f^{H_2-H_2(1)} = 2.5*10^{-4}T^{4.3}$
$H_2(2) + M \rightleftharpoons H_2(1) + M$	all species 4H <sub>2</sub> ,4H	$K_f^{H_2-H_2(2)} = 5.0*10^{-4}T^{4.3}$

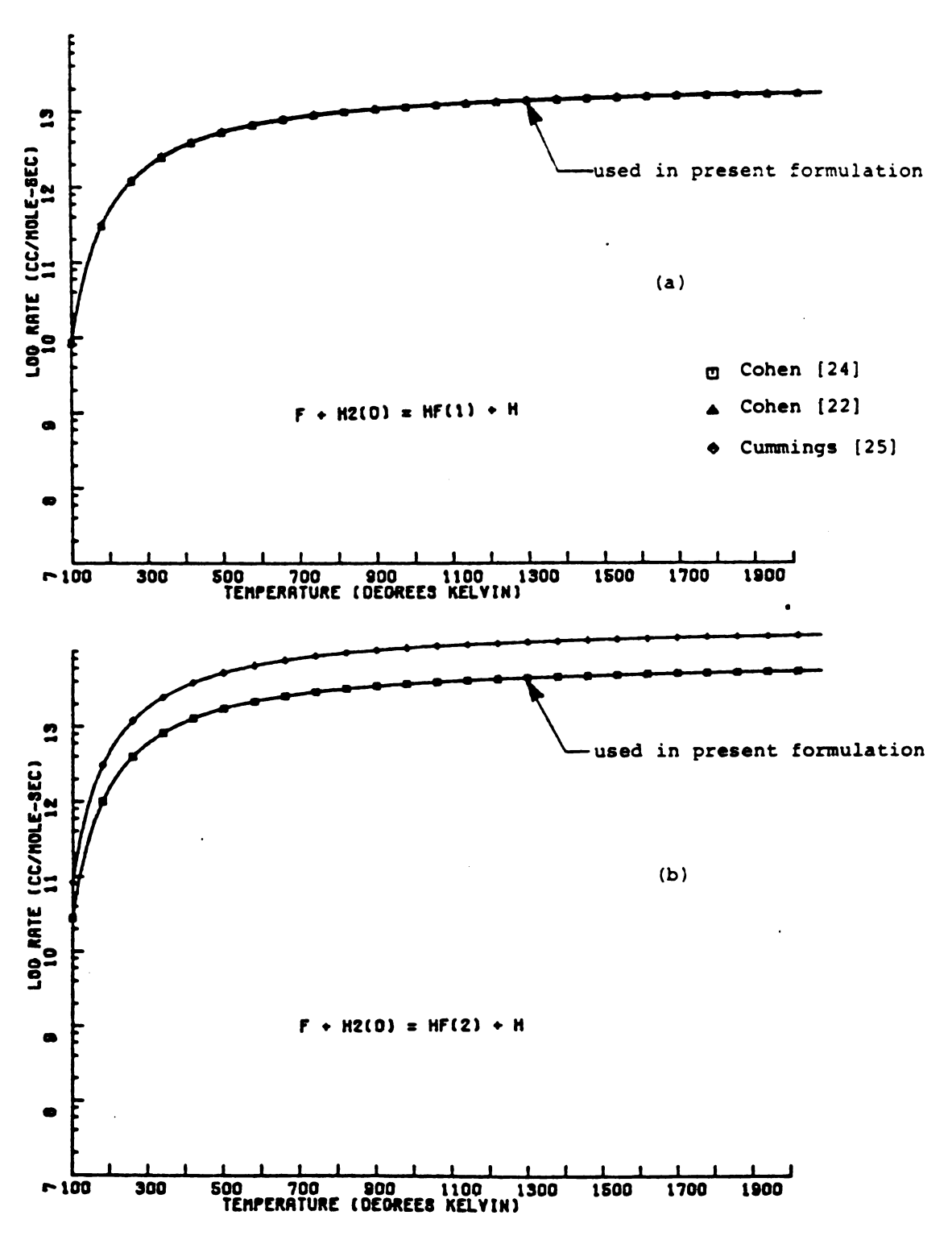


Figure A.1. Pumping rates for the cold reaction.

The pumping rates employed in the present formulation have been suggested by Cohen [24].

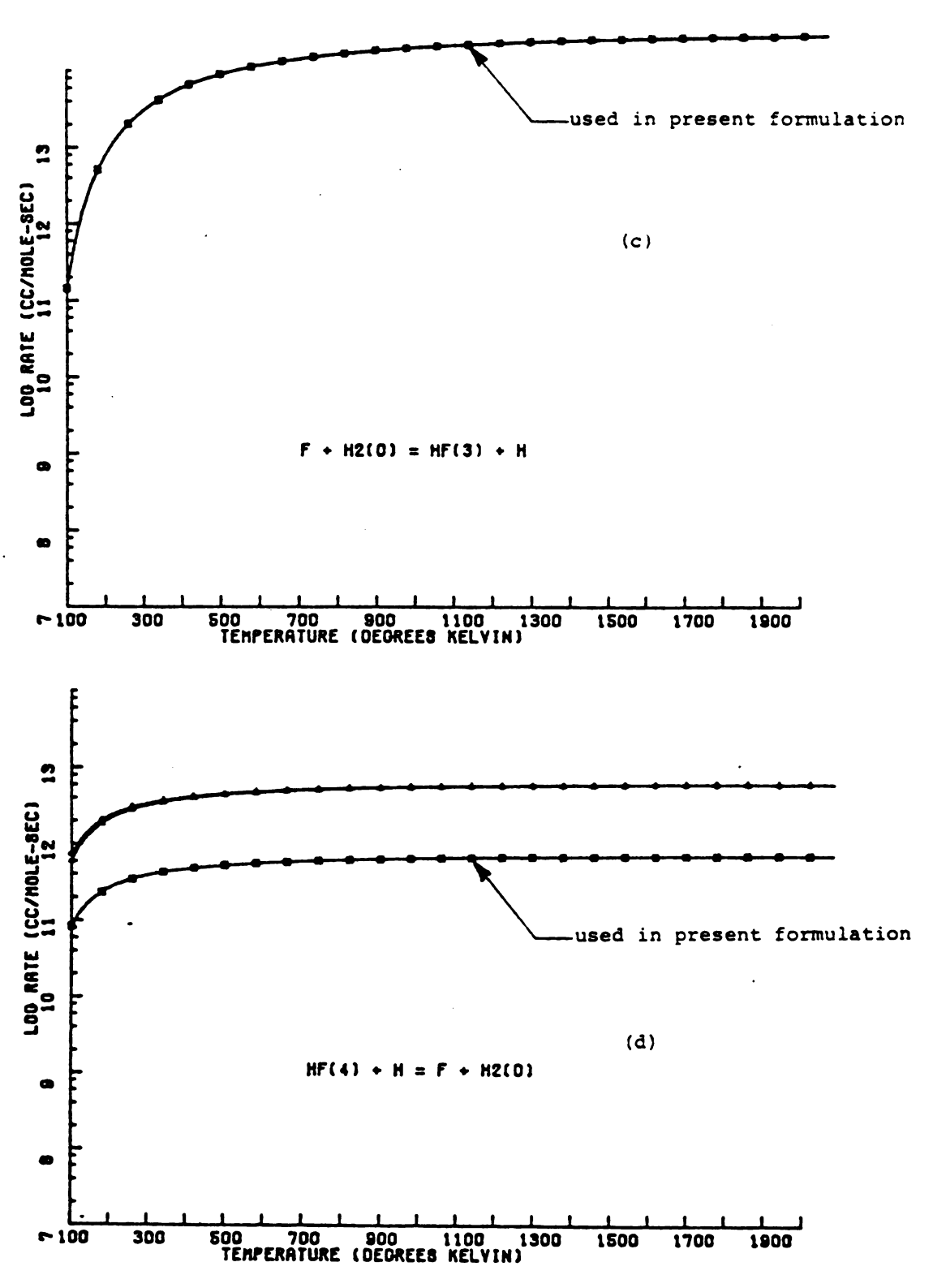
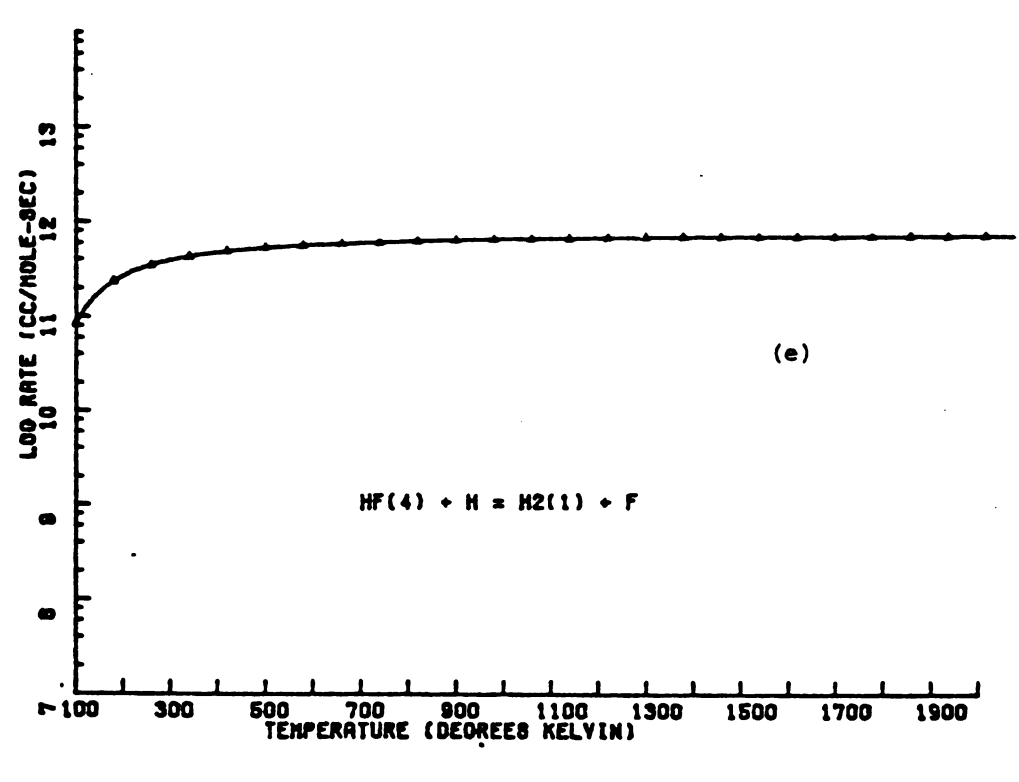


Figure A.1. (continued)



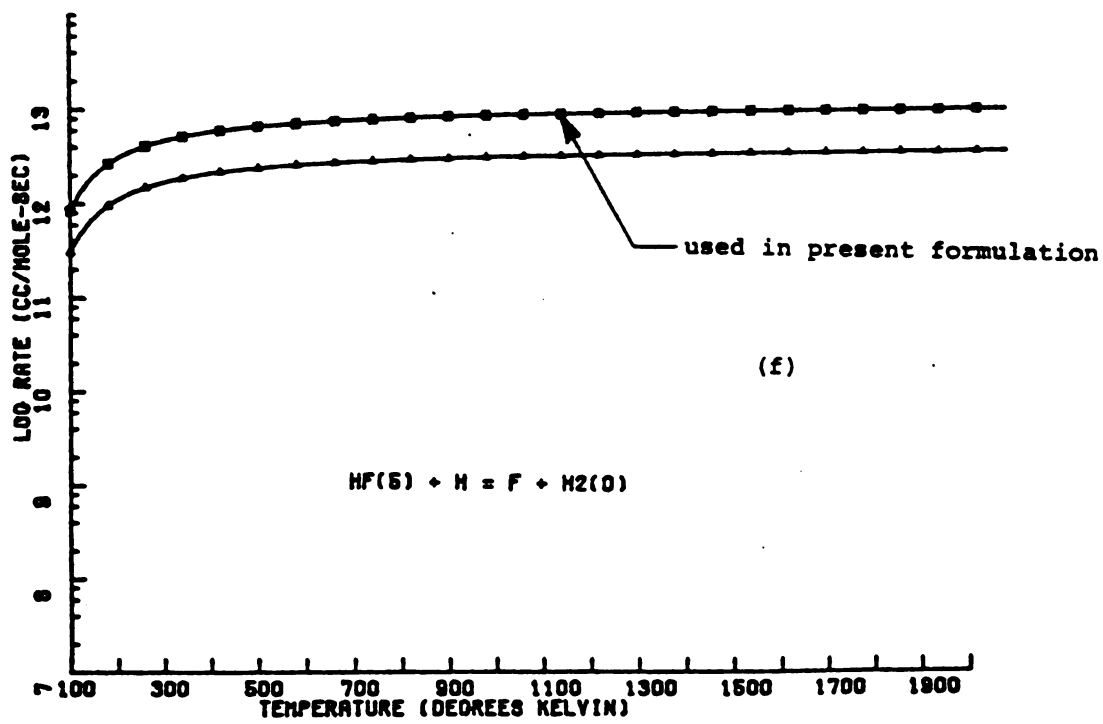


Figure A.1. (continued)

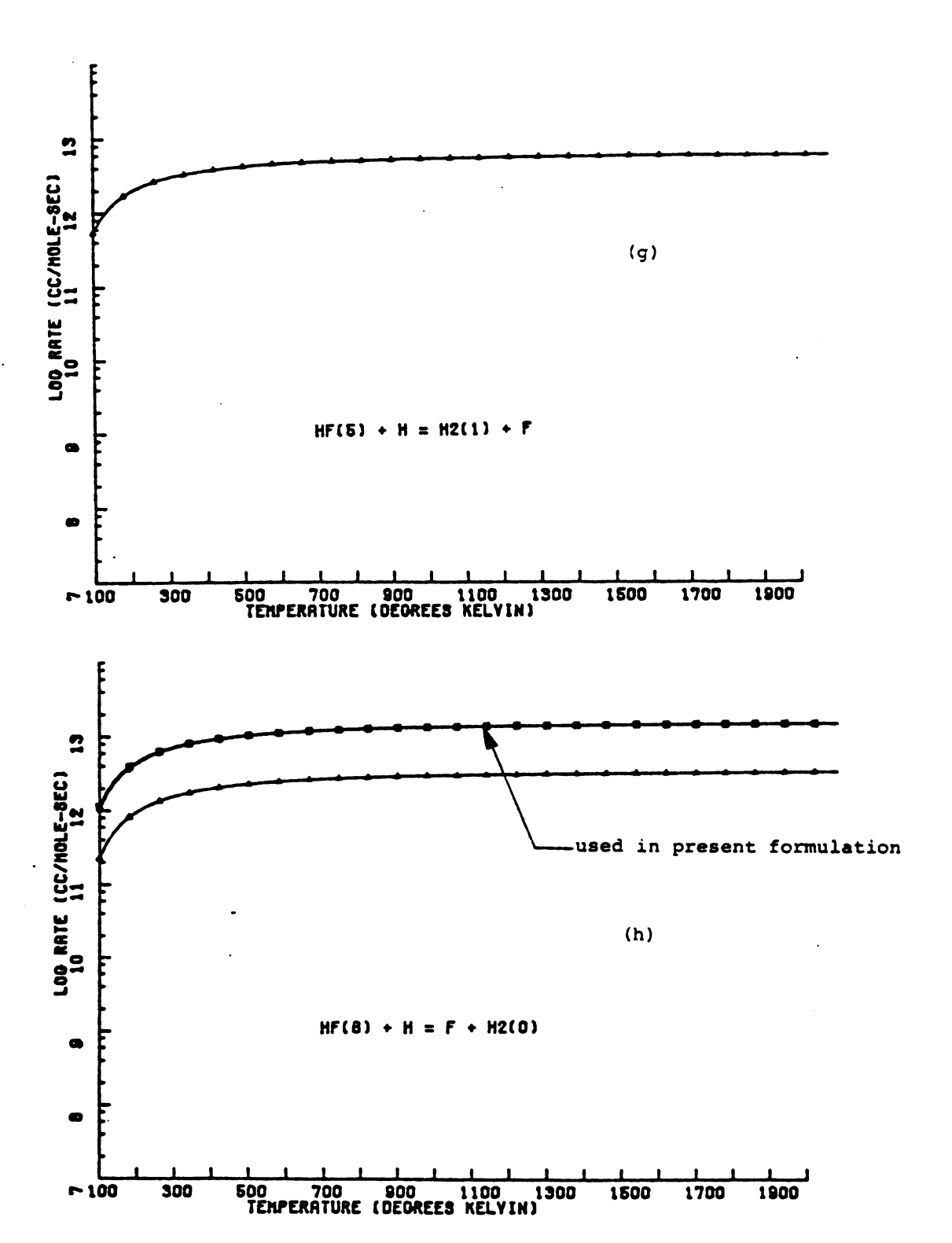


Figure A.1. (continued)

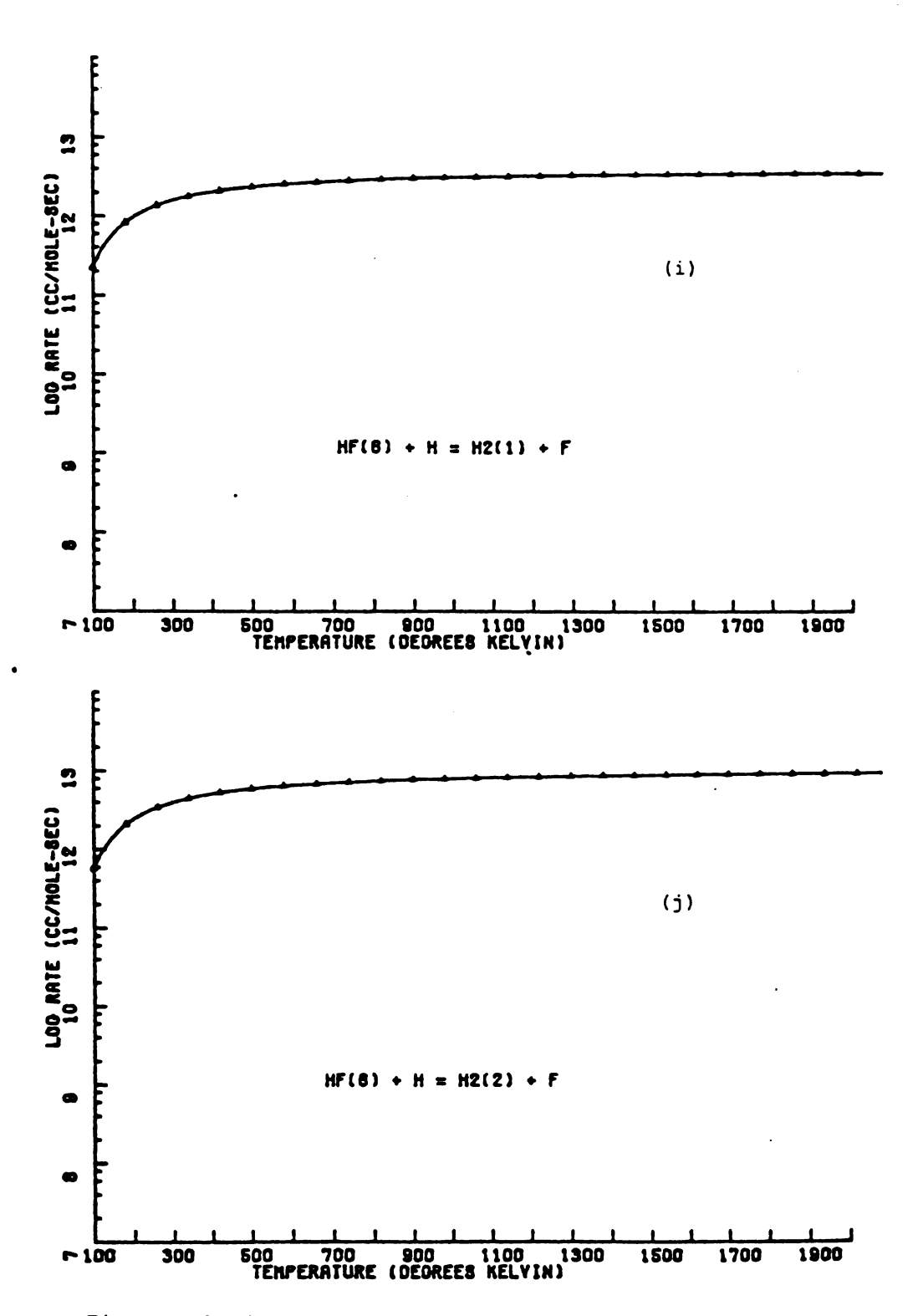


Figure A.1. (continued)

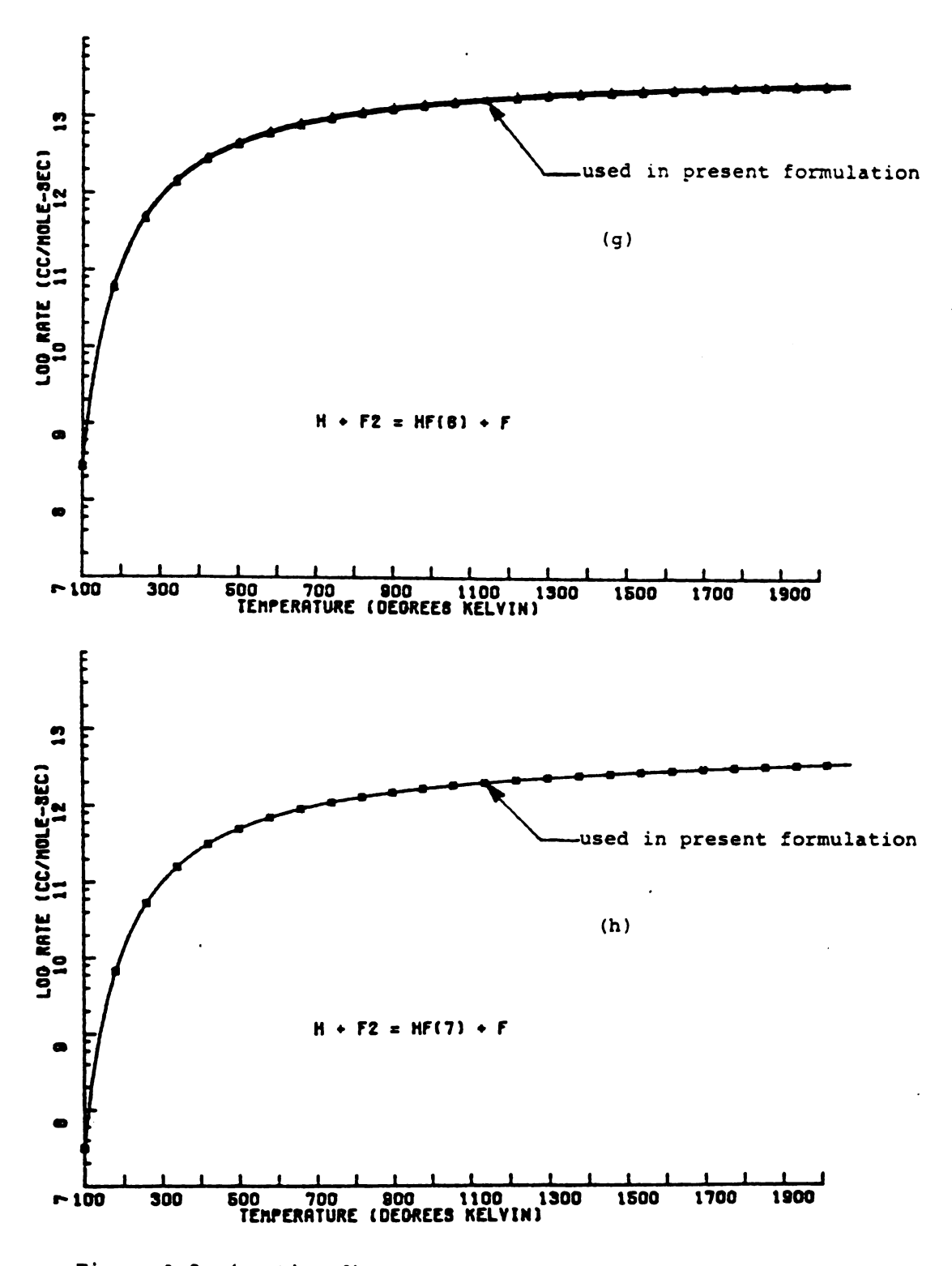


Figure A.2. (continued)

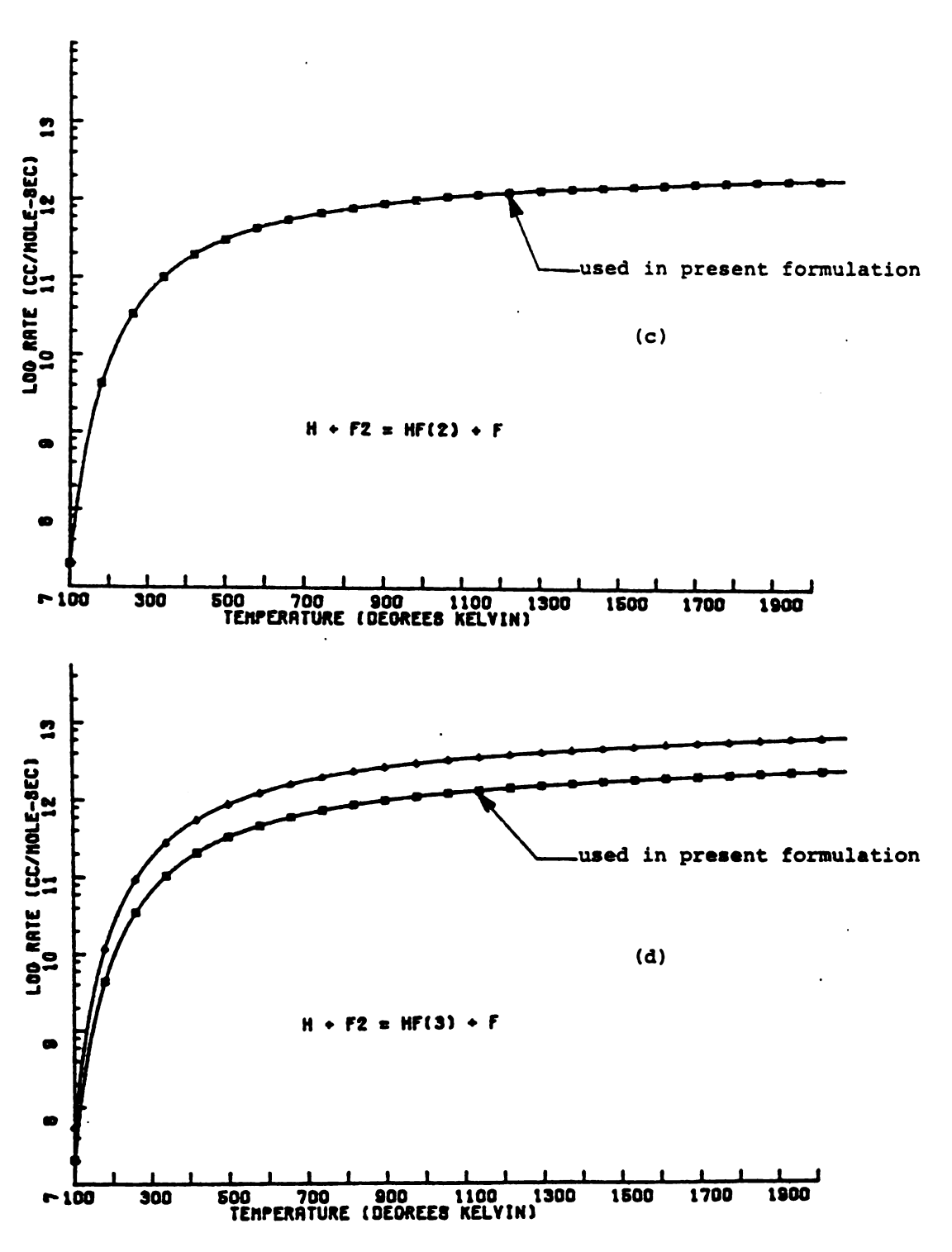


Figure A.2. (continued)

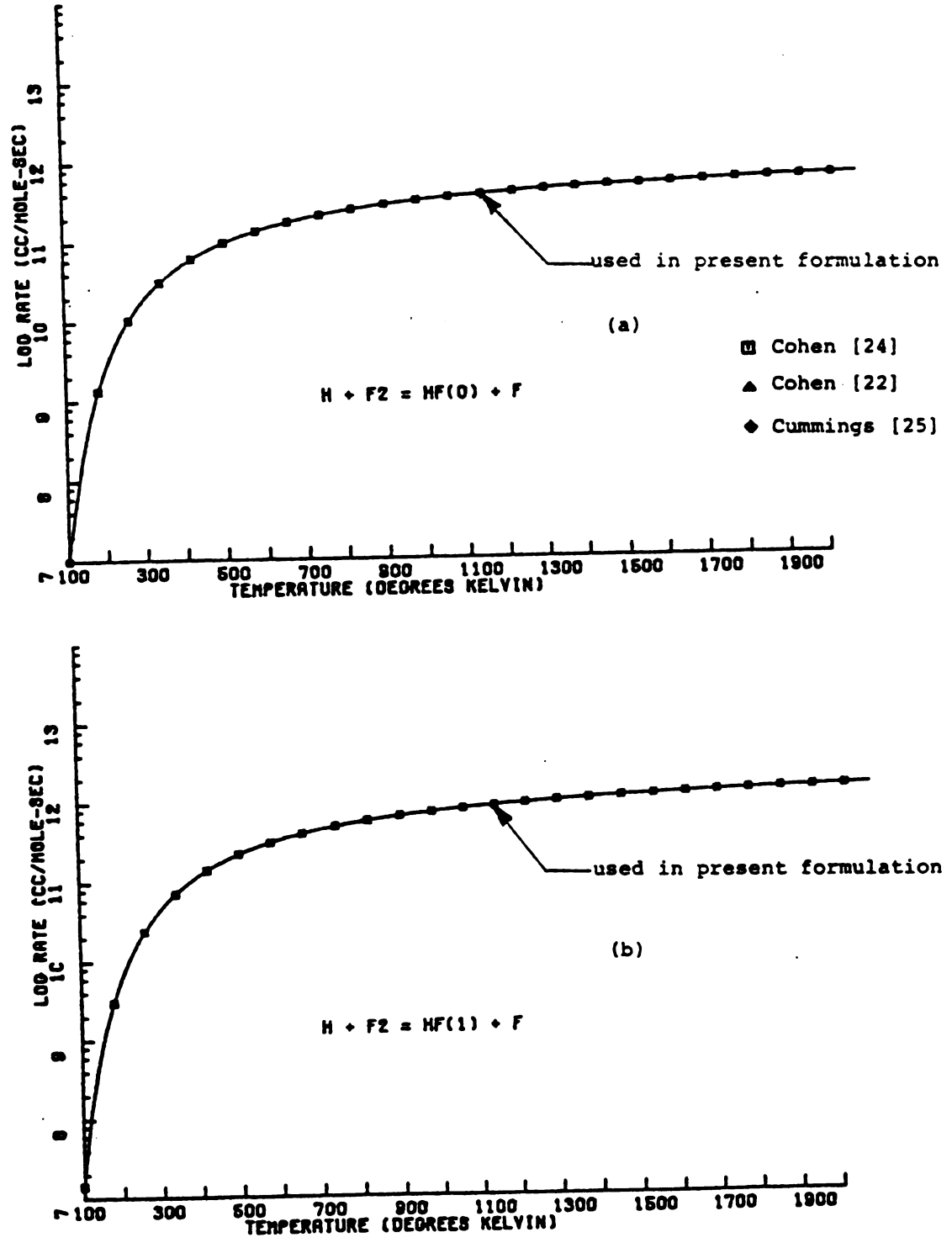


Figure A.2. Rate coefficients for the hot pumping reaction.

The present formulation uses the rate coefficients that have been suggested by Cohen [24].

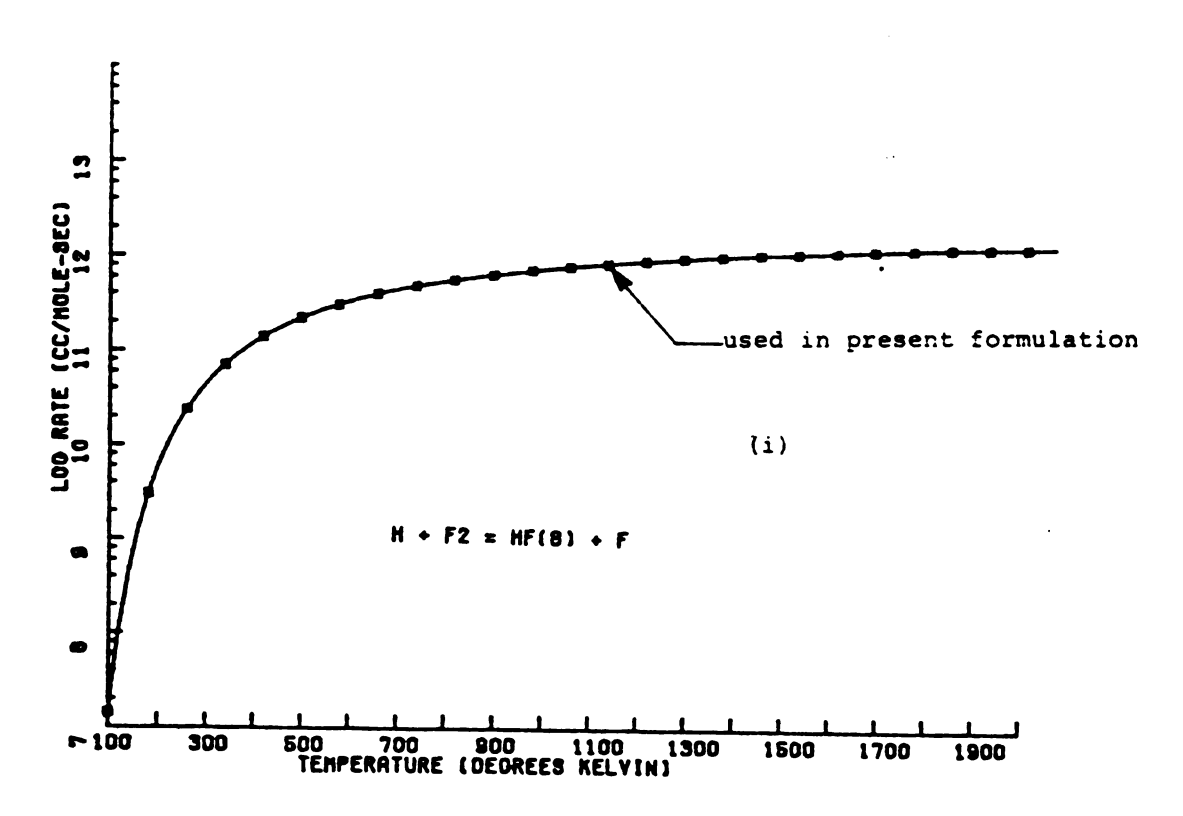


Figure A.2. (continued)

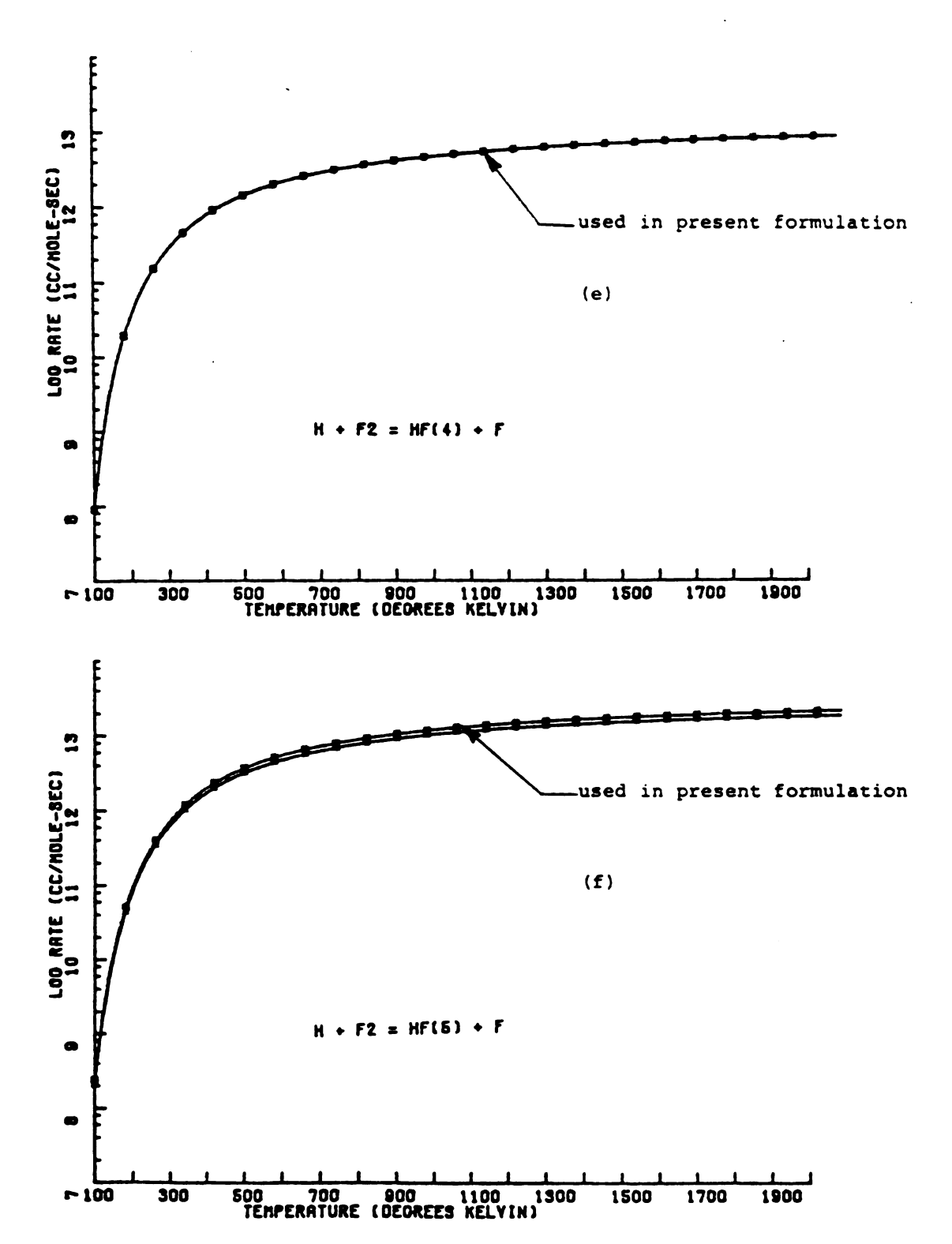


Figure A.2. (continued)

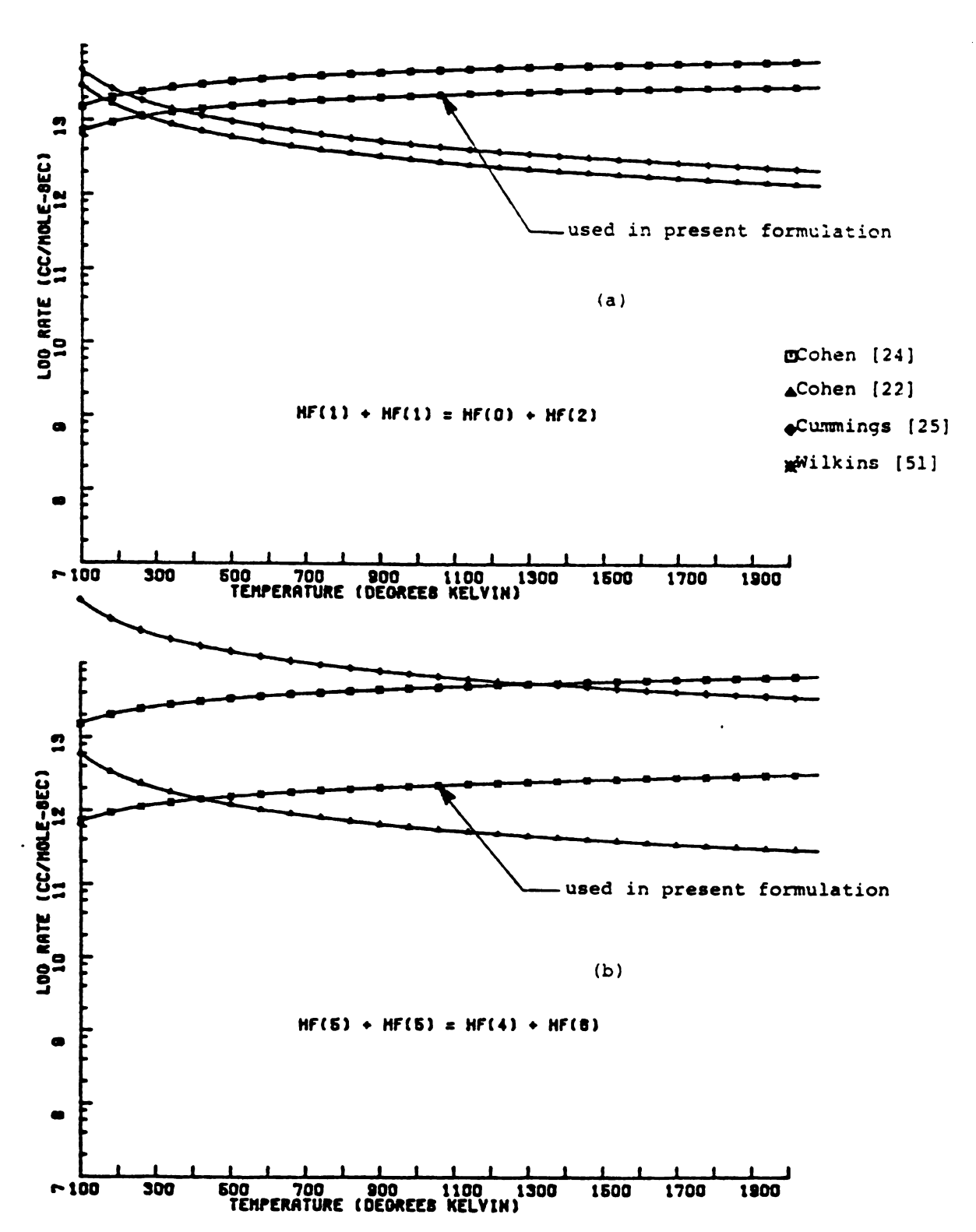
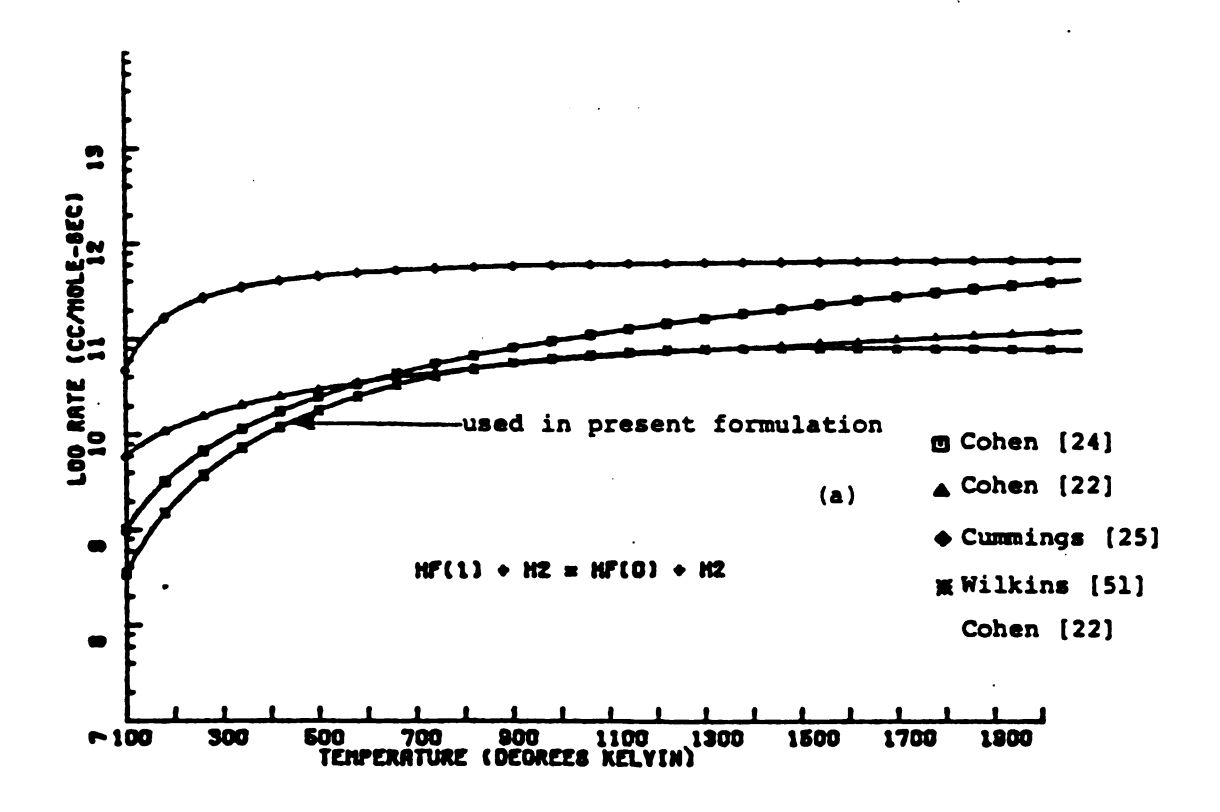


Figure A.3. The temperature dependence of selected vibrational to vibrational exchange rate coefficients. The VV rates calculated by Wilkins [51] and given in Table 1.5 are employed in the present formulation.



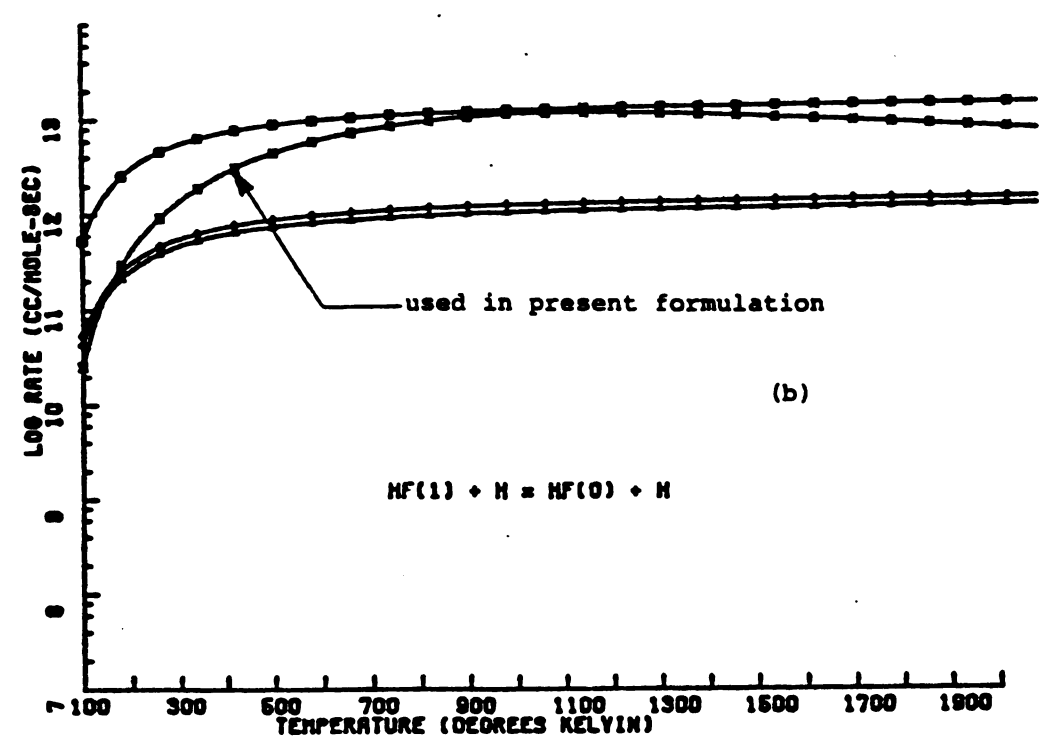
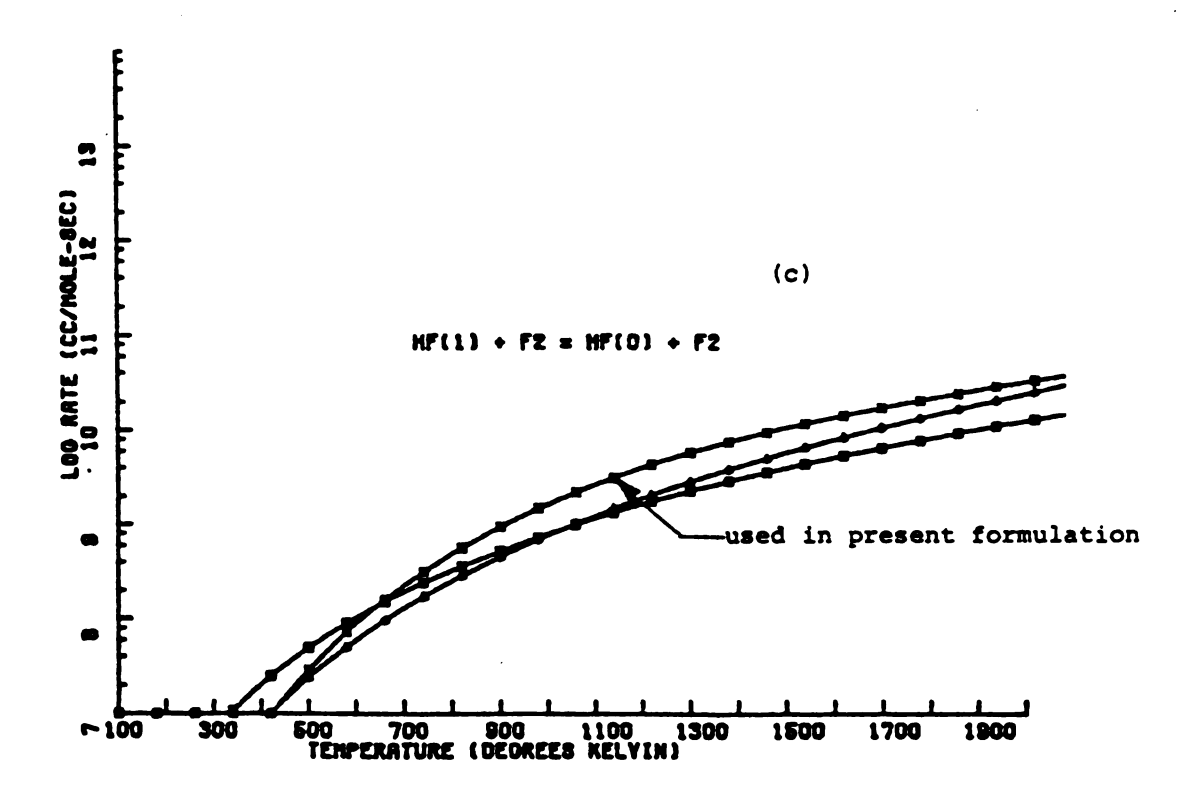


Figure A.4. Vibrational to rotational, translational rates.

Note that for HF+H2,H,F2,H, Wilkins [51] rates are scaled according to Cohen's [22] rates and are employed in the present formulation.



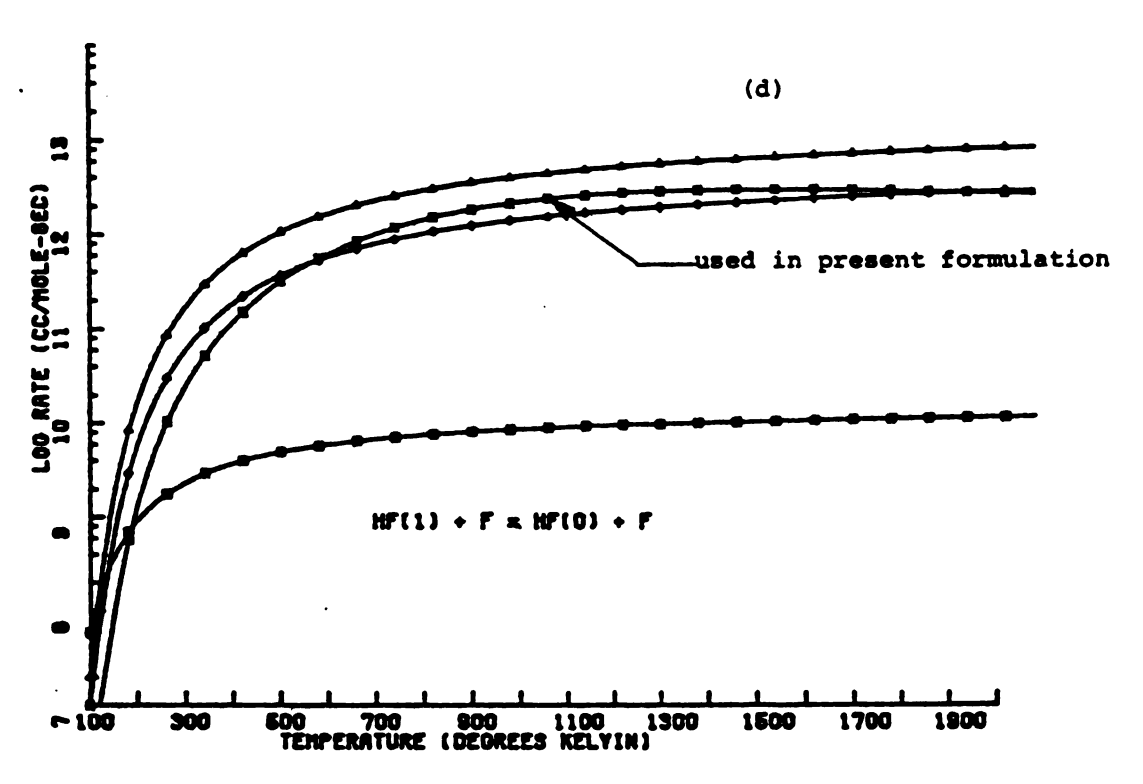


Figure A.4. (continued)

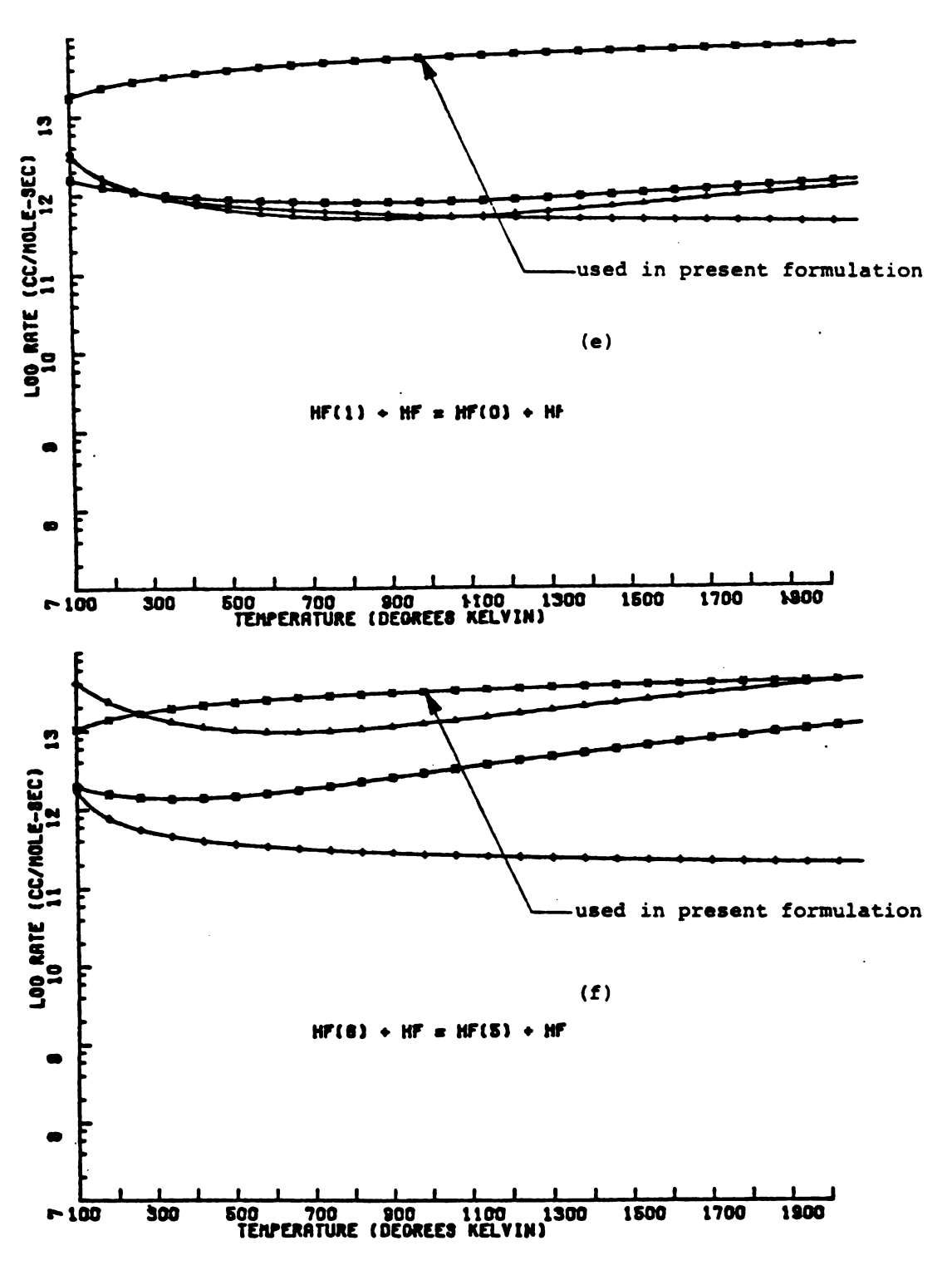


Figure A.4. (continued)

## APPENDIX B

DERIVATION OF X FOR ROTATIONAL LASING

The rate equation for HF(v,J) is

$$\frac{dHF(v,J)}{dt} = X(v,J) + X_{rad}(v,J+1) - X_{rad}(v,J) + A(v,J)$$
 (B.1)

where X(v,J) is the net change in HF(v,J) resulting from chemical reactions and P branch lasing. The rate of change in HF(v,J) due to rotational lasing can be expressed in terms of the gain,  $\alpha(v,J)$ , and  $X_{rad}(v,J)$ . The Einstein coefficient for spontaneous rotational decaying A(v,J) has been tabulated by Meredith [91] and can be expressed in terms of the Einstein isotropic absorption coefficient B(v,J) as shown in Equation B.2.

$$A(v,J) = 2hc\omega_{CR}(v,J)^{3}B(v,J) \text{ molecule}^{-1}-\sec^{-1} \qquad (B.2)$$

The gain coefficient for RR lasing is derived in terms of the Einstein B coefficient, the Voigt profile lineshape function  $\phi(v,J)$ , and the wave number  $\omega_{cR}(v,J)$  of the transition (v,J+1)+(v,J). This gain coefficient can be written as [72]

$$\alpha_{R}(v,J) = \frac{hN_{A}\omega_{cR}}{4\pi} (v,J)B(v,J)[\frac{2J+1}{2J+3}HF(v,J+1) - HF(v,J)]. \quad (B.3)$$

The gain coefficient has been estimated by Hinchen [34] to be on the order of 1 cm<sup>-1</sup> for a population difference of  $10^{-4}$  torr and cross section of  $2.2 \times 10^{13}$  cm<sup>2</sup>. Similar gains have been measured by Skirbanowitz et al. [43] with the same range of wavelength and pressure. The rate of photon emission  $X_{rad}(v,J)$  can be written in terms of the photon flux and the gain [72].

$$X_{rad}(v,J) = \alpha_{R}(v,J)f_{R}(v,J)$$
 (B.4)

The present formulation is capable of modeling rotational lasing based upon Equation (B.4) which requires up to 210 additional rotational lasing flux variables to be integrated. However, the model currently requires over 30 minutes on a CDC 7600 for a typical run and the additional variables may significantly increase computation time. An alternate expression for  $X_{\rm rad}(v,J)$  will be derived which does not require additional integration variables. If a population inversion exists then the following condition holds

$$\frac{2J+1}{2J+3} HF(v,J+1) - HF(v,J) \ge 0$$
 (B.5)

With the large gains that have been observed it may be reasonable to expect that during lasing

$$\frac{d\alpha_{R}(v,J)}{dt} = 0 (B.6)$$

hence Equation (B.3) reduces to

$$\frac{2J+1}{2J+3} \frac{dHF(v,J+1)}{dt} - \frac{dHF(v,J)}{dt} = 0.$$
 (B.7)

If equality is assumed in Equation (B.7) then Equations (B.1) and (B.7) may be solved for the rotational lasing photon emission rate  $X_{\rm rad}(v,J)$ .

$$\left[\frac{2J+1}{2J+3}+1\right] X_{rad}(v,J) = \frac{2J+1}{2J+3} X(v,J+1) - X(v,J)$$
 (B.8)

For two adjacent lasing transitions,  $X_{rad}(v,J)$  and  $X_{rad}(v,J+1)$  can be written as

$$\left[\frac{2J+1}{2J+3} + 1\right] X_{rad}(v,J) - \frac{2J+1}{2J+3} X_{rad}(v,J+1) = \frac{2J+1}{2J+3} X(v,J+L) - X(v,J)$$

$$- X_{rad}(v,J) + \left[\frac{2J+3}{2J+5} + 1\right] X_{rad}(v,J+1) = \frac{2J+3}{2J+5} X(v,J+3) - X(v,J+1) .$$
(B.9)

With inductive reasoning Equation (B.9) can be generalized to a system of n adjacent lasing transitions with n unknowns.

$$A = B X_{rad}$$
 (B.10)

where B(k) is given by

$$B(k) = G_k \frac{dHF(v,k+1)}{dt} - \frac{dHF(v,k)}{dt}$$
(B.12)

and the degeneracy factor  $G_{k}$  is given by

$$G_{k} = \frac{2k+1}{2k+3} \tag{B.13}$$

The matrix A defined by Equations (B.10) and (B.11) is a continuant matrix. The matrix A can be readily transformed to the upper triangular matrix A'.

$$A' = B'X_{rad}$$
 (E.14)

Since there are non zero terms only on the main diagonal and the diagonal above it, a simple algorithm can be developed to obtain  $\mathbf{X}_{\text{rad}}$  by noting that

$$X_{rad}(n) = \left[1+G_n - \frac{G_{n-1}}{1+G_{n-1}}\right] / \left[B(n) + \frac{B(n-1)}{1+G_{n-1}}\right]$$
 (B.16)

and through repeated substitution  $X_{rad}(k)$  is obtained

$$X_{rad}(k) = \left[ -G_k X_{rad}(k+1) - B(k) + \frac{B(k-1)}{1+G_{k-1}} \right] / \left[ 1+G_k - \frac{G_{k-1}}{1+G_{k-1}} \right]$$
 (B.17)

The photon emission rate for the  $k^{th}$  transition  $X_{rad}(k)$  can be obtained in terms of known quantities through Equation (B.16). This derivation assumes that all elements in  $X_{rad}$  are positive which means that if a negative  $X_{rad}(k)$  is obtained the system of n adjacent lasing transitions is re-evaluated for k-l adjacent transitions. Once the solution vector  $X_{rad}$  is obtained with all elements positive the matrix A' is reformulated for the subgroup of transitions from k+l to n. A new group of n transitions is then reformulated based upon the criterion of Equation (B.5). This process is repeated until all positive  $X_{rad}$  have been computed.

The rotational lasing power  $P_{RR}(v,J)$  may be expressed in terms of  $X_{rad}(v,J)$  as

$$P_{RR}(v,J) = hcN_A^{\omega}_{cR}(v,J) \quad X_{rad}(v,J) \quad . \tag{B.18}$$

where the rate of photon emission  $X_{rad}(v,J)$  can be written in terms of Equation (B.4) or (B.17).

#### APPENDIX C

# DESCRIPTION OF COMPUTER SIMULATIONS FOR THE PULSED HF CHEMICAL LASER

The simulation of the pulsed HF laser system is accomplished through the numerical integration of Equations (3.27), (3.30), and (3.38). The basic structure of the computer model consists of a controlling main program designated by MSUHFVR, and five major subroutines designated PRINT, HFRATE, GAIN, RKF45, and DIFFUN. The purpose of MSUHFVR is to initialize computational variables such as species concentration, photon flux, temperature and time; define the cavity conditions; obtain the necessary spectroscopic and thermodynamic data from data files; and provide control parameters that direct the laser simulation. Subroutine HFRATE obtains the forward reaction rate constants and the detailed balance factors. Subroutine GAIN is used to compute the medium gain of the laser for any given allowed P branch transition by means of Equation (3.32). The population difference in Equation (3.32) is computed in DIFFUN to reduce discontinuities in computing Equation (3.30).

Time progression within the model proceeds along user definable integration steps from time  $\tau$  to  $\tau_{\rm out}$ . Numerical integration is accomplished through subroutine DIFFUN, which utilizes a fourth order Runge-Kutta technique developed by Shampine and Watts [92]. The derivatives required for the integration are computed from rate Equations (3.27), (3.30), and (3.38) and are obtained by means of subroutine DIFFUN. Laser initiation may be accomplished by the introduction of a finite amount of F, F<sub>2</sub> and H<sub>2</sub> at a given temperature. Other gases such as HF, He, Ar, N<sub>2</sub> and SF<sub>6</sub> may also be present.

Fluorine atoms may also be produced by photodissociation of  $F_2$  in Equation (3.25).

A Warnier-Orr diagram describing the computer model is presented in Figure C.1. The important variables and symbols used in the computer program, listed in Figure C.1 and discussed in the text are defined in Table C.1. This diagram is an overview that illustrates the hierarchy and structure that produces a chain of commands and decisions that are followed to obtain the time evolution of species concentrations within the laser medium as well as temperature, and gain on all transitions and the intensity on all lasing transitions. The Warnier-Orr diagram illustrates the hierarchy of the processes involved in the simulation of the pulsed HF laser by observing that the leftmost brace denotes the main program MSUHFVR. The series of braces to the right of MSUHFVR brace. The computer simulation proceeds from the first process in the first level INPUT through the tree structure to the last process in the first level TERMINATE RUN. The initial conditions are printed by subroutine PRINT prior to the INTEGRATION LOOP. The INTEGRATION LOOP is a recursive structure that calls subroutine RKF45 which computes the solution vector  $Y_i$  at  $T_{out}$  based upon the values of  $Y_i$  at T and the derivatives of  $Y_i$ . The variables  $Y_i$  constitute a 298 variable one-dimensional array and contain the species concentration, photon flux and temperature. The INTEGRATION LOOP calls subroutines RKF45, GAIN, HFRATE, and PRINT. The computer simulation is terminated when the total power P drops below 1% of the maximum power P and the time is greater than the expected pulse duration T<sub>Final</sub>. For computer simulations where P branch lasing is suppressed the simulation is terminated when T is greater than T final. Due to

program execution times exceeding 30 minutes on a CDC 7600 the Fortran

Program MSUHFVR produces a file that is capable of restarting the simulation at a later date if desired.

	BECIN MSUNFVR		
		/ Concentrations	{ F, F <sub>2</sub> , II <sub>2</sub> , HF, He, Ar, N <sub>2</sub> , SF <sub>6</sub>
		Cavity Conditions	{ R, R <sub>0</sub> , L, t, T <sub>1</sub> ,Flux, T <sub>Flash</sub> , Z <sub>1</sub> , Z <sub>2</sub>
	ţ	Spectroscopic	{ E(v,J), w <sub>c</sub> (v,J), B(v,J), Jeran(kkk), Q <sub>v</sub> (T)
		Thermodynamic	{ F <sub>B</sub> (J,T), H <sub>1</sub> (T), C <sub>V1</sub> (T), F(J,T), CCC
		Lusing	SSG, Av. 2 Boltzmann Pumping. Igain
			N Variables = 298
		Integration Control	Time = 0.0
			T <sub>Out</sub> = Stepsize
		Define Constants	{ $hcN_A$ , $\frac{cL}{t}$ , $u_{cR}(v,J)$ , $\alpha_{thr} = -\frac{1}{2L} \ln(R_0 I_L)$
MSUNFVR	INITIALIZATION	Pumping Rotational	$P_{c}(v, J)$ $F + H_{2}(v') \neq HF(v, J) + H$
		Discribution	$\begin{cases} P_h(v,J) & \{H+F_2 + HF(v,J) + F \} \end{cases}$
		Initialize to Zero	Pyk(v,J),PRR(v,J), EyR(v,J), ERR(v,J), "((v,J), Pyk' Pkk' Ekk'
			Y <sub>1</sub> , 1t 1t 1t N Steps, N Unsuccessful, Ktdiff, P <sub>Mix</sub>
		Convert from lorr to mol/cc and Place in Y	{ F, F <sub>2</sub> , H <sub>2</sub> (v'), He, Ar, N <sub>2</sub> , SF <sub>6</sub>
	I <sub>Restart</sub> " ()	B ≠ 0	Place infrigible to vibrational (v) and rotational (I) thermal equilibrium
	Restart # 0	RESTART MSHIIFVR	Start the simulation from prior conditions. Call RESTART $\{$ Time, Y, $E_{VR}(v,J)$ , $E_{RR}(v,J)$ , $T_{Max}$ , $T_{Max}$
	PRINT	Print the initial conditions Call PRINT	Time, Y.o.(v.1), Pur, Eur, Pur(v.1), Eur(v.1), Per, Err Per(v.1), Err(v.1), Theft

Figure C.1. A Warmier-Our [90] diagram of the Fortran program MSUHEVE, a comprehensive computer model of the pulsed  ${\rm H}_2+{\rm F}_2$  laser system.

Figure C.1. (Continued)

Four and Energy due to P branch lasting (v, J) < Flux   ((v, J) - Flux   Flux   ((v, J) - Flux   ((v, J) - Flux   Flux   Flux   ((v, J) - Flux   Flux   Flux   ((v, J) - Flux   Flux   Flux   Flux   ((v, J) - Flux   Flux   Flux   ((v, J) - Flux   Flux   Flux   Flux   ((v, J) - Flux   Flux   Flux   Flux   ((v, J) - Flux   Fl	HI - Time - Told		
Compute Power and Energy (v=0,5) (J=0,12)  Computer Power and Energy (v=0,6) (J=0,28)  A new peak power has Pax = FyR The power is less that The power is less that The power is less that	Tout - Time + Stepsi	. ze	
Compute Power and Energy (v=0,5) (J=0,12)  Computer Power and Energy (v=0,6) (J=0,28)  A new peak power has Pax			Power and Energy due to P branch lasing f(v,J) < Flux { (v,J) = Flux PyR(v,J) = hcNathrac(v,J)f(v,J) PyR = PyR + PyR(v,J)
Computer Power and Energy (v=0,6) (J=0,28) A new peak power has Pax = VR Thax = VR The power is less that the powe		Compute Power and Energy (v=0,5) (J=0,12)	$P_{VR}^{Out} = P_{VR} \begin{bmatrix} 1 & -R_0 \\ 1 & +\sqrt{\frac{R_0}{L_0}} \end{bmatrix} \begin{bmatrix} 1 - \sqrt{\frac{R_0}{R_0}} \end{bmatrix}$
Computer Power and Energy (w=0,6) (J=0,28) A new peak power has Pax = FyR Thax = FyR The power is less that The power is less that The power is less that Terrinal: RUN			$E_{VR}(v,J) = E_{VR}(v,J) + P_{VR}(v,J)HI$ $E_{VR} = E_{VR} + E_{VR}(v,J)$
(v=0,6) (J=0,28) A new peak power has Pax PvR Thax Time The power is less that The power is less that The power is less that Tenninal! Run		Computer Power	Power and Energy due to Rotational lasing $P_{RR}(\mathbf{v}, \mathbf{J}) = hcN_{oc}(\mathbf{k}, \mathbf{v}, \mathbf{J}) \times_{rad}(\mathbf{v}, \mathbf{J})$
T en	Print	(w=0,6) (J=0,28)	PRR = PRR + PRR (v, J) H
Ten .	PVR PHJX	A new peak power   P Nax PVR	nas been found
	Time -0.27 Final	T <sub>Max</sub> Time	
	P.N. 100	The power is less TERMINAL: RUN	than 1% of the maximum

Figure C.1. (Continued)

	IssG = 1 .AND. Time < Trinal	The time is greater than the user specified time limit. TERMINATE RUN for small signal gain cases.
	T <sub>Left</sub> < 10.	Less than ten seconds of program execution time is left on a CDC 7600. RESTART MSUHFVR a later date. TERMINATE RUN.
	Time>T Start	Return to BEGIN INTEGRATION LOOP
	Tstort Tstart + Tskip	•
		Print the Time, Concentrations, Gain, Power and Energy. Call PRINT [ Time, Y.a(v,J), P, E, P(v,J), E(v,J),
•	PRINT	
	Return to BEGIN INTEGRATION LOOP	Loop
ABNORHAL TERMINATION	Print diagnostic message	I Flag, Time, Y, dY
		Print the final conditions
	PRINT	Call PRINT   Time, Y, a(v,J), PyR, EyR, PyR(v,J), EyR(v,J),
		( PRR' ERR' PRR(V, J), FRK(V, J), TIIL
TERMINATE	1 S S C = 0	Print Phux, Thax, relative band energies
	Create a file for RESTART	Time, Y, FyR, EyR(v,J), ERR, ERR(v,J), THAX, I'HAX
END MSUNFVR		

Figure C.1. (continued)

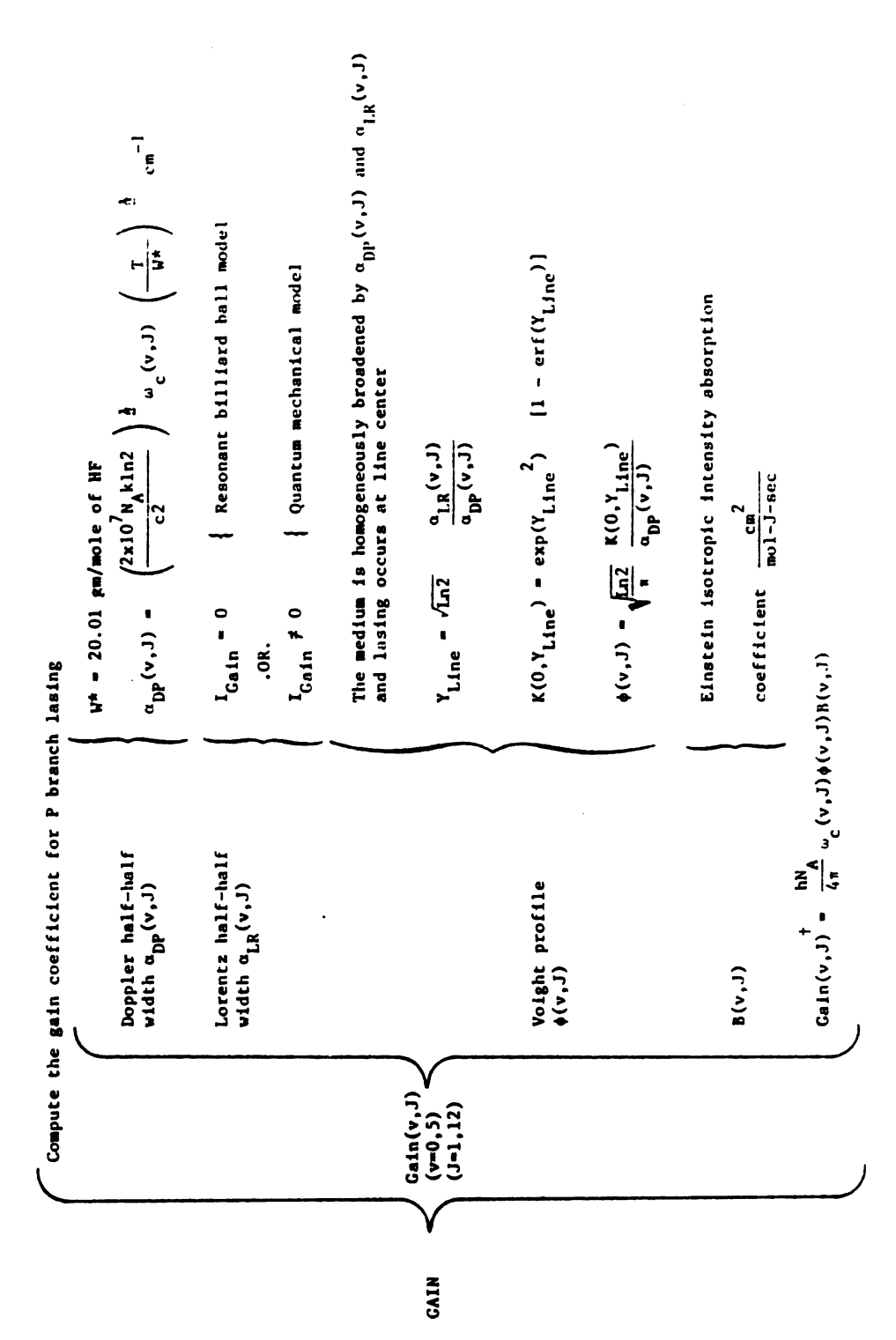


Figure C.1. (Continued)

 $^{\dagger}$ Gain (v,J) is multiplied by the population difference to give a(v,J) in DIFFUN

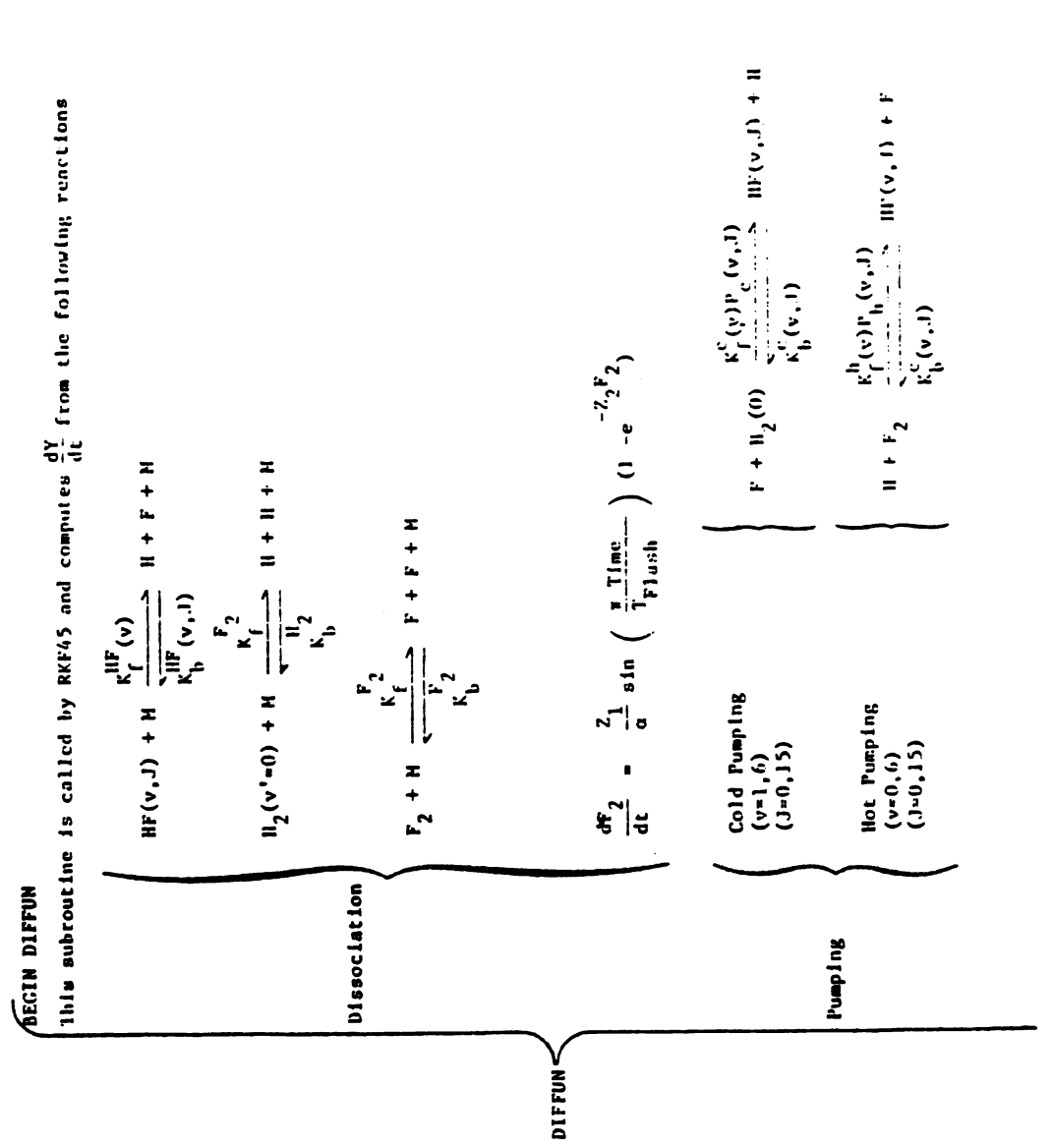
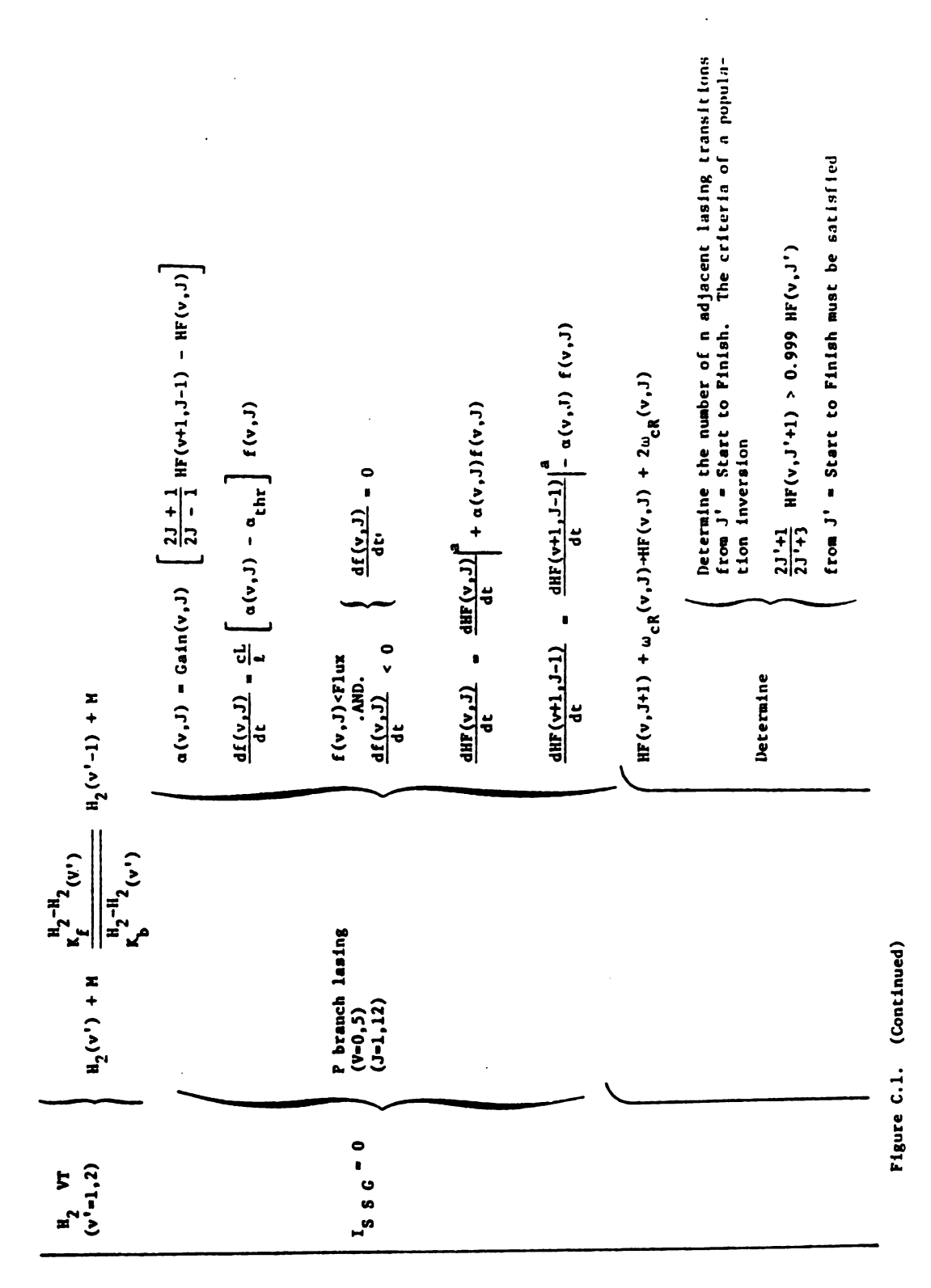


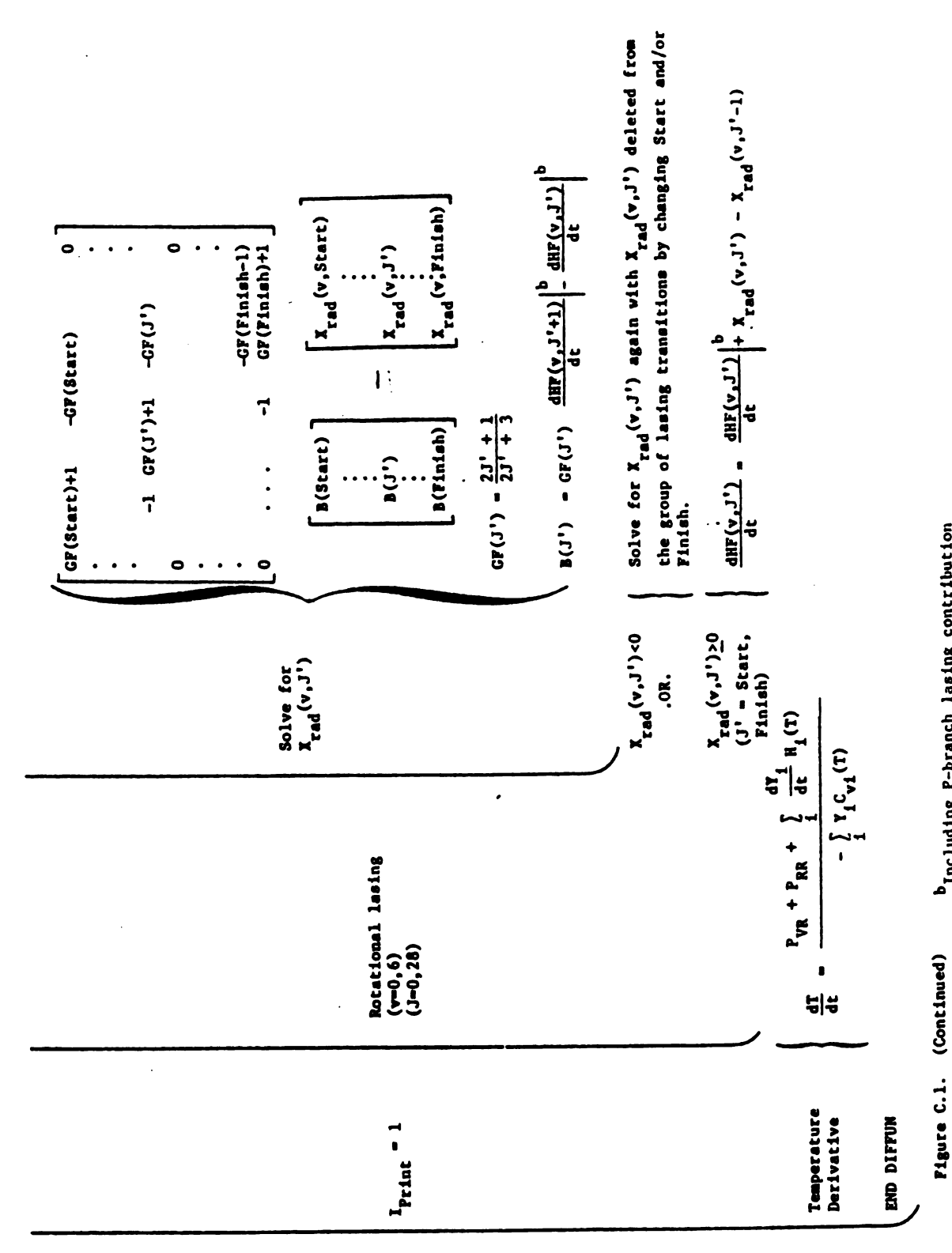
Figure C.1. (Continued)

Δv = 1  HF(v, J) + H  KVR (v, v')  KVR (v, v')  KVR (v, v')  KVR (v, v')  KVR (v, v') + H  KVR (v, v', J, J')	Δv >1	$\frac{K_{\rm C}^{\rm VV}(v,v')}{\frac{K_{\rm C}^{\rm VV}(v,v')}{\frac{V_{\rm V}(v,v',J,J')}{V_{\rm C}}}}$ HF(v'+1,J')	$\begin{array}{c} K^{RT}(\mathbf{v},J) + H & \frac{K^{RT}_{\mathbf{f}}(\mathbf{v},J,\Delta J)}{\sqrt{K^{RT}_{\mathbf{f}}(\mathbf{v},J,\Delta J)}} & HF(\mathbf{v},J-\Delta J) + H \\ K^{RT}_{\mathbf{b}}(\mathbf{v},J,\Delta J) \end{array}$	$\frac{K_{f}^{RR}(v, J, \Delta J)}{f}$ $\frac{K_{f}^{RR}(v, J, \Delta J)}{K_{b}^{RR}(v, J, J', \Delta J)}$ $\frac{K_{f}^{RR}(v, J, J', \Delta J)}{K_{b}^{RR}(v, J, J', \Delta J)}$	$\frac{\kappa^{\text{HF-H}_2(\mathbf{v},\mathbf{v}')}}{\kappa^{\text{HF-H}_2(\mathbf{v},\mathbf{v}',\mathbf{v}')}}$ $\frac{\kappa^{\text{HF-H}_2(\mathbf{v},\mathbf{v}',\mathbf{v}')}}{\kappa^{\text{HF-H}_2(\mathbf{v},\mathbf{v}',\mathbf{J})}}$ $\frac{\text{HF}(\mathbf{v}+1,\mathbf{J}) + \text{H}_2(\mathbf{v}'-1)}{\kappa^{\text{HF-H}_2(\mathbf{v},\mathbf{v}',\mathbf{J})}}$
	VR (v=0,6) (v' <v) (J=0,29) (J<sub>Hax</sub>+2)</v) 	VV (v=1,6) (y <v') (J=0,29) (J<j')< th=""><th>KT (v=0,6) (J=∆1,29) (AJ=1,2)</th><th>RR (v=0,6) (v<v') (J=ΔJ,28) (J<j'),δj=1< th=""><th>H<sub>2</sub> VV (v=0.5) (v=1.2) (J=0.29)</th></j'),δj=1<></v') </th></j')<></v') 	KT (v=0,6) (J=∆1,29) (AJ=1,2)	RR (v=0,6) (v <v') (J=ΔJ,28) (J<j'),δj=1< th=""><th>H<sub>2</sub> VV (v=0.5) (v=1.2) (J=0.29)</th></j'),δj=1<></v') 	H <sub>2</sub> VV (v=0.5) (v=1.2) (J=0.29)

Figure C.1. (Continued)



\*Without lasing contribution



broluding P-branch lasing contribution

## Table C.1. Nomenclature

Ar	Concentration of argon, mol/cc
B(v, J)	Einstein isotropic intensity absorption coefficient, cm <sup>2</sup> /molecule-J-sec
C <sub>vi</sub> (T)	Molar specific heat at constant volume of species i, cal/mol - °K
E(v,J)	Rotational energy of state (v,J), cm <sup>-1</sup>
$E_{RR}(v,J), E_{RR}$	Energy density of laser output due to rotational lasing, J/cc
f(v,J)	Photon flux for the transition $(v,J+1)+(v,J)$ mol/cm <sup>2</sup> -sec
fr'(v, J)	Photon flux for the transition $(v,J+1)+(v,J)$ mol/cm <sup>2</sup> -sec
F	Concentration of fluorine atoms, mol/cc
F <sub>2</sub>	Concentration of fluorine molecules, mol/cc
F <sub>B</sub> (J,T)	HF self broadening coefficients recommended by Hough [86]
Flux	Background photon flux. Typically 10 <sup>-14</sup> mol/cm <sup>2</sup> -sec
hc/k	The gas constant is k, h is Plancks constant, c is the speed of light in units of 1.4387886 cm-°K
н	Concentration of atomic hydrogen, mol/cc
H <sub>1</sub> (T)	Molar enthalpy of species i, Kcal/mol
H <sub>2</sub> (v')	Concentration of hydrogen in vibrational level v', mol/cc
Не	Concentration of helium, mol/cc
HF(v,J)	Concentration of hydrogen fluoride in vibrational level v and rotational level J, mol/cc
Print	A flag which controls the output from the laser simulation and the rotational lasing option included in the simulation
I Restart	A flag which specifies whether or not the simulation is started from previous conditions

I ssg	A flag which specifies whether or not there is P branch lasing
J,J <sup>†</sup>	Rotational energy level
J <sub>Max</sub>	Rotational energy level that minimizes the energy defect in the VR reaction $HF(v,J) \rightarrow HF(v',J_{max})$
J <sub>P</sub>	Rotational energy level on a given vibrational band of maximum gain
K <sub>b</sub> F2	F atom recomination rate coefficient
K <sub>b</sub> <sup>H</sup> 2	H atom recombination rate coefficient
K <sub>b</sub> <sup>HF</sup> (v,J)	HF recombination rate coefficient
K <sub>b</sub> <sup>VR</sup> (v,v',J,J')	Detailed balance factor for multiquanta VR, where J' ranges from -4 to +2 of $J_{max}$ . The most probable VR path is denotes as $J_{max}$ .
$K_{b}^{RT}(v,J,\Delta J)$	Detailed balance factor for RT with $\Delta J = 1$ or 2
$K_b^{RR}(v,v^*,J,\Delta J)$	Detailed balance factor for RR with $\Delta J = 1$
$K_{b}^{VV}(v,v^{*},J,J')$	Detailed balance factor for HF-HF VV
$K_f^c(v)(K_f^h(v))$	Forward rate coefficient of cold (hot) pumping from reference [24], cc/mol-sec
K <sub>f</sub> <sup>F</sup> 2	Forward rate coefficient for F dissociation recommended by Cohen [24], cc/mol-sec
K <sub>f</sub> <sup>H</sup> 2	Forward rate coefficient for $H_2$ dissociation recommended by Cohen [24], cc/mol-sec
H <sub>f</sub> (v)	Forward rate coefficient for HF dissociation recommended by Cohen [24], cc/mol-sec
K <sub>f</sub> <sup>R</sup> (v)	Forward rate coefficient for rotational relaxation recommended by Wilkins [51], cc/mol-sec
$K_{f}^{RR}(v,J,\Delta J=1)$	Forward rate coefficient for rotational to rotational quantum exchange, cc/mol-sec
$K_{f}^{RT}(v,J,\Delta J)$	Forward rate coefficient for rotational to translational relaxation, cc/mol-sec
K <sub>f</sub> <sup>VR</sup> (v,v')	Forward rate coefficient for mulitquanta VR, cc/mol-sec
K <sub>f</sub> <sup>VV</sup> (v,v*)	Forward HF VV rate coefficients recommended by Wilkins [51], cc/mol-sec

K <sub>HF</sub>	HF-HF VT rate recommended by Cohen [23], cc/mol-sec
<b>L</b>	Spacing between $R_0$ and $R_L$ , cm
N <sub>2</sub>	Concentration of nitrogen, mol/cc
P <sub>c</sub> (v, J)	Normalized cold pumping distribution of Polanyi and Woodall [11]
P <sub>h</sub> (v,J)	Normalized hot pumping distribution of Polanyi and Sloan [26]
P <sub>RR</sub> (v, J)	Power density of laser output from rotational lasing for the transition $(v,J+1)+(v,J)$ , w/cc
P <sub>RR</sub>	Total power due to rotational lasing, w/cc
P <sub>VR</sub> (v,J)	Power density of laser output from P branch lasing for the transition $(v+1,J-1)\rightarrow(v,J)$ , w/cc
P <sub>VR</sub>	Total power from P branch lasing, w/cc
P <sub>VR</sub> <sup>out</sup> (v,J)	Power density of laser output through $R_0$ for the transition $(v+1,J-1)+(v,J)$ , w/cc
P <sub>VR</sub>	Total power from P branch lasing through mirror $R_0$ , w/cc
$P_{\Delta J}(J)$	HF rotational relaxation probability for the transition $J\!\!\to\!\! J\!-\!\Delta J$
Q <sub>v</sub> (T)	Rotational partition function for level v
R	Universal gas constant, 1.98725 cal/mol-°K
R <sub>L</sub>	Reflectivity of the back mirror
R <sub>O</sub>	Reflectivity of the output mirror
SF <sub>6</sub>	Concentration of sulfurhexafluoride in mol/cc
Stepsize, H	The integration stepsize is T <sub>out</sub> -T, sec
T	The gas temperature, °K
<sup>T</sup> Final	Expected duration of the simulation
<sup>T</sup> Flash	Length of time of the photodissociation of F2, sec
<sup>T</sup> Left	The amount of remaining program execution time in- sec
T <sub>Out</sub>	The integrator RKF45 integrates $dY/dt$ from Time to $T_{Out}$

<sup>T</sup> Start' <sup>T</sup> Skip	Controls the time at which the output is printed in MSUHFVR
Time (t)	Time, sec
v,v'	Vibrational energy level
Y	The variable list Y contains 298 variables, $HF(v)$ , $HF(v,J)$ , $H_2(v')$ , H, $F_2$ , F, T, and $f(v,J)$
dY <sub>i</sub> /dt	The derivitive of Y evaluated in DIFFUN
z <sub>1</sub>	Maximum value of flashlamp output in moles of photons per unit volume, mol/cc-sec
z <sub>2</sub>	Photon absorption parameter of F2, cc/mol
α( <b>v</b> , <b>J</b> )	Gain of transition $(v+1,J-1)+(v,J)$ , cm <sup>-1</sup>
α <sub>LR</sub> (v,J)	Lorentz half-half width, cm <sup>-1</sup>
α <sub>DP</sub> (v,J)	Doppler half-half width, cm <sup>-1</sup>
$\alpha_{R}^{(v,J)}$	Gain of transition $(v,J+1)+(v,J)$ , cm <sup>-1</sup>
α <sub>thr</sub>	Threshold gain, cm <sup>-1</sup>
ρ	Density of the gas mixture, mol/cc
$\Delta {f v}$	Number of vibrational quanta lost in VR
φ( <b>v</b> ,J)	Normalized line profile, cm
X <sub>rad</sub> (v,J)	Rate of photon emission of transition $(v,J+1)+(v,J)$ mol/cc-sec
$\omega_{c}(v,J)$	Wave number of transition $(v+1,J-1)+(v,J)$ , cm <sup>-1</sup>
ω <sub>cR</sub> (v,J)	Wave number of transition $(v,J+1)+(v,J)$ , cm <sup>-1</sup>

## APPENDIX D

## MINIMUM ENERGY DEFECTS FOR VIBRATIONAL-ROTATIONAL RELAXATION

The J' levels associated with the vibrational-rotational relaxation processes given in Equation (1.12) with minimum energy defect for the relaxation paths of interest are tabulated in Table D.1. The corresponding energy defect is also noted.

Table D.1 Most Probable Multiquanta VR Transitions and Their Energy Defect  $\Delta E$  in cm $^{-1}$ 

	V=1	, V *=0	V=2	, V * = Q	V=2	,V*=1	V=3	, V = 0	V=3	,V'=1	V= 3	. V " = 2	V=4	, V°=0
J	J.	ΔE	J·	ΔE	J.	ΔE	J·	ΔE	J.	ΔΕ	. J•	ΔE	J.	ΔE
1	15	- 263	20	236	14	256	25	-231	28	182	14	223	28	436
2	15	-223	20	274	15	-237	25	-194	20	219	15	-258	28	471
	15	-144	20	350	15	-161	25	-121	20	292	15	-177	29	-438
	15	-26	21	-292	15	-47	25	-12	21	-326	15	-68	29	-332
5	15	131	21	-141	15	104	25	133	21	-188	15	77	29	-192
6	16	-260	21	46	16	-273	25	315	21	1	15	259	29	-17
7	16	-24	21	274	16	-46	26	-37 0	21	219	16	-66	29	191
8	16	249	22	-250	16	21 7	26	-116	22	-285	16	186	29	434
9	17	-62	22	50	17	-82	26	171	22	3	17	-101	30	-290
10	17	287	22	387	17	254	27	-435	22	327	17	222	30	20
11	16	16	23	- 59	18	-6	27	-76	23	-101	18	-28	30	364
12	19	- 251	23	349	19	-254	27	315	23	29 0	19	-276	31	-283
13	19	209	24	-56	19	179	28	-214	24	-98	19	149	31	125
14	20	-19	24	421	20	-48	28	244	24	360	20	-61	32	-480
15	21	-244	25	56	21	-257	29	-244	25	8	21	-270	32	-8
16	21	321	26	- 302	21	286	29	278	56	-336	21	25 2	32	493
17	22	133	26	274	22	105	30	-159	26	217	22	78	33	-48
18	23	-52	27	-47	23	-72	30	414	27	- 91	23	-92	33	521
19	24	-235	28	-363	24	-247	31	4	28	- 394	24	-260	34	27
20	25	-413	28	306	25	-420	32	-397	28	248	24	382	35	-456
21	25	314	29	26	25	279	. 32	274	<b>9</b>	-20	25	245	35	188
25	26	168	30	-248	26	139	33	-92	30	-284	26	119	36	-258
23	27	25	30	587	27	1	34	-458	30	441	27	-21	36	437
24	85	-115	31	265	28	-133	34	300	31	209	28	-151	37	25
25	29	- 252	32	29	29	-265	35	-23	32	-18	29	-277	38	-375
26	30	-386	33	-282	30	-394	36	-340	33	-248	30	-401	38	391
27	30	507	34	-428	30	463	36	48 2	34	-457	30	421	39	21
28	31	400	34	452	31	360	37	194	34	387	31	355	40	-337
29	35	295	35	254	32	259	38	-85	35	196	32	225	40	491
38	33	192	36	61	33	151	39	-357	36	10	33	131	41	161

Table D.1 (continued)

	V=4	,V°=1	V=4;	۷°=2	V=4,	, V '=3	V=5	, Y ° = 0	V=5	, v ·=1	V=5	, <b>* * =</b> 2	V=5	, <b>V</b> *= 3
J	J·	ΔE	J	ΔE	ှာ•	ΔE	J·	. ΔΕ	. J•	ΔE	J.	ΔE	.jė	ΔE
1	25	-290	20	130	14	192	<b>,</b> 35	-318	28	328	25	- 347	29	79
_	25	-255	20	165	14	227	32	-284	28	361	25	-313	20	113
	25	-184	20	235	15	-193	32	-217	28	429	25	-246	20	181
_	25	-79	28	. 341	15	-87	32	-116	29	-410	25	-145	20	28 2
	25	60	21	-218	15	52	32	18	29	-276	25	-10	21	-255
	25	235	21	-43	15	227	32	186	29	-108	25	157	21	-87
7	26	-424	21	165	16	-86	32	387	29	92	25	358	21	113
8	26	-180	22	-319	16	156	33	-444	29	326	26	-241	21	347
9	26	96	. 22	· -41	17	-120	33	-178	30	-370	26	24	22	-85
10	26	407	22	- 269	17	190	33	119	38	-71	26	322	ZZ	212
11	27	-142	23	-142	18	-49	33	449	30	258	27	-205	23	-183
12	27	234	23	233	19	-287	34	-272	31	-364	27	156	23	. 178
13	28	-274	24	-140	19	121	34	119	31	28	28	- 332	24	-180
14	28	166	24	300	20	-81	. 34	542	31	450	28	90	24	241
15	29	- 302	25	-37	21	-282	35	-106	32	-100	29	-360	25	-82
16	29	199	26	-369	21	220	35	375	32	380	29	121	25	. 399
17	30	- 231	26	162	22	52	36	-231	33	-130	30	- 232	25	189
18	30	329	27	-133	23	-111	36	386	33	407	30	245	27	-175
19	31	-64	28	-424	24	-273	37	-260	34	- 67	31	-132	27	390
20	32	-450	28	192	24	344	37	331	34	524	31	459	28	137
21	32	193	29	-65	25	212	38	-196	35	86	32	114	29	-110
22	33	-157	30	-319	26	82	38	446	36	-343	33	-222	38	-353
23	34	-501	30	376	27	- 44	39	-45	36	323	33	443	30	312
24	34	218	31	153	28	-168	40	-523	37	-71	34	136	31	· 98
25	35	- 93	32	-54	29	-289	40	159	38	-456	35	-161	32	-116
26	36	-398	33	-277	. 30	-408	41	-255	38	277	36	-454	33	-315
<b>27</b>	36	389	34	-486	30	379	.41	498	39	-77	36	299	33	438
28	37	113	34	322	31	284	42	36	+0	- 421	37	34	34	258
29	38	-154	35	140	32	. 191	43	-312	<b>, 40</b>	371	38	- 222	35	83
30	39	-415	36	-37	33	. 181	43	497	41	54	39	-472	36	-87

Table D.1 (continued)

	V=5 , V * =4		, V=5,V'=0 V=6,V'=1			V=6, V'=2 V=6, V'=3			V= <b>5</b>		V=6,V'=5			
J	J·	ΔE	J.	ΔE	,	ΔΕ	J·		J·		J.	ΔE	٠,٠	ΔΕ
4	14	162	35	-426	32	-421	28	222	24	374	20	30	4.	4 7 2
	14	196	35	-394	32	-388	28	254	25	-370	28	5 <b>u</b> 62	14	132
	15	-202	35	-329	32	-324	28	319		- 305			14	164
	15	-107	35	-232	32	-227	28	416	25 25	-208	20 20	127	15	-222
	15	27	35	-103	32	-98		-357				224	15	-125
	15	195	35	57			29		25	-79	21	-291	15	3
	16	-106			32	62	29	-196	25	81	21	-130	15	164
			35	250	32	255	29	-3	25	274	21		16	-125
	16	127	35	474	32	479	29	220	26	-301	21	286	16	99
_	17	-138	36	-387	33	-287	30	-448	26	-46	22	-129	17	-155
10		160	36	-101	33	-1	30	-162	26	239	22	157	17	130
11		-70	36	214	33	315	30	153	27	-267	23	-222	1.5	-91
12		290	36	561	34	-378	31	-443	27	79	23	123	18	254
	19	93	37	-195	34	-2	31	-67	28	-30 5	24	- 220	19	65
14		-101	37	209	34	4 B Z	31	337	28	15	24	184	20	-121
15		-293	38	-502	35	-219	32	-191	29	-416	25	-126	21	-385
	21	187	38	- 40	35	241	35	270	29	45	25	335	21	155
17	22	27	38	447	36	-341	33	-221	30	- 352	2 €	56	22	2
18	23	-130	39	-194	36	173	33	294	30	163	27	- 215	23	-149
19	24	-285	39	346	37	- 370	34	-161	31	-199	27	325	24	-297
20	24	306	40	-255	37	196	34	484	31	366	28	82	24	. 598
21	25	179	40	335	38	-309	35	-15	32	35	29	-155	25	147
22	26	55	41	-227	38	304	36	-426	33	-287	30	- 388	26	26
23	27	-65	41	409	39	-166	36	210	33	349	30	249	27	-68
24	28	-185	42	-116	39	49 2	37	-168	34	55	31	43	28	-202
25	29	-301	42	564	40	55	37	512	35	- 231	32	-157	29	-314
26	30	-416	43	73	41	-378	38	153	35	469	33	-353	23	386
27	30	337	44	-403	41	349	39	-176	36	2 08	33	366	30	296
28	31	246	44	335	42	-45	40	-506	37	-44	34	194	31	209
29	32	157	45	-109	43	-428	40	249	38	- 291	35	25	32	123
30	33	7L	46	-539	43	344	41	-54	38	481	36	-137	33	40

Table D.1 (continued)

	V=7, V *=0		V=7	, V*=1	V=7, V*=2		V=7.V*=3		V=7 ,V*=4		V=7 ,V *=5		V=7,V*=6	
J	٠,	ΔΞ	,	ΔE	J·	ΔE	J•	•	J•		J	-	J•	•
1	37	311	34	505	31	439	28	117	24	287	20	-18	14	103
2	37	342	35	-519	31	470	28	148	24	318	20	12	14	134
3	37	4 D-+	35	-457	32	-429	28	210	25	- 36 4	25	74	14	196
4	37	497	35	-364	32	-336	28	303	25	- 27 1	20	167	15	-144
5	38	- 523	35	-241	32	-212	28	427	25	-147	20	298	15	-21
6	38	- 36 <del>4</del>	35	-87	32	-58	29	-283	25	6	21	-172	15	133
7	38	-185	35	97	32	125	29	-99	25	190	21	11	16	-143
8	38	29	35	311	32	340	29	115	26	-361	21	226	16	70
9	38	273	36	-515	33	-395	29	359	26	-116	22	-171	17	-173
10	38	547	36	-241	33	-121	30	- 252	26	156	22	181	17	100
11	39	- 307	36	60	33	181	36	3 €	27	- 328	23	- 251	15	-112
12	39	24	36	392	34	-483	30	332	27	3	23	69	18	219
13	39	363	37	-332	34	-124	31	-162	27	363	24	-250	19	38
14	40	<b>-</b> 396	37	54	34	263	31	225	28	-56	24	127	20	-140
15	40	10	37	L69	35	-332	32	-231	25	356	25	- 170	20	273
16	40	459	36	-186	35	108	32	159	29	- 31	25	270	21	124
17	41	- 251	36	280	36	-450	33	-311	30	-412	26	4	22	-23
18	41	241	39	-335	36	42	33	151	30	80	27	-256	23	-168
19	42	-427	39	181	37	-479	34	-255	31	-267	27	260	24	-310
20	42	113	40	-394	37	61	34	255	31	274	28	27	24	230
21	43	-513	40	169	36	-423	35	-117	32	- 43	29	-200	25	114
22	43	73	41	-370	38	163	35	459	33	-353	29	396	26	9
23	44	-51+	41	238	39	-287	36	97	33	255	30	164	27	-110
24	44	114	42	-266	39	341	37	-255	34	-26	31	-11	28	-220
25	45	- 436	42	383	L 0	-77	37	354	35	- 301	32	-204	29	- 326
26	45	231	43	-66	41	-486	38	49	35	366	33	- 391	29	341
27	46	- 265	44	-544	41	199	39	-277	36	117	· 33	234	30	255
8 \$	46	418	44	159	42	-178	39	426	37	-125	34	126	31	171
29	47	-62	45	-265	42	542	40	127	38	-361	35	-31	32	90
30	48	- 526	45	469	43	190	41	-163	38	373	36	-188	33	9

Table D.1 (continued)

	V=8, Y *=0		V=8, V'=1		V=8, V'=2		V=8,V'=3		Y=6,V *=4		V =8,V *=5		V=8,V°=6	
J	J·	ΔE	J·	ΔE	J	ΔE	J•	ΔΕ	J·	ΔE	J.	ΔΕ	١.	ΔΕ
1	40	- 323	37	128	34	336	31	298	28	14	24	200	20	-67
2	40	-293	37	157	34	366	31	328	8 5	44	24	230	20	-37
3	40	-234	37	216	34	425	31	397	28	103	24	269	20	2:
4	40	-145	37	305	35	-496	32	-445	28	192	25	- 334	20	109
5	40	-27	37	423	35	-378	32	-327	28	318	25	-216	20	228
6	40	119	36	-525	35	-231	32	-180	29	-371	25	-68	21	-215
7	40	296	38	-349	35	-54	32	- 3	29	-194	25	107	21	-39
8	40	501	38	-144	35	150	32	201	29	10	25	312	21	16€
9	41	-443	38	89	35	383	32	434	29	244	26	-187	22	-215
10	41	-181	38	3 51	36	-380	33	-241	30	-342	2 €	74	22	46
11	41	107	39	-468	36	-91	33	47	30	- 52	<b>26</b>	353	23	-361
12	41	424	39	-151	36	225	33	364	30	263	27	-73	23	15
13	42	-417	39	191	37	-469	34	-2+5	31	- 257	27	270	24	-300
14	42	-47	40	-555	37	-99	34	124	31	112	28	-133	5.4	5 9
15	42	346	40	-159	37	296	35	-447	3 2	- 37 3	28	262	25	-215
16	43	-422	40	261	38	-332	35	-26	32	48	29	-109	25	20€
17	43	23	41	-419	38	113	35	419	33	-482	29	336	26	-43
18	43	493	41	50	39	-476	36	-91	33	67	30	- 3	27	-293
19	44	-209	41	543	39	17	36	402	34	- 350	31	-335	27	19-
20	44	306	42	-73	39	533	37	-73	34	165	31	186	28	-20
21	45	- 356	42	464	40	Z	37	464	35	- 22 0	32	-123	29	-246
22	45	203	43	-115	41	-514	38	21	35	338	33	-419	29	313
23	46	-419	43	464	41	65	39	-411	36	-17	33	150	30	120
24	46	179	44	-79	42	-417	39	157	37	-365	34	-110	31	-68
25	47	-404	44	538	42	200	40	-214	37	253	35	- 373	32	-252
26	47	231	45	28	43	-250	40	421	38	-67	35	262	35	38 4
27	48	- 315	46	-465	43	403	41	49	39	- 376	36	23	33	221
28	48	352	46	203	44	-19	42	-314	39	289	37	-209	34	6 1
29	49	- 160	47	-257	45	-425	42	379	40	2	38	-434	35	-91
30	49	537	47	440	45	27 <b>2</b>	43	33	41	-276	36	263	36	-241

## References

- 1. K. L. Kompa and G. C. Pimentel, "Hydroflouric acid chemical laser," J. Chem. Phys. <u>47</u>, pp. 857-858 (1967).
- 2. J.V.V. Kasper and J. C. Pimentel, "HCL chemical laser," Phys. Rev. Letters 14, pp. 352-354 (1964).
- 3. T. F. Deutsch, "Molecular laser action in hydrogen and deuterium halides," Appl. Phys. Letters <u>10</u>, pp. 234-236 (1967).
- 4. R.W.F. Gross and J. F. Bott, <u>Handbook of Chemical Lasers</u>, John Wiley and Sons, New York (1976).
- 5. R. L. Kerber, A. Ching, M. L. Lundquist, and J. S. Whittier, "An efficiently initiated pulsed H<sub>2</sub>+F<sub>2</sub> laser," IEEE J. Quantum Electron. <u>QE-9</u>, pp. 607-609 (1973).
- 6. N. R. Greiner, L. S. Blair, E. L. Patterson, and R. A. Gerber, "A 100 gigawatt H<sub>2</sub>-F<sub>2</sub> laser initiated by an electron beam," IEEE J. Quantum Electron. QE-10, p. 780 (1974).
- 7. W. D. Adams, E. B. Turner, J. F. Hold, D. G. Sutton, and H. Mirels,

  The RESALE Chemical Laser Program, TR-0075(5530)-5, The

  Aerospace Corporation, El Segundo, California (February 1975).
- 8. R. L. Kerber, G. Emanuel, J. S. Whittier, "Computer modeling and parametric study for a pulsed H<sub>2</sub>+F<sub>2</sub> laser," Appl. Optics 11, pp. 1112-1123 (1972).
- 9. J. G. Skifstad, "Theory of an HF chemical laser," Combustion Science and Tech. 6, pp. 287-306 (1973).
- 10. S. N. Suchard, R. L. Kerber, G. Emanuel, and J. S. Whittier, "Effect of H<sub>2</sub> pressure on pulsed H<sub>2</sub> + F<sub>2</sub> laser. Experiment and theory," J. Chem. Phys. <u>57</u>, pp. 5065-5075 (1972).
- 12. D. J. Douglas and J. C. Polanyi, "Effect of changing reagent energy on reaction dynamics. VII. Dependence of product energy distribution on reagent rotational excitation in F+H<sub>2</sub>(J) + HF+H," Chem. Phys. <u>16</u>, pp. 1-8 (1976).
- 13. D. S. Perry and J. C. Polanyi, "Energy distribution among reaction products. IX. F+H<sub>2</sub>, HD and D<sub>2</sub>," Chem. Phys. <u>12</u>, pp. 419-431 (1976).
- 14. M. J. Berry, "F+H<sub>2</sub>,D<sub>2</sub>, HD reactions: Chemical laser determination of the product vibrational state populations and the F+HD intramolecular kinetic isotope effect," J. Chem. Phys. <u>59</u>, pp. 6229-6253 (1973).

- 15. R. L. Wilkins, "Monte Carlo calculations of reaction rates and energy distribution among reaction products. II. H+HF(v)+
  H<sub>2</sub>(v')+F and H+HF(v)+HF(v')+H," J. Chem. Phys. <u>58</u>,
  pp. 3038-3046 (1973).
- 16. R. L. Wilkins, "Monte Carlo calculation of reaction rates and energy distribution among reaction products. I. F+H<sub>2</sub>→HF+H," Chem. Phys. <u>57</u>, pp. 912-917 (1972).
- 17. J. T. Muckerman, "Monte Carlo calculations of energy partitioning and isotope effects in reactions of flourine atoms with H<sub>2</sub>, HD, and D<sub>2</sub>" J. Chem. Phys. <u>54</u>, pp. 1155-1164 (1971).
- 18. R. L. Jaffe and J. B. Anderson, "Classical trajectory analysis of the reaction F+H<sub>2</sub>+HF+H," J. Chem. Phys. <u>54</u>, pp. 2234-2236 (1971), erratum, 56, p. 682 (1972).
- 19. J. C. Polanyi and J. C. Schreiber, "The reaction of F+H<sub>2</sub>+HF+H, a case study in reaction dynamics," Faraday Disc. Chem. Soc. 62, pp. 267-290 (1977).
- 20. J. N. L. Connor, W. Jakubetz, and J. Manz, "Information theoretic analysis and collinear to three-dimensional transformation of reaction probabilities for F+H<sub>2</sub>, H+F<sub>2</sub>, H+Cl<sub>2</sub>, and D+Cl<sub>2</sub>," Chem. Phys. <u>17</u>, pp. 451-469 (1976).
- 21. K. G. Anlauf, P. J. Kuntz, D. H. Maylotte, P. D. Pacey, and J. C. Polanyi, "Energy distribution among reaction products, Part 2. H+X<sub>2</sub> and X+HY," Faraday Disc. Chem. Soc. <u>44</u>, pp. 183-192 (1967).
- 22. N. Cohen, A Review of Rate Coefficients in the H<sub>2</sub>+F<sub>2</sub> Chemical Laser System, TR-0076(6603)-2, The Aerospace Corporation, El Segundo, California (April 1976).
- 23. N. Cohen, A Review of Rate Coefficients in the H<sub>2</sub>-F<sub>2</sub> Chemical
  Laser System Supplement (1977), TR-0078(3603)-4 The
  Aerospace Corporation, El Segundo, California (June 1978).
- 24. N. Cohen, A Review of Rate Coefficients for Reactions in the H<sub>2</sub>+F<sub>2</sub> Laser System, TR-0073(3430)-9, The Aerospace Corporation, El Segundo, California (November 1972).
- 25. J. C. Cummings, J. E. Broadwell, W. L. Shackleford, A. B. Whie, J. E. Trost, and G. Emanuel, "H<sub>2</sub>+F<sub>2</sub> Chain reaction rate investigation," J. Quant. Spectrosc. Radiat. Transfer <u>17</u>, pp. 97-116 (1977).
- 26. J. C. Polanyi and J. J. Sloan, "Energy distribution among reaction products. VII. H+F<sub>2</sub>," J. Chem. Phys. <u>57</u>, pp. 4988-4998 (1972).

- 27. N. Jonathan, S. Okuda, and D. Timlin, "Initial vibrational energy distributions determined by infra-red chemiluminescence III. Experimental results and classical trajectory calculations for the H+F<sub>2</sub> system," Molecular Physics <u>24</u>, pp. 1143-1164 (1972).
- 28. J. C. Polanyi, J. L. Schreiber, and J. J. Sloan, "Distribution of reaction products (theory). XI. H+F<sub>2</sub>," Chem. Phys. <u>9</u>, pp. 403-421 (1975).
- 29. R. L. Wilkins, "Monte Carlo calculations of reaction rates and energy distribution among reaction products. III H+F<sub>2</sub>+HF+F and D+F<sub>2</sub>+DF+F," J. Chem. Phys. <u>58</u>, pp. 2326-2332 (1973)
- 30. R. G. Albright, A. F. Dodonov, G. K. Lavrovskaya, I. I. Morosov, and V. L. Tal'roze, "Mass-spectrometric determination of rate constants for H atom reactions with Cl<sub>2</sub> and F<sub>2</sub>," J. Chem. Phys. 50, pp. 3632-3633 (1969).
- 31. J. C. Polanyi and K. B. Woodall, "Mechanism of rotational relaxation," J. Chem. Phys. <u>56</u>, pp. 1563-1572 (1972).
- 32. A. M. G. Ding and J. C. Polanyi, "Energy transfer as a function of collision energy. I Collision partners: Hydrogen halides + inert gases, hydrogen halides, H<sub>2</sub>S and propane," Chem. Phys. 10, pp. 39-49 (1975).
- 33. J. J. Hinchen and R. H. Hobbs, <u>Rotational population transfer in</u>
  <u>HF</u>, R77-952595-1, United Technologies Research Center, East
  Hartford, Connecticut (August 1977).
- 34. J. J. Hinchen and R. H. Hobbs, "Rotational relaxation studies of HF using ir double resonance," J. Chem. Phys. 65, pp. 2732-2739 (1976).
- 35. L. M. Peterson, G. H. Lingquist, and C. B. Arnold, "Rotational relaxation measurements of laser-excited hydrogen flouride," J. Chem. Phys. 61, pp. 3480-3482 (1974).
- 36. G. K. Vasil'ev, E. F. Mokarov, A. G. Ryabenko, and V. L. Tal'roze, "Rotational and vibrational deactivation of excited HF molecules," Sov. Physics JETP 41, pp. 617-621 (1976).
- 37. V. I. Gur'ev, G. K. Vasil'ev and O. M. Batovskii, "Measurement of the rate of rotational relaxation of HF molecules," JETP Lett. 23, pp. 230-232 (1976).
- 38. G. Emanuel, "Chemiluminescent measurement sensitivity of a nonuniform gas," J. Quant. Spectrosc. Radiat. Transfer, 19, pp. 397-406 (1978).

- 52. R. L. Wilkins, "Vibrational relaxation in the HF-DF and DF-HF systems," (to be published).
- 53. J. D. Kelly, "Intra-and intermolecular vibrational deexcitation in impulsive atom-diatomic molecule collisions," J. Chem. Phys. 53, pp. 3864-3868 (1970).
- 54. L. L. Poulsen, P. L. Houston, and J. I. Steinfeld, "Near-resonant vibration-rotation energy transfer," J. Chem. Phys. <u>58</u>, pp. 3381-3388 (1973).
- 55. D. Frankel, J. I. Steinfeld, R. D. Sharma, and L. Poulsen, "Temperature dependence of near-resonant vibration-rotation energy transfer," Chem. Phys. Lett. <u>28</u>, pp. 485-489 (1974).
- 56. P. McGuire and J. P. Toennies, "A priori low temperature vibrational relaxation rates for He-H<sub>2</sub>," J. Chem. Phys. <u>62</u>, pp. 4623-4627 (1975).
- 57. T. A. Dillon and J. C. Stephenson, "Multiquantum vibrational-energy exchange," Phys. Rev. A., 6, pp. 1460-1468 (1972).
- 58. H. K. Shin, "Vibration-to-rotation energy transfer in hydrogen fluoride: Effects of the dipole-dipole and hydrogen-bond interactions, J. Chem. Phys. <u>59</u>, pp. 879-884 (1973).
- 59. H. K. Shin, "A collision model for the vibrational relaxation of hydrogen fluoride at low temperatures," Chem. Phys. Lett. 26, pp. 450-456 (1974).
- 60. J. R. Airey, S. F. Fried, "Vibrational relaxation of hydrogen fluoride," Chem. Phys. Lett. 8, pp. 23-26 (1971).
- 61. H. K. Shin and Y. H. Kim, "Temperature dependence of the vibration-vibration de-excitation rates of HF(v=n) + HF(v=o)→HF(v=n-1) + HF(v=1) for n=2-5," J. Chem. Phys. 64, pp. 3634-3638 (1976).
- 62. M. A. Kwok and R. L. Wilkins, "Flow-tube studies of vibrational energy transfer in HF(v) + HF, DF(v) + HF, and DF(v) + Dz systems," J. Chem. Phys. 6, pp. 2453-2460 (1975).
- 63. J. A. Airey and I.W.M. Smith, "Quenching of infrared chemilumine-scence: Rates of energy transfer from HF(v<5) to CO<sub>2</sub> and HF and from DF (v<5) to CO<sub>2</sub> and HF," J. Chem. Phys. <u>57</u>, pp. 1669-1676 (1972).
- 64. R. M. Osgood Jr., P. B. Sackett, and A. Javan, "Measurement of vibrational-vibrational exchange rates for excited vibrational levels (2<v<4) in hydrogen fluoride gas," J. Chem. Phys. 60, pp. 1464-1480 (1974).

- 39. G. H. Lindquist, L. M. Peterson, and C. B. Arnold, <u>Rotational relaxation measurements and resonant phenomena in laser-excited hydrogen fluoride</u>, 101300-18-15, Environmental Research Institute of Michigan, Ann Arbor, Michigan (June 1974).
- 40. R. F. Deutsch, "Laser emission from HF rotational transitions," Appl. Phys. Lett. 11, pp. 18-20 (1967).
- 41. E. R. Sirkin, E. Cuellar, and G. C. Pimentel, "Laser emission between high rotational states of HX resulting from photo-elimination of halogenated olefins," presented at the 5th Conference of Chemical and Molecular Lasers, St. Louis, Missouri, April 18-20, 1977.
- 42. O. D. Krogh and G. C. Pimentel, "CIF<sub>x</sub>-H<sub>2</sub> chemical lasers: vibration-rotation emission by HF from states with high rotational excitation," presented at the 5th Conference of Chemical and Molecular Lasers, St. Louis, Missouri, April 18-20, 1977 and J. Chem. Phys. 67, pp. 2993-3001 (1977).
- 43. N. Skribanowitz, I. P. Herman, R. M. Osgood Jr., M. S. Feld, and A. Javan, "Anisotropic ultrahigh gain emission observed in rotational transitions in optically pumped HF gas," Appl. Phys. Lett. 20, pp. 428-431 (1972).
- 44. H. Chen, R. L. Taylor, J. Wilson, P. Lewis, and W. Fyfe,
  "Atmospheric pressure pulsed HF chemical laser," J. Chem.
  Phys. 61, pp. 306-318 (1974).
- 45. D. P. Akitt and J. T. Yardley, "Far-infrared laser emission in gas discharges containing boron trihalides," IEEE J. Quantum Electron. QE-6, pp. 113-116 (1972).
- 46. E. Cuellar, J. H. Parker, and G. C. Pimental, "Rotational chemical lasers from hydrogen fluoride elimination reactions," J. Chem. Phys. 61, pp. 422-423 (1974).
- 47. W. W. Rice, R. C. Oldenborg, "Pure rotational HF laser oscillations from exploding-wire laser," IEEE J. Quantum Electron. QE-13, pp. 86-88 (1977).
- 48. L. H. Sentman, "Rotational relaxation of HF," J. Chem. Phys. <u>67</u>, pp. 966-969 (1977).
- 49. F. J. Zeleznik, "Rotational relaxation in polar gases," J. Chem. Phys. 47, pp. 3410-3424 (1967).
- 50. R. L. Wilkins, <u>Vibration-rotation bands of HF and DF</u>, TR-0077 (2603)-7 Aerospace Corp. Los Angeles, CA (September 1977).
- 51. R. L. Wilkins, "Mechanisms of energy transfer in hydrogen fluoride systems," J. Chem. Phys. 67, pp. 5838-5854 (1977).

- 65. D. L. Thompson, "Mechanisms for hydrogen halide vibrational relaxation," J. Chem. Phys. <u>57</u>, pp. 2584-2590 (1972).
- 67. M. A. Nazar, J. C. Polanyi, W. J. Skrlak, J. J. Sloan, "Experimental evidence for "coscading"; rapid vibration with retention of rotational quantum number," Chem. Phys. <u>16</u>, pp. 411-418 (1976).
- 68. S. N. Suchard, R.W.F. Gross, and J. S. Whittier, "Time-resolved spectroscopy of a flash-initiated H<sub>2</sub>-F<sub>2</sub> laser," Appl. Phys. Lett. 19, pp. 411-413 (1971).
- 69. D. B. Nichols, K. H. Wrolstad, and J. D. McClure, "Time-resolved spectroscopy of a pulsed H<sub>2</sub>-F<sub>2</sub> laser with well-defined initial conditions," J. Appl. Ph ys. <u>45</u>, pp. 5360-5366 (1974).
- 70. J. V. Parker and R. R. Stephens, "Pulsed HF chemical laser with high electrical efficiency," Appl. Phys. Lett. 22, pp. 450-452 (1973).
- 71. S. N. Suchard, "Lasing from the upper vibrational levels of a flash-initiated  $H_2$ - $F_2$  laser," Appl. Phys. Lett. 23, pp. 68-70 (1973).
- 72. J.J.T. Hough and R. L. Kerber, "Effect of cavity transients and rotational relaxation on the performance of pulsed HF chemical lasers: A theoretical investigation," Appl. Optics 14, pp. 2960-2970 (1975).
- 73. R. L. Kerber, J.J.T. Hough, "Rotational nonequilibrium mechanisms in pulsed  $H_2+F_2$  chain reaction lasers I. Effect on gross laser performance parameters," Appl. Optics <u>17</u>, pp. 2369-2380 (1978).
- 74. R. L. Kerber, K. Emery, and J.J.T. Hough, "Evaluation of rotational nonequilibrium mechanisms in pulsed H<sub>2</sub>+F<sub>2</sub> lasers," Presented at the 5th Conference of Chemical and Molecular Lasers, St. Louis, Missouri, April 19-20, 1977.
- 75. A. Ben-Shaul, K. L. Kompa, and V. Schmailzl, "Vib-rotational energy distributions and relaxation processes in pulsed HF chemical lasers," J. Chem. Phys. 65, pp. 1711-1728 (1976).
- 76. J. B. Moreno, "Computer model for the  $H_2+F_2$  superradient laser," AIAA paper #73-36 13th Aerospace Sciences Meeting, Pasadena, California, January 20-22, 1975.
- 77. J. R. Creighton and R. K. Pearson, "A numerical investigations of the pulsed NF<sub>3</sub>+H<sub>2</sub> chemical laser using a model which includes rotational relaxation and semi-classical laser equations,"

  Technical Report #UCRL 51931, Lawrence Livermore Laboratory, University of California/Livermore, September 1, 1975.

- 78. L. H. Sentmen, "Rotational nonequilibrium in cw chemical lasers," J. Chem. Phys. 62, pp. 3523-3537 (1975).
- 79. L. H. Sentman, "Chemical laser power spectral performance: a coupled fluid dynamic, kinetic, and physical optics model," Appl. Optics 17, pp. 2244-2249 (1978).
- 80. J. G. Skifstad and C. M. Chao, "Rotational relaxation in a line-selected continuous HF chemical laser," Appl. Optics 14, pp. 1713-1718 (1975).
- 81. R. J. Hall, "Rotational nonequilibrium and line-selected operation in cw DF chemical lasers," IEEE J. Quantum Electron. QE-12, pp. 453-462 (1976).
- 82. A. F. Trotman-Dickenson and G.S. Milne, <u>Tables of Bi-molecular</u>
  <u>Gas Reactions</u>, Washington D.C., NSRAS-NBS, 1967.
- 83. A. Persky, "Kinetic isotope effects in the reaction of fluorine atoms with molecular hydrogen," J. Chem. Phys. <u>59</u>, pp. 3612-3615 (1973).
- 84. J. G. Moehlman, J. D. McDonald, "Infrared chemiluminescence of fluorine atom substitution reactions," J. Chem. Phys. 62, pp. 3052-3060 (1975).
- 85. R. Herman and K. E. Shuler, "Studies in nonequilibrium rate processes. IV. The rotational and vibrational relaxation of a system of rotating oscillators," J. Chem. Phys. 29, pp. 366-374 (1958).
- 86. J.J.T. Hough, "Lorentz broadening in the modeling of the HF chemical laser." Appl. Optics 16, pp. 2297-2307 (1977).
- 87. D. L. Thompson, "Monte Carlo classical trajectory calculation of the rates of H-atom vibrational relaxation of HF and DF," J. Chem. Phys. 57, pp. 4164-4169 (1972).
- 88. R. L. Wilkins, "Monte Carlo calculations of reaction rates and energy distributions among reaction products IV. F+HF(v)+HF(v')+F and F+DF(v)+DF(v')+F," J. Chem. Phys. <u>59</u>, pp. 698-704 (1973).
- 89. E. B. Turner, G. Emanuel, R. L. Wilkins, The Nest Chemistry
  Computer Program Vol. 1, TR-0059-(6240-20)-1, Vol. I, The
  Aerospace Corporation, El Segundo, California (July 1970).
- 90. J. D. Warnier, Logical Construction of Programs, Van Nostrand Reinhold Company, New York (1976).

- 91. R. E. Meredith and F. J. Smith, <u>Investigations of Fundamental</u>
  Laser Processes Vol. II: <u>Computation of Electric Dipole</u>
  Matrix Elements for Hydrogen Fluoride and <u>Deuterium Fluoride</u>,
  84130-39-T(II), The Environmental Research Institute of
  Michigan, Ann Arbor, Michigan, November 1971.
- 92. L. F. Shampine and H. A. Watts, <u>Practical Solution of Ordinary Differential Equations by Runge-Kutta Methods</u>, SAND76-0585, Sanda Laboratories, Albuquerque, New Mexico 87115 (December 1976).